

TECHNISCHE UNIVERSITÄT MÜNCHEN

Wissenschaftszentrum Weihenstephan für Ernährung, Landnutzung und Umwelt

Lehrstuhl für Siedlungswasserwirtschaft

Long-distance electron transfer by cable bacteria in aquifer sediments

Hubert Müller

Vollständiger Abdruck der von der Fakultät Wissenschaftszentrum Weihenstephan für Ernährung, Landnutzung und Umwelt der Technischen Universität München zur Erlangung des akademischen Grades eines Doktors der Naturwissenschaften genehmigten Dissertation.

Vorsitzende(r): Univ.-Prof. Dr. Wolfgang Liebl

Prüfer der Dissertation:

1. Priv.-Doz. Dr. Tillmann Lueders
2. Univ.-Prof. Dr. Rainer Meckenstock

Die Dissertation wurde am 16.01.2017 bei der Technischen Universität München eingereicht und durch die Fakultät Wissenschaftszentrum Weihenstephan für Ernährung, Landnutzung und Umwelt am 28.02.2017 angenommen.

Abstract

The sequential depletion of electron acceptors leads to a distinct redox zonation in the upper layers of organic-rich sediments. In marine and freshwater sediments, a direct coupling of spatially-separated sulfide oxidation and oxygen reduction by an electron transfer over centimeter distances has been inferred from biogeochemical profiles. Cable bacteria of the family *Desulfobulbaceae* are supposed to mediate this long-distance electron transfer (LDET) by bridging a suboxic zone over centimeter distances where both sulfide and oxygen are absent.

Comparable small-scale gradients are found in hydrocarbon-contaminated aquifers where biodegradation is often limited by deficient availability of electron acceptors. According to the plume fringe concept, electron acceptors are mainly depleted within a narrow zone at the fringe of the contaminant plume where electron donors and acceptors encounter by dispersive mixing. There, cable bacteria might conduct electrons from the highly-reduced plume core to electron acceptors in the pristine groundwater outside the plume. An electron transfer across the redox boundary at the plume fringe might lead to a recycling of electron acceptors within the plume core and therefore enhance biodegradation.

Within this thesis, it was investigated if a LDET by cable bacteria exists in contaminated aquifers; and its potential impacts on the biogeochemistry and biodegradation were elucidated. Therefore, sediments from a contaminated site were amended with FeS, incubated in the laboratory exposed to air, and tested for the presence of LDET by biogeochemical measurements. Groundwater and sediments from the same contaminated field site were sampled in high resolution and analyzed in terms of redox chemistry, contaminants, and dissolved organic matter. Laboratory and field samples were investigated for the presence of cable bacteria by pyrosequencing, microbial community fingerprinting, and fluorescence in situ hybridization.

After 2-3 months, the sediment incubations showed the characteristic pore-water chemistry of LDET together with a high abundance of up to 40% of *Desulfobulbaceae* in the anoxic part of the sediment. Fluorescence in situ

hybridization identified up to 5.5-millimeter-long filaments as members of the *Desulfobulbaceae*. These groundwater cable bacteria formed a distinct phylogenetic lineage to previously published cable bacteria with only up to 88% similarity. High resolution field sampling showed a pronounced abundance of *Desulfobulbaceae* at the lower and upper fringe of the contaminant plume.

Surprisingly, cable bacteria were also found in a 1-methylnaphtalene degrading iron-reducing enrichment culture 1MN under anoxic conditions. Temporal monitoring of chemical parameters during growth of 1MN indicated that cable bacteria might catalyze iron reduction via a cryptic sulfur cycle.

High-resolution mass spectrometry revealed that the composition of dissolved organic matter (DOM) is strongly influenced by the prevailing sulfur redox chemistry in a hydrocarbon-contaminated aquifer. DOM scavenges toxic sulfide produced by sulfate-reducing bacteria which might be beneficial for contaminant degradation.

The results from laboratory experiments proofed the presence of cable bacteria and LDET in sediments from a contaminated aquifer. The high abundance of the same *Desulfobulbaceae* in field samples from the upper plume fringe indicated that cable bacteria might indeed be active *in situ* by recycling of electron acceptor sulfate at the plume fringe. The discovery cryptic sulfur cycle mediated by cable bacteria in the iron-reducing 1-methylnaphtalene degrading culture 1MN was the first indication that cable bacteria might actively support contaminant degradation.

Zusammenfassung

In den oberen Schichten organikreicher Sedimente führt der sukzessive Verbrauch von Elektronenakzeptoren zu einer deutlichen Redoxzonierung. In Meeres- und Süßwassersedimenten wurde eine direkte Kopplung von räumlich getrennter Sulfidoxidation und Sauerstoffreduktion durch einen Elektronentransfer über Zentimeter aus biogeochemischen Profilen abgeleitet. Es wird vermutet, dass Kabelbakterien aus der Familie *Desulfobulbaceae* diesen Elektronentransfer über große Distanzen vermitteln, indem sie eine suboxische Zone überbrücken, wo weder Sulfid noch Sauerstoff vorhanden ist.

In mit Kohlenwasserstoffen kontaminierten Grundwasserleitern, wo der biologische Abbau häufig durch eine mangelhafte Verfügbarkeit von Elektronenakzeptoren eingeschränkt ist, finden sich vergleichbar kleinskalige Gradienten. Entsprechend dem „Plume fringe concept“ werden die Elektronenakzeptoren in erster Linie innerhalb einer kleinen Zone an der Grenzfläche der Schadstofffahne abgebaut, wo Elektronendonator und -akzeptor durch dispersive Vermischung zusammentreffen. Kabelbakterien könnten Elektronen aus dem stark reduzierten Bereich im inneren der Schadstofffahne zu Elektronenakzeptoren im unberührten Grundwasser außerhalb der Fahne leiten. Ein Elektronentransfer über diese Redoxgrenzfläche hinweg könnte zu einem Recycling von Elektronenakzeptoren innerhalb der Fahne führen und dadurch den biologischen Abbau beschleunigen.

In dieser Arbeit wurde untersucht, ob ein solcher Elektronentransfer über große Distanzen durch Kabelbakterien in kontaminierten Grundwasserleitern vorkommt und welche möglichen Auswirkungen sich daraus auf die Biogeochemie und den biologischen Schadstoffabbau ergeben. Dafür wurden Sedimente aus einem kontaminierten Standort mit Eisensulfid versetzt, im Labor der Luft ausgesetzt inkubiert, und auf einen Elektronentransfer über große Distanzen durch biogeochemische Messungen untersucht. Grundwasser und Sedimente aus dem selben kontaminierten Standort wurden durch hochaufgelöste Probenahme und Analytik in Hinblick auf die Redoxchemie, die Kontamination und die gelöste Organik untersucht. Proben aus Labor und Feld wurden auf das Vorhandensein von

Kabelbakterien durch Pyrosequenzierung, Bestimmung des mikrobiellen Fingerabdrucks und Fluoreszenz-in-situ-Hybridisierung untersucht.

Nach 2-3 Monaten zeigten die im Labor inkubierten Sedimente die charakteristische Porenwasserchemie eines Elektronentransfers über große Distanzen in Verbindung mit einem starken Auftreten von *Desulfobulbaceae* von bis zu 40%. Durch Fluoreszenz-in-situ-Hybridisierung konnten bis zu 5,5 Millimeter lange Filamente als *Desulfobulbaceae* identifiziert werden. Diese Grundwasserkabelbakterien bildeten, im Vergleich zu bis dahin veröffentlichten Kabelbakterien, eine eigenständige phylogenetische Abstammungslinie mit nur 88% Übereinstimmung. Hochaufgelöste Probennahme im Feld zeigte, dass *Desulfobulbaceae* vor allem an den oberen und unteren Grenzflächen der Schadstofffahne vorhanden waren. Erstaunlicherweise wurden Kabelbakterien auch in der eisenreduzierenden, 1-Methylnaphthalin abbauenden Anreicherungskultur 1MN entdeckt. Eine zeitliche Verfolgung von chemischen Parametern während der Wachstumsphase von 1MN zeigte, dass die Kabelbakterien möglicherweise Eisenreduktion durch einen versteckten Schwefelzyklus katalysieren.

Durch hochaufgelöste Massenspektrometrie stellte sich heraus, dass die Zusammensetzung der gelösten Organik in einem mit Kohlenwasserstoffen kontaminierten Grundwasserleiter stark durch die vorherrschende Schwefelredoxchemie beeinflusst wird. Die gelöste Organik bindet giftiges Sulfid, welches von sulfatreduzierenden Bakterien gebildet wird, und begünstigt dadurch möglicherweise den mikrobiellen Schadstoffabbau.

Durch die Laborergebnisse konnte ein Elektronentransfer über große Distanzen durch Kabelbakterien in Sedimenten aus einem kontaminierten Grundwasserleiter nachgewiesen werden. Das bedeutende Vorkommen der selben *Desulfobulbaceae* in Feldproben aus dem oberen Rand der Schadstofffahne wies darauf hin, dass Kabelbakterien möglicherweise tatsächlich auch *in situ* aktiv sind, indem sie den Elektronenakzeptor Sulfat am Rand der Schadstofffahne recyceln. Die Entdeckung eines versteckten Schwefelzyklus durch Kabelbakterien in der eisenreduzierenden 1-Methylnaphthalin abbauenden Anreicherungskultur 1MN, wies erstmals darauf hin, dass Kabelbakterien möglicherweise aktiv den Schadstoffabbau unterstützen.

Table of Contents

Abstract.....	1
Zusammenfassung.....	3
List of Figures.....	8
List of Tables	10
Abbreviations and Symbols	11
1. Introduction	14
1.1. Microbial Energy Conservation in Aquatic Ecosystems	14
1.2. Biogebattery and Self-potentials	16
1.3. Long-distance Electron Transfer (LDET) in Marine Sediments.....	17
1.3.1 Exploitation of Marine Redox Gradients by Sediment Batteries.....	17
1.3.2 Spatial Decoupling of Redox Half-reactions by LDET.....	18
1.3.3 The Impact of LDET on Biogeochemical Cycling Processes	19
1.4. Evidences for Cable Bacteria as Main Drivers of LDET.....	20
1.4.1 Proliferation and Physiology of Marine Cable Bacteria	22
1.4.2 The Phylogeny of Cable Bacteria	23
1.4.3 Habitats of Cable Bacteria and Occurrence of LDET in Nature	24
1.5. The Plume Fringe Concept.....	26
1.6. LDET and Cable Bacteria in Hydrocarbon-contaminated Aquifers?	27
1.7. Outline of this Thesis	29
1.8. Coordination and Funding	32
2. Materials and Methods.....	33
2.1. The Tar-oil Contaminated Site in Düsseldorf-Flingern	33
2.1.1 Site Description and Sampling.....	33

2.1.2	Solid Phase Extraction of Dissolved Organic Matter (DOM)	34
2.1.3	Direct Analyses of Field Samples	35
2.1.4	Ultrahigh Resolution Mass Spectrometry.....	35
2.2.	Laboratory Sediment Incubations	38
2.2.1	Preparation	38
2.2.2	Column Biogeochemistry.....	38
2.3.	Culture 1MN.....	40
2.3.1	Cultivation.....	40
2.3.2	Growth Experiments with Culture 1MN.....	40
2.3.3	Temporal Monitoring of Chemical Parameters	41
2.3.4	Determination of Solid-phase Mineral Composition	42
2.3.5	Estimation of Nitrate Concentrations	42
2.4.	DNA Extraction and Molecular Methods	43
2.4.1	DNA Extraction from Sediments	43
2.4.2	DNA Extraction from Culture 1MN	43
2.4.3	PCR and Microbial Community Fingerprinting.....	44
2.4.4	Pyrosequencing and Phylogenetic Analyses	44
2.4.5	Fluorescence In Situ Hybridization	45
3.	Results	47
3.1.	LDET and Cable Bacteria in Laboratory Sediment Columns	47
3.2.	Possible LDET at the Capillary Fringe <i>In Situ</i>	51
3.3.	Cable Bacteria Couple Nitrate Reduction to Iron and Sulfur Cycles in Anaerobic Enrichment Culture	53
3.4.	Geochemistry of Dissolved Organic Matter in a Spatially Highly Resolved Groundwater Petroleum Hydrocarbon Plume Cross-Section	62
4.	Discussion	69
4.1.	Long-distance Electron Transfer by Cable Bacteria in Aquifer Sediments.....	69

4.2. Cable Bacteria Couple Nitrate Reduction to Iron and Sulfur Cycles in Anaerobic Enrichment Culture	72
4.3. Geochemistry of Dissolved Organic Matter in a Spatially Highly Resolved Groundwater Petroleum Hydrocarbon Plume Cross-Section	76
5. Conclusions and Outlook.....	78
6. References.....	80
Appendix	94
Publications	102
Authorship Clarification.....	103
Selected Contributions to Scientific Meetings	105
Lebenslauf	106
Acknowledgments.....	107

List of Figures

Figure 1. Characteristic porewater chemistry and geochemical impacts of LDET.....	18
Figure 2. Morphology of cable bacteria.....	21
Figure 3. Phylogenetic tree of cable bacteria.....	24
Figure 4. Concepts of governing redox processes in hydrocarbon-contaminated aquifers.....	27
Figure 5. Schematic vertical cross-section of the Düsseldorf-Flingern aquifer.....	33
Figure 6. Geochemical gradients and microbial community analysis from a representative incubation of sediments taken from the Flingern aquifer.....	48
Figure 7. Microscopy of groundwater cable bacteria.....	49
Figure 8. Phylogeny of groundwater cable bacteria.....	50
Figure 9. Depth profiles of geochemistry of water samples from a high-resolution monitoring well installed in Flingern and of microbial community compositions.....	52
Figure 10. Growth of culture 1MN.....	54
Figure 11. Development of pH values in active incubations of culture 1MN.....	55
Figure 12. X-ray diffraction patterns of freeze-dried matter from the culture bottles of culture 1MN.....	57
Figure 13. Transmission-Fourier transform infrared spectra of the freeze-dried matter from culture 1MN.....	57
Figure 14. Bacterial community composition of culture 1MN and phylogenetic affiliations of bacteria in culture 1MN.....	60

Figure 15. Filaments in culture 1MN.....	61
Figure 16. High-resolution vertical concentration profiles at the Düsseldorf-Flingern site	62
Figure 17. (A) Hierarchical cluster analysis of the assigned (-)ESI FT-ICR-MS derived molecular formulas observed in SPE-DOM	64
Figure 18. (A) (-)ESI and (B) (+)APPI FT-ICR mass spectra.....	65
Figure 19. (A) Hierarchical cluster analysis of the assigned (+)APPI FT-ICR-MS derived molecular formulas observed in SPE-DOM along the aquifer	66
Figure 20. Conceptual model of reactions involved in nitrogen, iron and sulfur cycling in culture 1MN	72
Figure 21. Conceptual model of the impact of LDET by cable bacteria on sulfur cycling and contaminant degradation at the plume fringe.	78

List of Tables

Table 1: Summary of locations and studies of LDET and cable bacteria	25
Table 2: Incubation conditions for the cultivation of the iron-reducing culture 1MN	41
Table 3: Oligonucleotide probes used for FISH.....	45
Table 4: Specificity of probe FlIDSB194	46
Table 5: Geochemical parameters associated with LDET detected in batch incubations.....	47
Table 6: Electron balance of redox reactions in culture 1MN	58
Table 7: Concentrations of O ₂ and HS ⁻ ; and pH values for Figure 6A	94
Table 8: Relative abundances of TRFs for Figure 6B.....	95
Table 9: Chemical composition of groundwater sampled at the Düsseldorf-Flingern site, in 2013, for Figures 9 and 16.....	97
Table 10: Relative abundances of TRFs for Figure 9B.....	98
Table 11: Concentrations of Fe(II), sulfate, sulfide, and nitrate during growth of culture 1MN and in abiotic controls for Figure 10	100
Table 12: Values of pH during growth of culture 1MN for Figure 11	101

Abbreviations and Symbols

Abbreviations

AC	Acenaphthene-5-carboxylic acid
ADMA	4-Amino-N,N-dimethylaniline sulfate
APPI	Atmospheric pressure photoionization
ATR	Attenuated total reflection
BTEX	Benzene, Toluene, Ethylbenzene, Xylene
COC	Cathodic oxygen consumption
DAPI	4',6-Diamidin-2-phenylindol
DOM	Dissolved organic matter
DOU	Diffusive oxygen uptake
ESI	Electrospray ionization
FISH	Fluorescence in situ hybridization
FT-ICR-MS	Fourier transform ion cyclotron resonance mass spectrometry
FTIR	Fourier transform infrared spectroscopy
GC-MS	Gas chromatography–mass spectrometry
LDET	Long-distance electron transfer
MNA	Methylnaphthoic acid
MNMS	Methylnaphthyl-2-methylsuccinic acid
NanoSIMS	Nanoscale secondary ion mass spectrometry
OPD	Oxygen penetration depth
PAHs	Polycyclic aromatic hydrocarbons
PLFA	Phospholipid-derived fatty acids

SIP	Stable isotope probing
SPE-DOM	Solid phase extracted dissolved organic matter
XRD	X-ray diffraction

Symbols

∇	Gradient
c	Concentration
D	Diffusion coefficient
F	Faraday constant
J	Flux
mV	Millivolts
n	Number of charges
R	Gas constant
R	Consumption rate
T	Temperature
t	Time
ϕ	Porosity

1. Introduction

One of the main prerequisites for all forms of life is the capability of energy conservation for maintaining cell function, growth, and reproduction (Hoehler and Jørgensen 2013; Sousa *et al.* 2013; LaRowe and Amend 2015). In dark habitats, such as sediments, soils, caves, and aquifers, organisms solely depend on energy conservation through redox reactions (Borch *et al.* 2009; Schoepp-Cothenet *et al.* 2013; Lower 2014). Unlike animals that require organic carbon as electron donor and oxygen as terminal electron acceptor, the metabolism of prokaryotic microorganisms is much more versatile (Jelen *et al.* 2016). Microbes can use oxidized forms of nitrogen, manganese, iron, sulfur, and carbon as electron acceptors. They are not restricted to organic carbon as electron donor, but can also oxidize reduced inorganic electron donors such as molecular hydrogen, sulfide, reduced iron and manganese, ammonium, and methane. In general, most combinations of electron donors and acceptors are conceivable as long as they are thermodynamically feasible. The amount of energy microbes can conserve from these reactions is given by two factors: The electrochemical potential difference between oxidation and reduction reactions given by the Nernst-equation and the supply with reactants (Rolle *et al.* 2011; McCarty and Criddle 2012; Schüring *et al.* 2013; Lower 2014). A single bacterium needs to have access to both electron donor and electron acceptor (McCarty and Criddle 2012). Such conditions are found at all kinds of chemical interphases – such as marine sediments or the fringes of a groundwater contaminant plume – making them to preferential habitats for microbial life and hotspots of substrate turnover.

1.1. Microbial Energy Conservation in Aquatic Ecosystems

Besides other factors, the redox conditions within a habitat have great influences on microbial community composition and metabolism (Frindte *et al.* 2016; Jelen *et al.* 2016). Generally, there is a trend in redox potential from high values at the earth surface – where molecular oxygen is generated by photosynthesis – towards more negative values over depth (Borch *et al.* 2009; Lower 2014). The transport of oxygen to the subsurface is limited especially in saturated aquatic habitats due to low

oxygen solubility in water. In organic rich sediments and soils, most oxygen is rapidly depleted by respiration during organic matter degradation (Jost *et al.* 2015). Below the upper oxic zone, alternate electron acceptors are depleted subsequently, almost exclusively by bacteria, according to their electrochemical energy yield (Zehnder 1988).

The preferential utilization of high-potential electron acceptors such as oxygen and nitrate leads to the formation of distinct biogeochemical zones (Bethke *et al.* 2011). After the depletion of oxygen and nitrate, dissimilatory iron reduction is followed by sulfate reduction. Here, the predominant process depends on the environmental conditions. At low pH, iron reduction is clearly favored as it exhibits a high redox potential of +0.77 V at pH 0 (Gorski *et al.* 2016). However, the redox potential of iron reduction decreases at neutral and alkaline conditions (Bird *et al.* 2011). Furthermore, ferric iron minerals are virtually not soluble at neutral pH and form iron oxides of different crystallinity with a high variety of redox potentials from around -0.3 V to +0.1 V (Weber *et al.* 2006; Bird *et al.* 2011). Intriguingly, the iron-reducing bacterium *Shewanella oneidensis* MR-1 cannot reduce goethite directly under alkaline conditions but switches to a sulfur-mediated electron shuttling. The bacterium reduces elemental sulfur instead of iron under these conditions (Flynn *et al.* 2014). The product sulfide is a strong reductant which can abiotically reduce highly crystalline iron oxides such as goethite by forming elemental sulfur and ferrous iron. Consequently, sulfate reduction can promote iron reduction at neutral to alkaline pH (Flynn *et al.* 2014; Hansel *et al.* 2015; Choi *et al.* 2016). Such interactions of the iron and sulfur cycles are often overlooked when evaluating the biogeochemistry in natural habitats, as free sulfide is scavenged by precipitation with ferrous iron to FeS and therefore often below detection limit. Therefore, cryptic sulfur cycles driven by iron reduction might be widespread in nature (Holmkvist *et al.* 2011; Hansel *et al.* 2015).

Bacteria developed different strategies to transport electrons to solid electron acceptors, such as iron or manganese oxides. The first one, direct cell contact, needs to be very close and is due to heterogeneous surfaces often difficult to achieve. The second strategy is utilizing extracellular substances such as humic acids or biogenic flavin molecules as electron shuttles (Kappler *et al.* 2004; Marsili

et al. 2008; Klüpfel *et al.* 2014). Bacteria can also use conductive nanowires for a direct extracellular electron transfer to ferric iron, but also to other solid matrices such as electrodes in microbial fuel cells (Reguera *et al.* 2005; Gorby *et al.* 2006). Even though not able to reduce nitrate directly, *Geobacter sulfurreducens* can transfer electrons to nitrate reducing bacteria, such as *Thiobacillus denitrificans*, by interspecies electron transfer through conductive minerals (Kato *et al.* 2012; Shrestha and Rotaru 2014; Reguera 2016). In the absence of electron acceptors, fermentation can take place where organic matter is degraded by functioning as electron donor and electron acceptor at the same time. The subsequent depletion of electron acceptors and the accumulation of reduced products lead to distinct geochemical zonation. A small upper oxic zone, followed by a suboxic zone containing high amounts of dissolved ferrous iron, and a lower sulfidic zone characterized by black ferrous sulfide precipitates and dissolved sulfide. At the boundaries between these zones, re-oxidation can take place by abiotic reactions and chemolithotrophic microbes which are, for example, re-oxidizing ferrous iron with molecular oxygen or nitrate (Melton *et al.* 2014). These re-oxidation reactions are characterized by low energy yields and often limited by transport of either electron acceptors or donors. Nevertheless, this leads to cycling processes at the boundary layers between different redox zone creating niches for specialized microbes (Jost and Pollehne 2012).

1.2. Biogeobattery and Self-potentials

A plenty of different microbial habitats exist at redox interphases where highly oxidized and highly reduced layers are close to each other separated by steep redox gradients. Sato and Mooney proposed the concept of a geobattery where a conductive ore body is connecting reduced and oxidized zones (Sato and Mooney 1960). Microbes at the lower part of the ore oxidize reduced sulfur minerals by using the ore body as electron acceptor. However, the ore body is not reduced itself, but the electrons are conducted to the oxidized zone at the upper part. There, distinct microbes take up the electrons to reduce molecular oxygen to water. This spatial segregation of redox half-reactions is in accordance with a battery where anodic oxidation couples with cathodic reduction by an electric current through a conductor

(Bigalke and Grabner 1997). Such geobatteries would enable microbes to shortcut the classical redox ladder, as electrons are directly conducted from a low potential electron donor to the high potential electron acceptor oxygen in the absence of energy and transport limited intermediate reactions. The electric current through the conductor creates strong electric potentials which are often referred to as self-potentials in literature (Sato and Mooney 1960; Bigalke and Grabner 1997; Revil *et al.* 2010). Electric potential signals of several hundred millivolts have been reported from contaminated aquifers at the Entressen landfill (Naudet *et al.* 2003; Naudet *et al.* 2004) and the Berre site (Revil *et al.* 2010) both located in the south of France. The electric potentials of -160 mV at the oil-contaminated Berre site are remarkable as they are directly related to biodegradation of oil in the absence of any known electrical conductors, such as pipes.

In the absence of an electric conductor between anode and cathode the concept of a geobattery can be developed further to the concept of a biogeobattery. In a biogeobattery, microbes are mediating the electron transport either by a conductive network of bacteria and minerals or by a conductive network of bacteria which are interconnected by conductive pili or nanowires (Revil *et al.* 2010).

1.3. Long-distance Electron Transfer (LDET) in Marine Sediments

1.3.1 Exploitation of Marine Redox Gradients by Sediment Batteries

In marine sediments, steep redox gradients form at the water-sediment interphase where oxic seawater infiltrates highly reduced sediments rich in organic carbon. These differences in redox potentials can be exploited by a sediment battery for electric energy generation by connecting an anode in the lower reduced sulfidic zone to a cathode at the oxic sediment surface (Reimers *et al.* 2001; Tender *et al.* 2002). This so-called sediment battery is in principle an artificial marine geobattery. In such settings, distinct microbes catalyze anodic oxidation as well as cathodic reduction reactions. The microbial community at the anode is often enriched in *deltaproteobacterial Geobacter* and *Desulfobulbaceae* in sediment batteries, but also in laboratory microbial fuel cells (Holmes *et al.* 2004a; Ryckelynck *et al.* 2005). The *Desulfobulbaceae* might oxidize elemental sulfur to sulfate using the anode as electron acceptor as proposed for *Desulfobulbus propionicus* (Holmes *et al.* 2004b).

Nevertheless, sediment batteries as well as microbial fuel cells require an electric conductor between anode and cathode.

1.3.2 Spatial Decoupling of Redox Half-reactions by LDET

Recently, electric currents have been inferred from biogeochemical profiles in marine sediment cores (Nielsen *et al.* 2010; Risgaard-Petersen *et al.* 2012; Meysman *et al.* 2015). Sulfidic sediment cores from Aarhus bay, Denmark, incubated for one month with overlying oxic seawater showed a spatial separation of a thin oxic zone at the sediment surface, followed by a suboxic zone of about 1.5 cm, and a lower sulfidic zone. In parallel to the development of the suboxic zone, a distinct pH profile developed in the sediment cores from Aarhus Bay: A pH maximum in the oxic zone followed by a sharp drop over depth towards a pH minimum at the transition between suboxic and sulfidic zone (Nielsen *et al.* 2010) (Figure 1A).

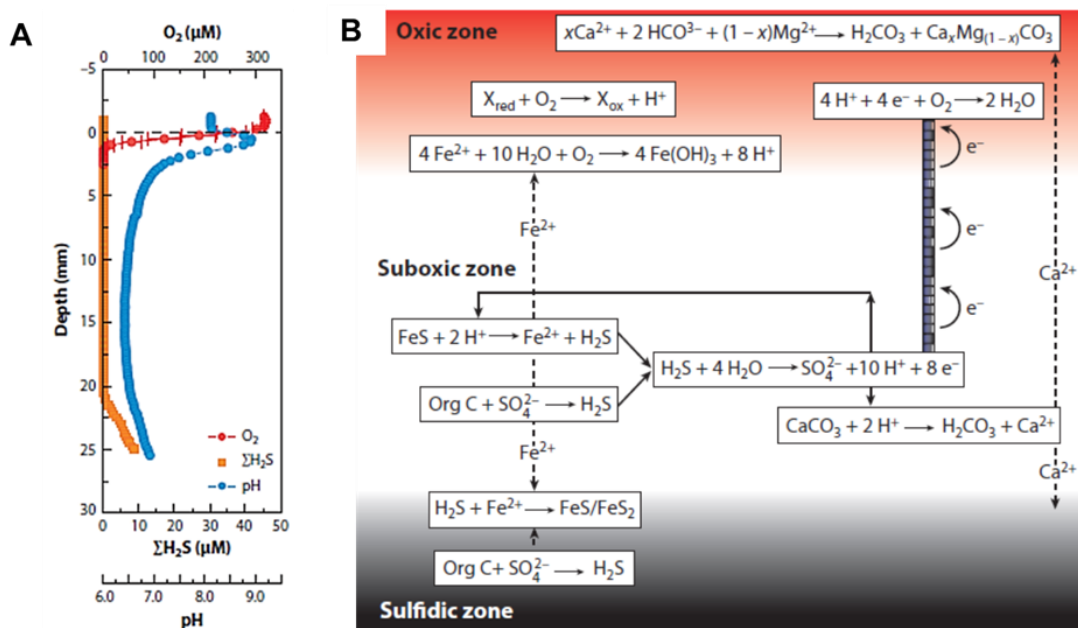


Figure 1. Characteristic porewater chemistry and geochemical impacts of LDET in marine sulfidic sediment cores incubated with overlying oxic sea water. **A)** Depth profile of pH, oxygen, and sulfide measured by microsensors. **B)** Impacts of LDET on the sediment geochemistry and proposed reactions (Nielsen and Risgaard-Petersen 2015)

Since all relevant reactions involving oxygen would be neutral or decrease the pH (Osburn *et al.* 2014), this observation can only be explained by a direct coupling of spatially segregated proton-consuming oxygen reduction and proton-producing sulfide oxidation half-reactions (Meysman *et al.* 2015). This coupling was reflected

by a rapid response of the sulfidic zone to alternating oxygen concentrations in the overlying seawater. As diffusion alone could not explain such rapid response, the sulfidic and the oxic zone must have been directly connected by an electric current over centimeter distances (Nielsen *et al.* 2010). This was supported by the observation of a constant electric field of a few mV cm⁻¹ throughout the suboxic zone inferred from electric potential measurements (Risgaard-Petersen *et al.* 2012; Damgaard *et al.* 2014; Risgaard-Petersen *et al.* 2014).

1.3.3 The Impact of LDET on Biogeochemical Cycling Processes

As up to 82% of the oxygen diffusing into the sediment is used for cathodic oxygen consumption, LDET has a high impact on all benthic processes at the sediment water interphase (Risgaard-Petersen *et al.* 2014; Nielsen and Risgaard-Petersen 2015). Sulfide is oxidized to sulfate by the anodic reaction leading to acidification of the pore water. The free protons – more precise hydroxonium ions – then dissolve ferrous sulfide precipitates leading to sulfide production as well as liberation of aqueous Fe²⁺ (Risgaard-Petersen *et al.* 2012). The stoichiometry of anodic sulfide oxidation coupled to FeS dissolution suggests a surplus of protons leading to acidification. Under certain conditions, even a net production of dissolved sulfide by anodic sulfide oxidation might be possible (Nielsen and Risgaard-Petersen 2015). The decrease in pH is partially buffered by dissolution of CaCO₃ and MgCO₃ which releases Ca²⁺ and Mg²⁺ ions. These cations are transported – together with Fe²⁺ – along the electric fields towards the cathode in the oxic zone balancing the flux of negatively charged electrons through LDET. This enhanced diffusion can be described mathematically by the macroscopic Nernst-Planck equation (Risgaard-Petersen *et al.* 2012):

$$J = -\phi D_s (\nabla C + (\pm 1) \frac{nf}{RT} C \nabla \psi) \quad (1)$$

Where J denotes the flux of the individual ionic species, ϕ the porosity, D_s the diffusion coefficient for ions in sediment, ∇C the concentration gradient, $\nabla \psi$ the electrostatic potential gradient, n the number of charges, f the Faraday constant, R the gas constant, and T the temperature.

The alkaline conditions in the oxic zone as well as the release of Fe²⁺ from the suboxic zone promote iron oxidation – visible by red crust formation of iron oxides

near the sediment surface. This pronounced iron oxide layer forms a reactive barrier after the breakdown of LDET. Upwelling sulfide is scavenged by reductive dissolution of ferric oxides and precipitation as ferrous sulfides in the upper layers of the sediment. This might explain why euxinia, i.e. the release of toxic sulfide from the sediment into the water column, is only rarely observed in marine sediments (Seitaj *et al.* 2015; Sulu-Gambari *et al.* 2016; Nielsen 2016; Sulu-Gambari *et al.* 2016). The top-layer iron oxides can also trap phosphates that are liberated from the lower sediments preventing their release into the water column (Sulu-Gambari *et al.* 2016).

In parallel, cathodic alkalinity production by LDET is buffered by CaCO_3 and MgCO_3 precipitation (Risgaard-Petersen *et al.* 2012). Microbial carbonate precipitation in marine sediments has been so far mainly attributed to photosynthetic cyanobacteria (Zhu and Dittrich 2016).

In contrast, the electric field causes lower fluxes of negatively charged ions, such as sulfate, towards the sediment surface as would be expected from diffusion alone. This could lead to an overestimation of sulfate fluxes by up to 50% (Risgaard-Petersen *et al.* 2012). The transport of cations and anions does not balance the electric field completely as otherwise no electric field would be detectable (Nielsen 2016).

1.4. Evidences for Cable Bacteria as Main Drivers of LDET

Long filamentous bacteria of the family *Desulfobulbaceae* are supposed to mediate this LDET by bridging the suboxic zone where neither oxygen nor sulfide is detectable. A single filament of these so-called “cable bacteria” is composed of thousands of individual cells characterized by a shared envelope with 15 to 58 marked ridges giving them a cable-like appearance (Pfeffer *et al.* 2012; Malkin *et al.* 2014). Periplasmic strings underneath the ridges might serve as electric conductors with the common outer membrane as isolation (Pfeffer *et al.* 2012; Malkin *et al.* 2014; Schauer *et al.* 2014; Meysman *et al.* 2015) (Figure 2).

Cutting the sediment beneath the oxic zone with a small tungsten wire led to an immediate breakdown of the electric potential signal within hours. The pH peak in

the oxic zone was less pronounced after one hour and disappeared completely one day after cutting. At the same time, oxygen and sulfide consumption declined reflected by deeper oxygen penetration into the sediment and upward diffusion of sulfide towards the oxic zone (Pfeffer *et al.* 2012; Vasquez-Cardenas *et al.* 2015).

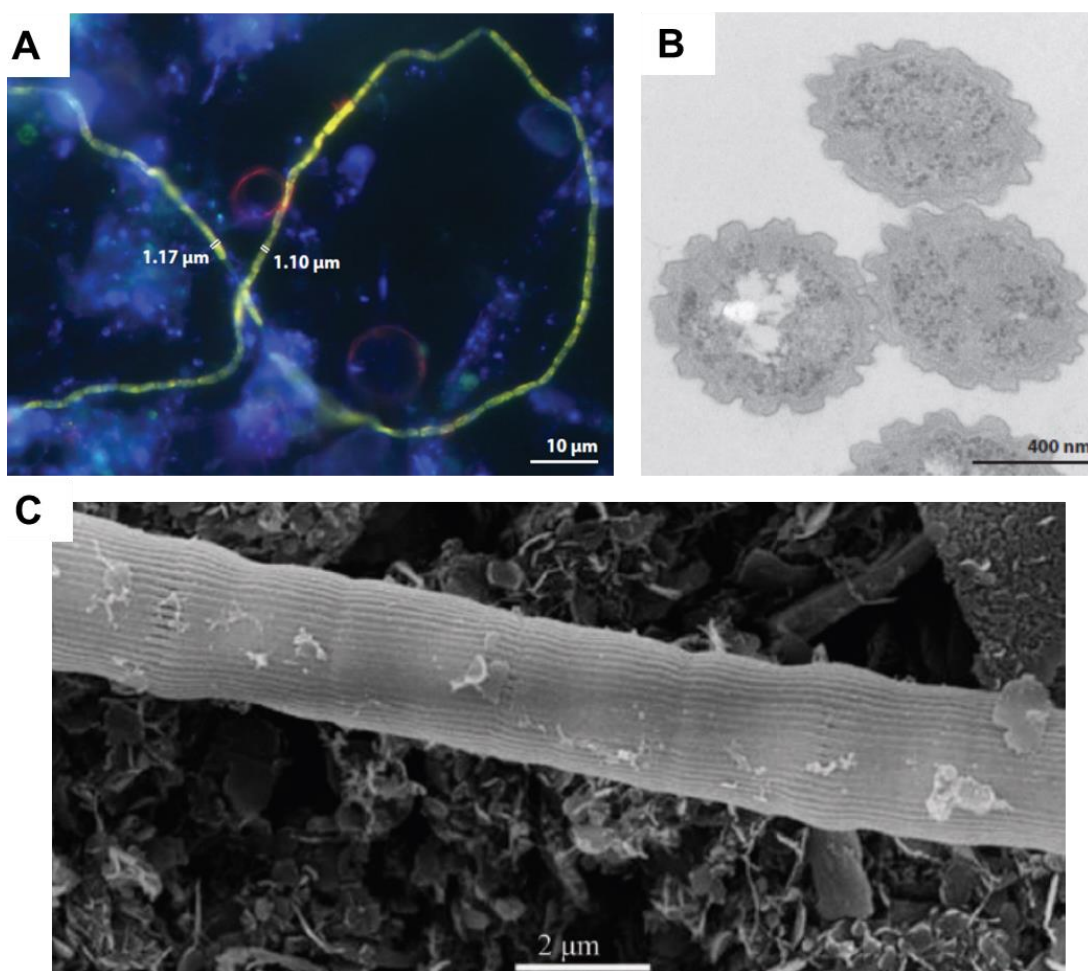


Figure 2. Morphology of cable bacteria. **A)** Identification of cable bacteria by FISH with probes DSB706 specific for *Desulfobulbaceae* and probe ELF654 specific for cable bacteria (Nielsen and Risgaard-Petersen 2015). **B)** Transmission electron microscopy of a filament cross-section (Nielsen and Risgaard-Petersen 2015). **C)** Characteristic cell envelope of cable bacteria with strings and ridges visualized by scanning electron microscopy (Malkin *et al.* 2014).

Besides oxygen, cable bacteria can also use nitrate as terminal electron acceptor. Sediments incubated with nitrate in the overlying sea water in the absence of oxygen also showed a characteristic pore water chemistry that can only be explained by a LDET. Nitrate and oxygen reducing cable bacteria cannot be distinguished by

phylogeny as they all cluster in the same monophyletic group based on sequencing of the 16S rRNA gene (Marzocchi *et al.* 2014).

Intriguingly, cable bacteria show active chemo-tactical movement by gliding motility on surfaces of $0.5 \mu\text{m s}^{-1} \pm 0.3 \mu\text{m s}^{-1}$ to orient themselves between the oxic and sulfidic zone. Frequently, cable bacteria are moving in loops at one end and often two cables closely associate by swirling around each other (Bjerg *et al.* 2016).

1.4.1 Proliferation and Physiology of Marine Cable Bacteria

Temporal monitoring by fluorescence in situ hybridization (FISH) of cable bacteria density in laboratory incubations with sediments from Aarhus Bay suggested a doubling time of 20 h. After 21 days, when the characteristic porewater chemistry of LDET had fully established, the filament density peaked at more than 2 km filaments below each cm^2 sediment (Schauer *et al.* 2014).

However, the filament density as well as the signal for LDET declined towards the end of the experiment on day 53 (Schauer *et al.* 2014). In a different study with sediments from the marine Lake Grevelingen (The Netherlands), a complete breakdown of the geochemical fingerprint of LDET was observed after 71 days of incubation (Rao *et al.* 2016). This collapse might be attributed to the depletion of the ferrous sulfide pool in the suboxic zone (Schauer *et al.* 2014; Rao *et al.* 2016).

The filament diameter in the sediment cores widely varied from 0.6 to 1.3 μm with a general trend to a raise in average cable-width towards the end of the experiment. Cable bacteria showed continuous cell divisions over the whole length of the filaments, not restricted to zones where either electron donor or electron acceptor was present (Schauer *et al.* 2014).

Consequently, the question arose what individual cells within the cable are living from. Following cable proliferation with labelled propionate by nanoscale secondary ion mass spectrometry (NanoSIMS) and phospholipid-derived fatty acids stable isotope probing (PLFA-SIP) indicated heterotrophic propionate incorporation and a fraction of 20% bicarbonate uptake for anaplerotic reactions. PLFA-SIP indicated that only a minor fraction (2%) of propionate was respired, whereas most was directly incorporated into the cell membrane. This pointed to a

chemolithoheterotrophic growth of cable bacteria. However, in the presence of LDET, sediments often exhibit fixation rates of inorganic carbon which cannot be explained by cable bacteria alone. Sequencing of sediment cDNA of 16S rRNA genes showed a high abundance of chemolithoautotrophic sulfide-oxidizing Gamma- and Epsilonproteobacteria in the oxic and suboxic zones. The nature of interactions between cable bacteria and chemolithoautotrophs is so far unresolved (Vasquez-Cardenas *et al.* 2015).

1.4.2 The Phylogeny of Cable Bacteria

Cable bacteria can be defined as long filamentous bacteria in sediments exhibiting the characteristic biogeochemistry of LDET. Hitherto, all cable bacteria are affiliated to the family *Desulfobulbaceae* within the Deltaproteobacteria based on 16S rRNA gene sequencing. They form a monophyletic group next to the genus *Desulfobulbus* showing 88.6% to 92.2% similarity to *Desulfobulbus mediterraneus* 86FS1 and 88.6% to 91.4% similarity to *Desulfobulbus propionicus* DSM 2023 (Figure 3).

16S rRNA gene sequences of cable bacteria can be grouped by similarity into 6 distinct clusters. This led to the proposal of two new genera: *Candidatus Electrothrix* and *Candidatus Electronema*. *Ca. Electrothrix* mostly originates from marine habitats. Based on 16S rRNA and *dsrAB* – coding for dissimilatory sulfite reductase – gene sequences, four candidate species were proposed: *Ca. E. marina*, *E. aarhusiense*, *E. communis*, and *E. japonica*. In contrast, sequences of *Electronema* are mostly found in freshwater habitats and cluster in two proposed candidate species: *Ca. E. nielsenii*, and *E. palustris* (Trojan *et al.* 2016) (Figure 3).

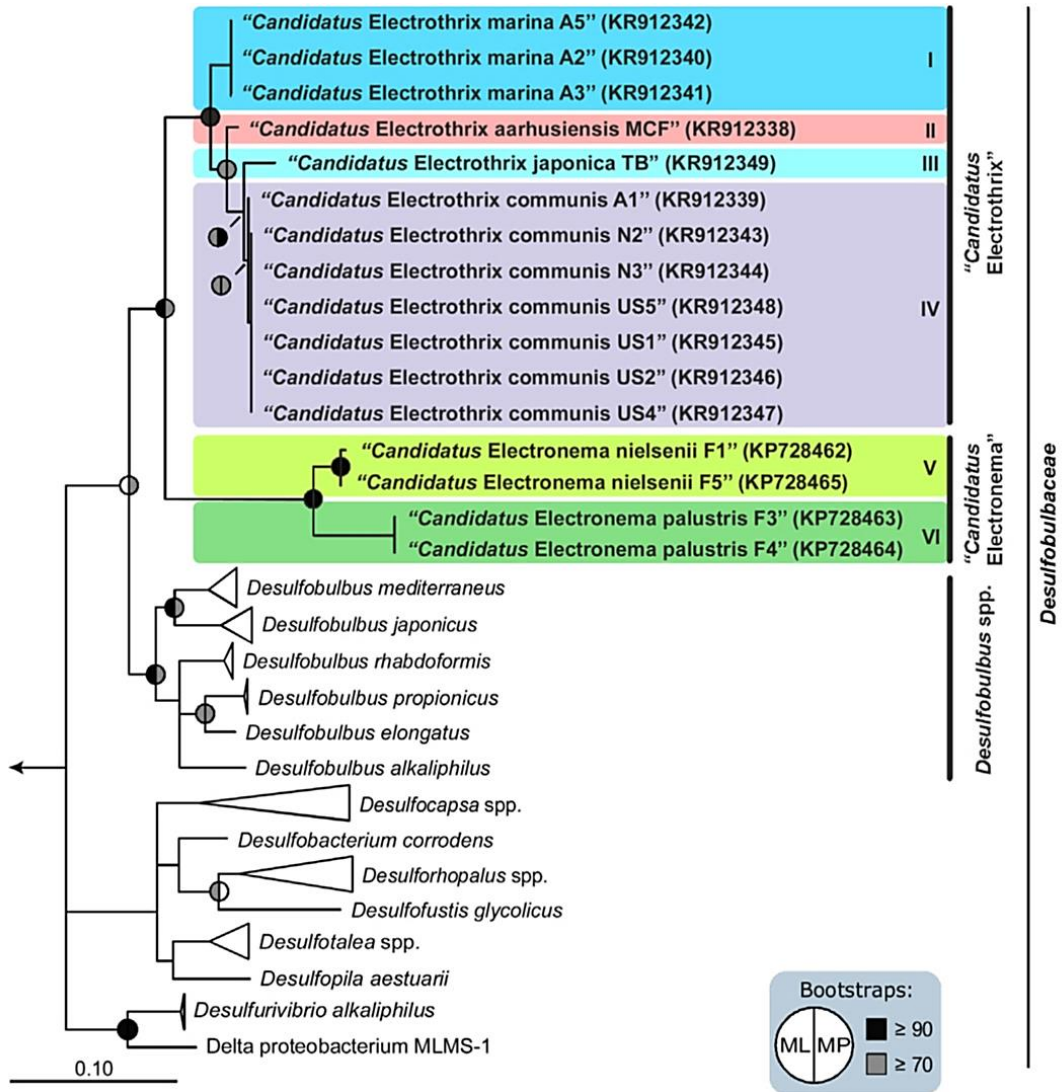


Figure 3. Phylogenetic tree of cable bacteria based on full-length 16S rRNA gene sequences containing the two proposed candidate genera for Electrothrix and Electronema and the six identified candidate species marked with different shadings (Trojan *et al.* 2016).

1.4.3 Habitats of Cable Bacteria and Occurrence of LDET in Nature

Since the discovery of LDET by cable bacteria in marine sediments from Aarhus Bay, numerous studies have been conducted to uncover the global distribution of cable bacteria and LDET (Table 1). Cable bacteria and the LDET were mainly detected in marine sediments and salt marshes during laboratory incubations and *in situ* (Table 1).

Table 1: Summary of locations and studies of LDET and cable bacteria

Location	Habitat	Detection	References
Aarhus harbor, Denmark	Marine	Laboratory	(Nielsen <i>et al.</i> 2010; Risgaard-Petersen <i>et al.</i> 2012; Damgaard <i>et al.</i> 2014; Risgaard-Petersen <i>et al.</i> 2014; Bjerg <i>et al.</i> 2016)
Aarhus Bay, Denmark	Marine	Laboratory	(Nielsen <i>et al.</i> 2010; Pfeffer <i>et al.</i> 2012; Marzocchi <i>et al.</i> 2014; Schauer <i>et al.</i> 2014)
Coastal Zone, Belgium	Marine	<i>In situ</i>	(Malkin <i>et al.</i> 2014)
Salt Marsh, The Netherlands	Salt marsh	<i>In situ</i> , laboratory	(Malkin and Meysman 2014; Malkin <i>et al.</i> 2014)
Lake Grevelingen, The Netherlands	Marine lake	<i>In situ</i> , laboratory	(Malkin <i>et al.</i> 2014; Rao <i>et al.</i> 2015; Seitaj <i>et al.</i> 2015; Sulu-Gambari <i>et al.</i> 2016; Vasquez-Cardenas <i>et al.</i> 2015; Sulu-Gambari <i>et al.</i> 2016)
New England, USA	Salt marsh	Laboratory	(Larsen <i>et al.</i> 2014)
St. Lawrence Estuary, Canada	Salt marsh	<i>In situ</i>	(Rao <i>et al.</i> 2016)
Freshwater stream, Denmark	Freshwater	Laboratory, <i>In situ</i>	(Risgaard-Petersen <i>et al.</i> 2015)
Mangrove forest, Australia	Mangrove	Laboratory, <i>In situ</i>	(Burdorf <i>et al.</i> 2016)
Southern Mariana Trough	Deep-sea sulfide chimney	-	(Kato and Yamagishi 2016)

Recently, cable bacteria together with the characteristic signal of LDET were also found in sediments of a freshwater stream in Denmark (Risgaard-Petersen *et al.* 2015). So far, all habitats of cable bacteria documented in literature are saturated, organic- and sulfate-rich sediments close to the surface.

Hitherto, nothing is known about the abundance of cable bacteria in deeper and more oligotrophic subsurface habitats, such as aquifers.

1.5. The Plume Fringe Concept

In many hydrocarbon-contaminated aquifers excess loads toxic pollutants enter a complex and highly-vulnerable ecosystem (Griebler and Lueders 2009). There, the contaminants are transported along with the groundwater flow forming a horizontal plume (Wiedemeier 1999). Microbes are capable of removing the contaminants by biodegradation during which the contaminant itself can function as electron donor and carbon source for microbial growth (Fuchs *et al.* 2011; Fahrenfeld *et al.* 2014).

However, in most cases biodegradation is hampered by a deficient availability of electron acceptors that are rapidly depleted and only slowly replenished in the aquifer (Christensen *et al.* 1994; Meckenstock *et al.* 2015).

Originally, it was suggested that under such conditions electron acceptors are subsequently depleted along the plume leading to a distinct redox zonation driven by thermodynamics (Chapelle 2000; Christensen *et al.* 2000) (Figure 4A).

However, several studies over the last decades indicated that biodegradation is mainly restricted to a narrow layer at the fringes of the contaminant plume where electron donors and acceptors encounter via dispersive mixing and diffusion (Cirpka *et al.* 2012). The inner plume core is often highly reduced allowing only for limited biodegradation by reduction of solid metal oxides or by fermentation coupled to syntrophic methanogenesis (Cirpka *et al.* 1999; Mayer *et al.* 2001; Thornton *et al.* 2001; Maier and Grathwohl 2006; Anneser *et al.* 2008; Bauer *et al.* 2008; Winderl *et al.* 2008; Meckenstock *et al.* 2015) (Figure 4). As the oxidation half reaction is not limiting in the presence of excess loads of organics, also a simultaneous reduction of different electron acceptors might occur at the plume fringes (Meckenstock *et al.* 2015).

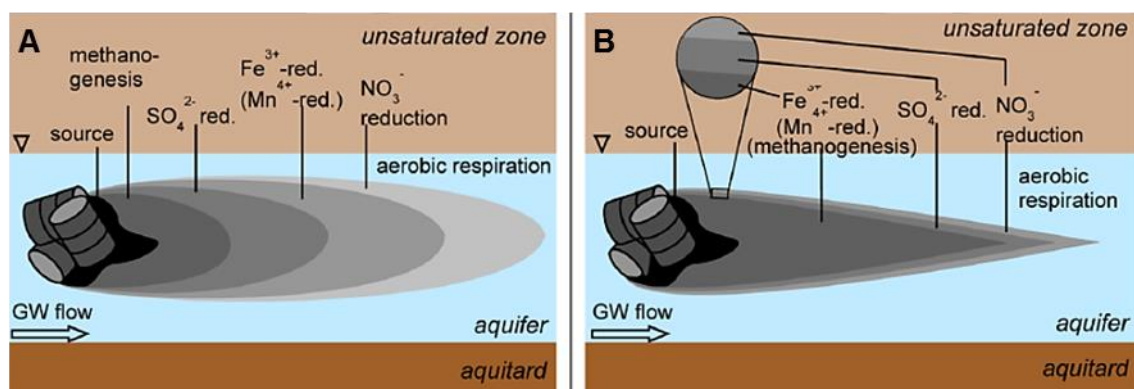


Figure 4. Concepts of governing redox processes in hydrocarbon-contaminated aquifers. **A)** Classical concept of a subsequent depletion of electron acceptors driven by thermodynamics. **B)** The plume fringe concept with predominant microbial biodegradation at the plume fringes (Meckenstock *et al.* 2015).

1.6. LDET and Cable Bacteria in Hydrocarbon-contaminated Aquifers?

High-resolution groundwater sampling and analyses at a tar-oil-contaminated site in Düsseldorf revealed that biogeochemical gradients at the plume fringes are much steeper and more pronounced than assumed from regular sampling campaigns (Anneser *et al.* 2008). The extent of the plume fringes is only in the centimeter to decimeter scale and might be even lower at higher resolution (Anneser *et al.* 2008).

Sequencing of 16S rRNA genes of sediment DNA from the same site showed a high abundance of different members of the family *Desulfobulbaceae*. (Winderl *et al.* 2008; Pilloni *et al.* 2011).

Furthermore, strong electric potentials in contaminated aquifers are reported in literature (Naudet *et al.* 2003; Naudet *et al.* 2004; Revil *et al.* 2010; Forté and Bentley 2013).

The small spatial scales of redox gradients at the plume fringes, the high abundance of *Desulfobulbaceae*, and the electric potentials reported in literature might indicate the presence of long-distance electron transfer (LDET) in aquifers upon contamination. In such settings, cable bacteria might overcome electron acceptor limitation by coupling sulfide oxidation insight the plume to reduction of electron acceptors, such as oxygen and nitrate, at the plume fringes by LDET.

The detection of LDET in contaminated aquifers could expand the knowledge about ongoing redox processes at the capillary fringe and might have huge implications on contaminant degradation and bioremediation.

Thus, the central research question of thesis was:

“Does LDET by cable bacteria naturally occur in contaminated aquifers and what are its impacts on contaminant degradation and groundwater biogeochemistry?”

I hypothesized that

- I. LDET by cable bacteria is present in aquifers upon contamination.
- II. LDET has a large impact on the biogeochemistry at the plume fringe.
- III. Electron acceptor sulfate is recycled by LDET which enhances contaminant degradation by specialized sulfate-reducing microbes.

The major aims of this thesis were:

- I. Detection of LDET in laboratory experiments with sediments from the tar oil contaminated aquifer in Düsseldorf.
- II. Search for evidences of LDET *in situ* by high-resolution sampling and analyses of groundwater and aquifer sediments.
- III. Evaluation of potential impacts of LDET on the biogeochemistry and contaminant degradation in contaminated aquifers.

1.7. Outline of this Thesis

I) Long-distance electron transfer by cable bacteria in aquifer sediments (Chapters 3.1, 3.2, 4.1)

The biodegradation of organic pollutants in aquifers is often restricted to the fringes of contaminant plumes where steep counter gradients of electron donors and acceptors are separated by limited dispersive mixing. However, long-distance electron transfer (LDET) by filamentous “cable bacteria” has recently been discovered in marine sediments to couple spatially separated redox half reactions over centimeter scales. Here, I provide primary evidence that such sulfur oxidizing cable bacteria can also be found at oxic-anoxic interfaces in aquifer sediments, where they provide a means for the direct recycling of sulfate by electron transfer over 1-2 cm distance. Sediments were taken from a hydrocarbon-contaminated aquifer, amended with iron sulfide, and saturated with water leaving the sediment surface exposed to air. Steep geochemical gradients developed in the upper 3 cm showing a spatial separation of oxygen and sulfide by 9 mm together with a pH profile characteristic for LDET. Bacterial filaments which were highly abundant in the suboxic zone were identified by sequencing of 16S rRNA genes and fluorescence in situ hybridization (FISH) as cable bacteria belonging to the *Desulfobulbaceae*. The detection of similar *Desulfobulbaceae* at the oxic-anoxic interface of fresh sediment cores taken at a contaminated aquifer suggests that LDET may indeed be active at the capillary fringe *in situ*. I propose that long-distance electron transport by sulfur oxidizing cable bacteria could increase the flux of electron acceptors at plume fringes and thereby might enhance contaminant biodegradation (Müller *et al.* 2016).

II) Cable bacteria couple nitrate reduction to iron and sulfur cycles in anaerobic enrichment culture (Chapters 3.3, 4.2)

Filamentous cable bacteria of the family *Desulfobulbaceae* couple spatially-separated sulfur oxidation and oxygen or nitrate reduction by a long-distance electron transfer over centimeter distances in marine sediments, freshwater streams, and contaminated aquifers. However, the function of closely related *Desulfobulbaceae* in habitats with high rates of iron reduction is presently unknown. Here, I report on the surprising detection of cable bacteria in an iron-reducing, 1-methylnaphthalene-degrading enrichment culture (1MN) and on the elucidation of their function in such habitats. Culture 1MN was grown in the presence of 1-methylnaphthalene, elemental sulfur, and FeS each with ferrihydrite and nitrate as electron acceptors in anoxic groundwater medium initially reduced with 0.3 to 2 mM sulfide. The microbial community composition was evaluated by T-RFLP, 454 pyrosequencing, and fluorescence in situ hybridization (FISH). Culture 1MN was capable of growing not only with 1-methylnaphthalene, but also with elemental sulfur and FeS as electron donor. This was accompanied with an increase of the *Desulfobulbaceae* abundance up to 95% providing strong evidence that *Desulfobulbaceae* are involved in sulfur cycling in culture 1MN. Fluorescence in situ hybridization revealed the presence of *Desulfobulbaceae* as filaments of several hundred micrometers length. These cable bacteria might catalyze iron reduction in 1MN by a cryptic sulfur cycle involving sulfur disproportionation, abiotic ferrihydrite reduction, and FeS oxidation with nitrate as electron acceptor.

III) Geochemistry of Dissolved Organic Matter in a Spatially Highly Resolved Groundwater Petroleum Hydrocarbon Plume Cross-Section (Chapters 3.4, 4.3)

This work is based on parts of the published manuscript from Sabine Dvorski (Dvorski *et al.* 2016) which the doctoral candidate co-authored. The contributions of the doctoral candidate are listed in detail in the authorship clarifications.

At numerous groundwater sites worldwide, natural dissolved organic matter (DOM) is quantitatively complemented with petroleum hydrocarbons. To date, research has been focused almost exclusively on the contaminants, but detailed insights of the interaction of contaminant biodegradation, dominant redox processes, and interactions with natural DOM are missing.

Here, high-resolution groundwater sampling at the tar oil contaminated site in Düsseldorf-Flingern was combined with high-resolution characterization of DOM by Electrospray- and atmospheric pressure photoionization (ESI, APPI) ultrahigh resolution mass spectrometry (FT-ICR-MS).

The composition of DOM appeared to be strongly influenced by the redox conditions across the vertical transect of the aquifer. At the upper part of the aquifer where the BTEX and naphthalene plume was located, the DOM composition and steep redox gradients followed congruent trends. There, the distinct sulfur chemistry strongly affected the DOM composition reflected by elevated concentrations of sulfur organic molecules.

1.8. Coordination and Funding

This thesis was conducted at the Institute of Groundwater Ecology (IGOE) of the Helmholtz Zentrum München (HMGU) in the frame of the Helmholtz WasserZentrum München (HWZM). This interdisciplinary platform of the HMGU, TU München, University of Tübingen, and University of Bayreuth investigated solute fluxes in regional water cycles. Its major aim was to expand the current knowledge of how groundwater quality is influenced by dynamic conditions and how to maintain good water quality.

2. Materials and Methods

2.1. The Tar-oil Contaminated Site in Düsseldorf-Flingern

2.1.1 Site Description and Sampling

Sediment was sampled from a tar-oil contaminated aquifer at a former coal gasification plant in Düsseldorf-Flingern, Germany (51°13'20.9"N 6°49'05.6"E). The site holds rather homogeneous quaternary sediment containing medium fine sand with grain sizes between 0.2-0.7 mm, a porosity of 0.34, and total organic carbon concentrations (TOC) of 0.2 to 0.6% (dry weight) (Anneser *et al.* 2008; Anneser *et al.* 2010). The aquifer is contaminated by a mixture of mono- and polycyclic aromatic hydrocarbons.

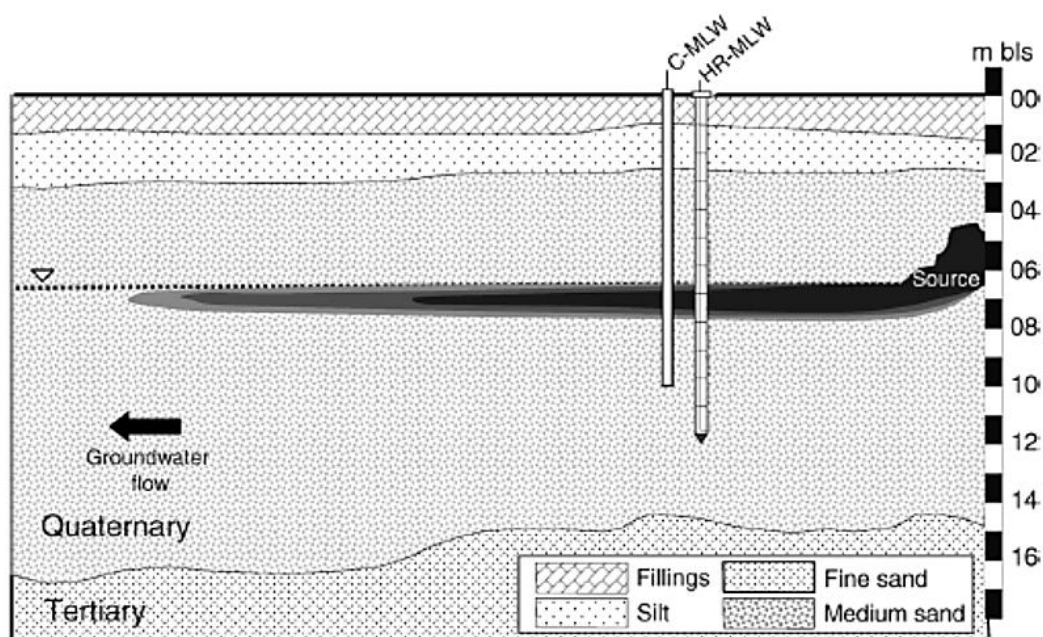


Figure 5. Schematic vertical cross-section of the Düsseldorf-Flingern aquifer. C-MLW: Conventional multi-level well; HR-MLW: High-resolution multi-level well (Anneser *et al.* 2008)

Reduced inorganic sulfur varied in a previous study between 0.6 and 15.6 $\mu\text{mol g}^{-1}$ (Anneser *et al.* 2010). The groundwater table was located at ~6.5 m below surface in 2013, but previous measurements between 2006 and 2009 indicated a dynamic groundwater table with fluctuations of up to 20 cm per year (Einsiedl *et al.* 2015). A high-resolution multi-level monitoring well has been installed previously, allowing for

groundwater sampling at 3 cm vertical resolution (Anneser *et al.* 2008) (Figure 5). Redox gradients and sediment microorganisms within the hydrocarbon plume were characterized in detail, previously (Schmitt *et al.* 1996; Anneser *et al.* 2008; Winderl *et al.* 2008; Pilloni *et al.* 2011).

For the present study, sediment samples were taken in September 2008 for incubation experiments in the laboratory and September 2013 for high resolution community profiling. Core liners of one meter each were retrieved over depths from 6 to 11 m below surface by hollow-stem auger drilling. The liners were opened by cutting with an angle grinder in the field under argon atmosphere in order to minimize oxygen exposure. Sediment subsamples (~10 g each) were sampled at 3 to 10 cm resolution from the liners in 2013 and stored at -20° C for later DNA extraction. Additionally, sediments of different depths were transferred to sterile anoxic tap water which was autoclaved under nitrogen atmosphere at 121°C for 20 min. The sediments were stored at 12° C under nitrogen for later batch experiments in the laboratory. For fluorescence in situ hybridization (FISH), sediments were sampled in 2013 from 10 cm above to 10 cm below groundwater table. Aliquots of 0.5 g sediment were taken in one-centimeter resolution along the core, directly transferred to either 4% paraformaldehyde or 2.5% glutardialdehyde, and stored at 4° C.

Groundwater was sampled in 3 cm resolution from the previously installed high-resolution multi-level well via steel capillaries connected to multi-channel peristaltic pumps (Anneser *et al.* 2008). The retrieved groundwater from each depth was subsampled in the field and treated for chemical analyses on site.

2.1.2 Solid Phase Extraction of Dissolved Organic Matter (DOM)

Dissolved organic matter (DOM) from 0.2 µm filtered 250 mL and 1 L groundwater samples was isolated by an established solid phase extraction (SPE) method (Dittmar *et al.* 2008). Briefly, the water samples (250 mL and 1 L) were acidified to pH 2 with hydrochloric acid (32%, p.a., Merck KGaA, Darmstadt, Germany) and passed through Agilent Bond Elut PPL SPE cartridges (100 mg and 500 mg with a flowrate of <4 mL min⁻¹ and <10 mL min⁻¹, respectively). To prevent loss of organics caused by overloading of the first SPE cartridge, a second cartridge was attached below the first one. Then, the cartridges were rinsed with acidified (pH 2) purified

water (MilliQ-Integral, Merck KGaA, Darmstadt, Germany) and dried under vacuum. The DOM was eluted with 2 mL (100 mg PPL cartridges) and 10 mL (500 mg PPL cartridges) methanol (Chromasolv® LC-MS grade methanol, Sigma Aldrich, Taufkirchen, Germany), respectively.

2.1.3 Direct Analyses of Field Samples

For dissolved sulfide analyses, 200 µl of sample were fixed in 1 ml of 2% (w/v) Zn-acetate solution. Sulfide concentrations were determined within 3 hours after sampling, following the protocol of Cline (Cline 1969).

Fe(II) concentrations of groundwater samples were measured by the ferrozine assay (Stookey 1970) as previously described (Anneser *et al.* 2008). Toluene was measured by headspace analysis on a GC-MS (Thermo Electron, Dreieich, Germany) as previously described (Anneser *et al.* 2008). Redox potentials were measured in the field directly after sampling with field redox electrodes (SenTix, WTW, Weilheim, Germany). Concentrations of nitrate and sulfate of field samples were measured by ion chromatography (Dionex DC-100, Idstein, Germany) as previously described (Anneser *et al.* 2008).

Intracellular ATP concentration of aquifer microbes was determined as proxy for viable microbial biomass in water and sediment samples immediately after sampling according to a modified protocol (Hammes *et al.* 2010) of the BacTiter-Glo Microbial Cell Viability Assay (G8231; Promega, Mannheim, Germany). As correction for extracellular ATP in groundwater, samples were filtered (pore size 0.1 µm) and then measured as described above. Intracellular ATP was calculated according to: Intracellular ATP = Total ATP – Extracellular ATP. For sediment samples, only total ATP concentrations were measured and no correction for extracellular ATP was applied. Cell numbers were calculated from intracellular ATP concentrations according to Hammes *et al.* 2010, who reported an average amount of 1.75×10^{-10} nmol ATP per cell (Hammes *et al.* 2010).

2.1.4 Ultrahigh Resolution Mass Spectrometry

Ultrahigh resolution mass spectra were acquired with a Bruker (Bremen, Germany) Solarix Qe FT-ICR-MS equipped with a 12 T superconducting magnet. Prior to

negative mode electrospray ionization ((-)ESI) FT-ICR-MS analysis, the SPE-DOM samples were diluted 1:20 with methanol and continuously infused with a flowrate of 120 $\mu\text{L h}^{-1}$. The dilution of the samples ensured a good compromise of signal intensity and comparable transient spectra in the ion cyclotron resonance (ICR) cell (same quantities of molecules entering the ICR cell), as well as avoided effects from ion-ion and ion-molecule interaction (e.g. peak splitting). Spectra were acquired in the range of m/z 123–1000 with 500 scans per spectrum averaged.

To address limited sensitivity of some compounds in (-)ESI FT-ICR-MS due to low ionization efficiency and suppression (+)APPI FT-ICR-MS was performed as a nearly orthogonal ionization mode (Hertkorn *et al.* 2008; D'Andrilli *et al.* 2010; Sleighter and Hatcher 2011). (+)APPI is the method of choice for the detection of molecules with extended, conjugated π -electron systems such as petroleum contaminants and their degradation products (Sleighter and Hatcher 2011). As an effect of the sample preparation, which was not optimized for the extraction of nonpolar contaminants but for DOM extraction, a mere 6% of the annotated molecular formulas of the whole data set were oxygen-free molecules. Therefore, only the results of the oxygen containing CHNOS molecular formulas are presented and discussed. For (+)APPI, the SPE-DOM extracts were diluted 1:20 with a solution of 90% methanol and 10% toluene as a dopant (Podgorski *et al.* 2012). The samples were continuously infused with a flowrate of 1 mL h^{-1} . Because of the low molecular mass of typical contamination molecules, spectra were acquired in the range of m/z 100–1000 with 500 scans per spectrum averaged. To prevent carry over and cross-contamination in (+)APPI FT-ICR-MS, the APPI source was rinsed thoroughly with a solution of 90% methanol and 10% toluene between the measurements. Blank methanol samples were frequently recorded and did not show any signs of sample carryover. Additionally, SPE extraction blanks were measured and the sample spectra were corrected after acquisition in Excel by filtering peaks resulting from the SPE resin and always present contaminants from methanol and the instrumentation itself.

Reproducibility of the mass spectra was assured by measuring SPE-DOM from 250 mL and 1 L samples collected at the same depths, also indicating no extraction volume effect. Additionally, FT-ICR mass spectra of samples taken in close vicinity

to each other (enabled by the high spatial resolution sampling in the centimeter range) resemble in principle composition, indicating indirectly reproducibility of FT-ICR mass spectra.

The mass spectra were internally calibrated to known and high abundant masses of DOM with a mass accuracy of 0.1 ppm. For both (-)ESI and (+)APPI FT-ICR-MS spectra, only singly charged molecular ions were found. Peak tables were exported with a signal to noise ratio of ≥ 4 . The formula assignment of the mass spectra was performed with the in-house written FormCalc software tool and the NetCalc network approach described previously (Tziotis *et al.* 2011). The mass accuracy window for the formula assignment was set 82 to ± 0.2 ppm. The assigned formulas were validated by setting sensible chemical constraints (N rule; O/C ratio ≤ 1 ; H/C ratio $\leq 2n+2$ (C_nH_{2n+2}), double bond equivalents) in conjunction with isotope pattern comparison. Final formulas were classified into molecular groups containing CHO, CHNO, CHOS, or CHNOS.

Hierarchical cluster analysis based on Pearson's correlations coefficient and average linkage of assigned FT-ICR-MS peaks for both ionization modes were performed with Hierarchical Clustering Explorer Version 3.0 and R (Version 3.0.0). The assigned peaks were almost normally distributed; therefore, the usage of Pearson's correlation was adequate. This was further confirmed by hierarchical cluster analysis based on Spearman's correlation, which led to analogous clustering results. To evaluate the molecular formulas explaining the main characteristics of each subcluster, formulas with a Pearson's correlations coefficient $r > 0.9$ were extracted for the individual subclusters. These molecular formulas are characteristic for the DOM chemistry in the specific depth region of the individual subclusters. The results were visualized by the use of van Krevelen diagrams in which the hydrogen to carbon ratio (H/C) was plotted against the oxygen to carbon ratio (O/C) (Van Krevelen 1950). The different bubble areas represent the mean intensity of the characteristic molecular formula within the respective subcluster.

FT-ICR-MS is a semiquantitative method owing to the lack of calibration standards in nontargeted analysis and differential ionization efficiency in complex and chemically diverse mixtures. The signal intensities of mass peaks are not necessarily directly proportional to their respective concentration; however, increase

and decrease of mass peak intensities follow the changes in relative concentrations. To address the limited detection of some compounds due to low ionization efficiency and suppression, two orthogonal ionization modes were performed.

2.2. Laboratory Sediment Incubations

2.2.1 Preparation

Laboratory sediment incubations were prepared in 100 ml glass syringes (Fortuna Optima, Poulten und Graf, Wertheim, Germany). The syringes were filled with 40 to 50 ml sediment which was homogenized by stirring with 2 $\mu\text{mol g}^{-1}$ (wet weight) freshly precipitated, solid FeS. The addition of electron donor FeS was necessary due to de-watering of sediment cores during sampling which also removed natural electron donors like dissolved organic carbon or sulfide. To equilibrate, the columns were percolated twice with three pore volumes of anoxic, sterile (autoclaved under nitrogen for 20 min at 121° C) tap water (80 ml) removing residual oxygen and dissolved ions from FeS synthesis. This water typically contains $\sim 100 \mu\text{M NO}_3^-$ and $\sim 200 \mu\text{M SO}_4^{2-}$. The water table was adjusted through the bottom outlet until it was approximately 1 mm above the sediment surface. Each of four replicate columns was incubated at 20°C in the dark for up to four months. Duplicate abiotic control columns were amended with FeS, autoclaved under nitrogen for 30 min at 121°C, and treated similar to the biotic incubations afterwards. FeS was synthesized freshly in the laboratory by mixing equal volumes of 1 M FeCl₂ and 1 M Na₂S dissolved in anoxic MilliQ water. The precipitated black FeS was washed twice with anoxic MilliQ water in order to remove any sodium and chloride ions released during synthesis.

2.2.2 Column Biogeochemistry

Microprofiles of oxygen in columns were measured by microsensors with a tip size of 0.1 mm (Revsbech 1989) (Unisense, Aarhus, Denmark) in 0.25 mm resolution. Porewater pH was measured in 1 mm resolution by a Perpfect Ross Micro Combination pH electrode (Thermo Fisher Scientific Inc., Waltham, MA, USA) with a tip size of 3 mm connected to a pH-meter (WTW series pH 730, InoLab, Weilheim, Germany) with a motorized micromanipulator (Unisense) for depth adjustment. The porewater chemistry in replicate columns developed in a similar way and fluxes

associated with LDET were reproducible (Table 5). After 2.5 and 3 months of column incubation two replicate sediment cores were shock-frozen in liquid nitrogen and cut into 3 to 12 mm slices with a circular diamond blade (Proxxon, Föhren, Germany). After thawing, pore water for sulfide measurements was collected with an automatic pipet in an oxygen free glove box. Sulfide was measured with a colorimetric assay (Cline 1969) which was downscaled to a reaction volume of 2 ml and a corresponding sample size of 40 μ l. Three aliquots of each reaction were analyzed at 660 nm on a Wallac 1420 Viktor3 plate reader (Perkin Elmer, Waltham, MA, USA). Sulfide concentrations were derived by linear regression from a Na₂S standard curve with a calibration range between 10 μ M and 10 mM. Ion chromatography was not conducted for laboratory incubations due to limited amounts of recovered pore water. Porewater alkalinity was determined by titration with 0.1 M HCl (APHA *et al.* 1998) of the anoxic tap water which was used for equilibration.

Cathodic proton consumption, diffusive oxygen uptake, and cathodic oxygen consumption were calculated from geochemical gradients as previously described (Nielsen *et al.* 2010; Risgaard-Petersen *et al.* 2012). Diffusive fluxes were calculated according to the formula:

$$J = \frac{\varphi}{(1-2\ln\varphi)} D_0 \frac{\delta C}{\partial x} \quad (2)$$

Where φ is the sediment porosity of 0.34 (Anneser *et al.* 2010); D_0 is the molecular diffusion coefficient, derived from literature (Cussler 2009) and adjusted to a temperature of 20° C assuming a linear correlation with temperature according to the Stokes–Einstein equation. This led to diffusion coefficients at 20° C for O₂, HCO₃⁻, CO₃²⁻, OH⁻, and H⁺ of 2.06, 1.16, 0.94, 5.51 and 9.14 (each multiplied by 10⁻⁵ cm² s⁻¹) respectively. C is the concentration and x the depth.

Cathodic proton consumption was calculated as sum of alkalinity fluxes above and below the pH maximum. Alkalinity fluxes were calculated from diffusive fluxes of individual compounds contributing to alkalinity as previously described (Malkin *et al.* 2014) by assuming constant values of dissolved inorganic carbon with depth according to the formula:

$$J_{TA} = J_{HCO_3^-} + 2J_{CO_3^{2-}} + J_{OH^-} + J_{H^+} \quad (3)$$

Current densities were determined from Cathodic proton consumption (CPC) by using a conversion factor of $1.036 \times 10^{-5} \text{ mol e}^{-} \text{ s}^{-1} \text{ A}^{-1}$. Assuming a consumption of 4 protons per oxygen molecule reduced by LDET, cathodic oxygen consumption was derived from: $\text{COC} = \text{CPC} \times 0.25$

2.3. Culture 1MN

2.3.1 Cultivation

The iron-reducing 1-methylnaphtalene-degrading enrichment was grown in 65 ml anoxic freshwater mineral medium (Widdel and Bak 1992) filled in 125 ml serum bottles and sealed with a butyl rubber stopper under 80% N₂ and 20% CO₂ (Linde, Germany) atmosphere. The medium was reduced with 1 mM Na₂S and buffered to pH 7 with 30 mM carbonate buffer. 20 mM amorphous ferrihydrite (Lovley and Phillips 1988) served as sole electron acceptor while 0.35 mM 1-methylnaphtalene was added as electron donor and carbon source. Fresh cultures were started by inoculation with 10% from a previous culture and incubated at 30° C.

2.3.2 Growth Experiments with Culture 1MN

In order to investigate if sulfur and iron cycles are coupled in culture 1MN and to elucidate the function of the *Desulfobulbaceae* in this culture, 2% (v/v) of a 1MN culture grown with ferrihydrite and 1-methylnaphtalene were transferred to fresh medium reduced with 0.3 and 2 mM Na₂S amended with 1-methylnaphtalene, elemental sulfur, or FeS as electron donor (Table 2). In contrast to the regular cultivation of culture 1MN (see above), ferrihydrite for the growth experiments was synthesized by preparing a 25 mM Fe(NO₃)₃ solution which was heated to 75°C for 20 min under constant stirring followed by a two-step cooling at room temperature and an ice bath for 15 min each (Carta *et al.* 2009). The solution was titrated with NaOH to pH 7. The precipitated ferrihydrite was washed five times with deionized water. However, not all nitrate from synthesis was removed by this washing step. Ion chromatography (Dionex DC-100, Idstein, Germany) revealed nitrate concentrations of 1 to 3 mM in the medium amended with ferrihydrite. To analyze if all the nitrate was dissolved in the medium or if some nitrate were still complexed with Fe(III), the iron sludge was dissolved in 5 mM HCl and the iron was precipitated

again by neutralizing the pH with NaOH. The nitrate concentrations did not increase indicating that all nitrate was dissolved in the medium. The medium contained 30 mM carbonate buffer as described above and the pH was adjusted to pH 6.5 to promote iron reduction. Each of the different cultivations was performed in at least four replicates and two abiotic controls. Elemental sulfur was suspended in deionized water and sterilized two times by autoclaving at 110° C for 30 min.

Table 2: Incubation conditions for the cultivation of the iron-reducing culture 1MN

E-Acceptors	E-Donor	Reducing agent
15 mM Fe(OH) ₃ , 0.9 mM NO ₃	0.35 mM 1-methyl-naphthlene	2 mM Na ₂ S
15 mM Fe(OH) ₃ , 1.3 mM NO ₃	5 mM FeS	0.3 mM Na ₂ S
30 mM Fe(OH) ₃ , 3.0 mM NO ₃	30 mM S ₀	0.3 mM Na ₂ S

2.3.3 Temporal Monitoring of Chemical Parameters

Every 1-2 weeks, serum bottles were homogenized by manual shaking and 600 µl of the culture were sampled by a syringe through the stopper. Samples were processed immediately for further analysis to minimize oxygen exposure. For iron measurements, 20 µl sample were dissolved in 180 µl of 1M HCl for ~3 hours under regular mixing. Fe(II) concentrations were determined by the ferrozine assay on a 96-well plate reader (Perkin Elmer, USA) by measuring the absorbance at 560 nm (Stookey 1970). For sulfide analysis, 20 µl of sample were fixed in 400 µl of a 1% ZnAc solution. Sulfide concentrations were measured within 2 hours by the methylene blue method (Cline 1969) which was downscaled to 96-well plate volumes. Therefore, 100 µl of the sample trapped in ZnAc was mixed directly in the 96-well plate with 100 µl H₂O, 25 µl 4-Amino-N,N-dimethylaniline sulfate (ADMA) solution and oxidized to methylene blue with 25 µl of ferric ammonium sulfate solution. The absorbance of triplicate samples was measured at 670 nm on a 96-well plate reader. Sulfide concentrations were calculated from a standard curve derived from different dilutions of a 100 mM Na₂S standard solution covering a range between 50 µM and 5 mM. The pH in the medium was measured with a Perphect Ross Micro Combination pH electrode (Thermo Fisher Scientific Inc., USA). For sulfate measurements, 500 µl of sample were centrifuged for about 10 seconds in an Eppendorf centrifuge. Triplicates of 100 µl supernatant were mixed in wells of 96-well plate with 200 µl of a BaCl₂ (4% w/v)-gelatine (0.3% w/v) solution acidified

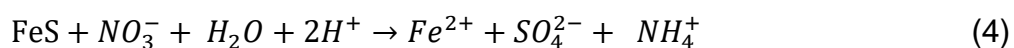
1:1 (v/v) with 0.5 N HCl (Tabatabai 1974). After half an hour, the 96-well plate was put into the 96-well plate reader, agitated continuously for 10 min followed by measuring the turbidity at 450 nm. Sulfate concentrations between 0.1 mM and 5 mM could be directly determined from a standard curve of different Na₂SO₄ concentrations. For concentrations exceeding 5 mM, samples were analyzed in 1:10 dilutions.

2.3.4 Determination of Solid-phase Mineral Composition

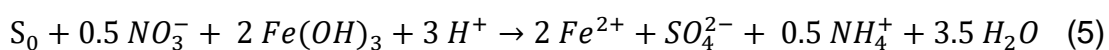
After the experiment, serum bottles containing culture 1MN grown on elemental sulfur or FeS were centrifuged (10 min, 3000 rpm), the supernatant was removed, and the solid minerals were washed in 40 ml anoxic MilliQ water. This procedure was repeated three times. After the last washing step, most of the supernatant was removed and the iron sludge was freeze-dried under anoxic conditions. The obtained powder was stored under nitrogen until mineral analyses by X-ray diffraction (XRD) and Fourier transform infrared spectroscopy (FTIR) as previously described (Höss *et al.* 2014).

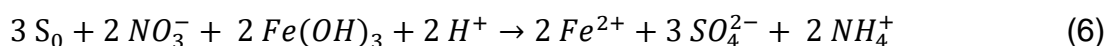
2.3.5 Estimation of Nitrate Concentrations

Nitrate concentrations were measured prior to inoculation and after each experiment. Nitrate concentrations at a certain time point were estimated from electron balance calculations. In all active incubations, nitrate was completely converted to ammonium over the course of the experiments. For FeS as electron donor, a direct oxidation of FeS to sulfate was assumed leading to a ratio of sulfate production to nitrate reduction of 1:1 according to:



For inoculations with elemental sulfur, Fe(II) was produced in parallel to sulfate indicating a coupling of FeS oxidation by nitrate reduction –which liberated Fe²⁺– and iron reduction by sulfide from sulfur disproportionation. Here, a partial oxidation of FeS to elemental sulfur followed by disproportionation or a direct oxidation of FeS to sulfate were possible as long as nitrate was present as electron acceptor.





The maximum nitrate concentration was therefore calculated according to reaction (5) assuming a ratio of sulfate production to nitrate reduction rate of 2:1. The same ratio was applied for cultures with 1-methylnaphthalene as electron donor in which elemental sulfur and FeS were present from initial reduction with sulfide. However, 1-methylnaphthalene might have been also directly oxidized with nitrate as electron acceptor which would have led to much faster nitrate depletion.

2.4. DNA Extraction and Molecular Methods

2.4.1 DNA Extraction from Sediments

DNA from sediment of batch and field samples was extracted in triplicates each with 1 g sediment according to a previously described protocol (Winderl *et al.* 2008).

2.4.2 DNA Extraction from Culture 1MN

DNA was extracted from culture 1MN following a modified version of a previously published protocol (Lueders *et al.* 2004). After the course of each experiment, serum bottles were manually mixed and 2 ml of each culture were taken with syringes. Each sample was centrifuged for 30 min at 14,000 rpm at 4°C. The supernatant was discarded. The pellet was re-suspended in 600 µl PTN buffer – containing 120 mM NaPO₄, 125 mM Tris, 25 mM NaCl at pH 8 – and transferred to bead beating vials containing ~0.2 ml of a 1:1-mix of 0.1 mm and 0.7 mm Zirkonia/Silica beads (BioSpec, USA). 40 µl of Lysozyme (50 mg/ml) and 10 µl of Proteinase K (10 mg/ml) were added and incubated at 37° for 15 min. Then, 100 µl of 20% SDS were added, followed by an incubation at 65°C for 15 min. After adding 100 µl Phenol/Chloroform/Isoamylalcohol and beat beating at 6.0 m s⁻¹ for 45 s, the vials were centrifuged at 7,500 rpm for 5 min. 750 µl of supernatant were taken and shaken with 750 µl of Phenol/Chloroform/Isoamylalcohol and centrifuged (14,000 rpm, 5 min, 4° C). Then, 800 µl of supernatant was transferred to Phase-Lock-Gel-Heavy tubes (Eppendorf, Germany), mixed with 800 µl Chloroform/Isoamylalcohol (24/1), and centrifuged for 4 min at 14,000 rpm (4° C). The DNA of 650 µl of supernatant was precipitated in two volumes of 30% polyethylene glycol solution

over night at 4° C. The precipitate was spun down for 30 min at 14,000 rpm (20° C). The polyethylene glycol solution was discarded and the pellet washed with 500 µl of cold (-20° C) 70% ethanol. After removing the ethanol and drying the pellet, the precipitated DNA was eluted in 30 µl elution buffer (EB buffer, Qiagen, Germany). In most cases, the extracted DNA still contained a high amount of iron impurities which could have interfered with downstream applications such as PCR. Therefore, all extracts were additionally purified by Sephadex Gel Filtration using DyeEx Spin Columns (Qiagen, Germany) according to the manufacturer's instructions.

2.4.3 PCR and Microbial Community Fingerprinting

For fingerprinting of the microbial communities by terminal-restriction fragment length polymorphism (T-RFLP) analysis, the 16S rRNA gene was amplified with primers Ba27f-FAM and 907r as described (Pilloni *et al.* 2011). The PCR conditions were: initial denaturation at 94° C (5 min), followed by 28 cycles of denaturation (94° C; 30 sec), annealing (52° C; 30 sec) and elongation (70° C; 60 sec) and a final elongation (70° C; 5 min). 80 ng of Fam-labeled amplicons were digested with 0.3 µl MSPI in Tango buffer with 10 µl total reaction volume at 37° C for 2 h. Fragments were desalted with DyeEx 2.0 Spin Kit (Quiagen, Hilden, Germany). 1 µl of the desalted fragments were mixed with 13 µl HiDi Formamide (Thermo Fisher Scientific) which contained a 1/300 dilution of MapMarker-100 ROX Size Standard. Fragments were denatured for 5 min at 95° C and analyzed by capillary electrophoresis on ABI 3730 DNA analyzer (Thermo Fisher Scientific). Data were evaluated with the Gene Mapper software 5.1 (Thermo Fisher Scientific) and further processed with the T-REX online tool for T-RFLP analysis (Culman *et al.* 2009). Peak heights were normalized and the T-RF clustering threshold was adjusted to 2 bp.

2.4.4 Pyrosequencing and Phylogenetic Analyses

Amplicon pyrosequencing, data processing, and taxon assessment were performed as previously published (Pilloni *et al.* 2011). Maximum likelihood phylogenetic trees of 16S rRNA genes were constructed with the MEGA6 (Tamura *et al.* 2013) software (Version 6.06) by creating an alignment of representative sequences with the MUSCLE algorithm (Edgar 2004). The chosen amplicon contigs were deposited at

GenBank under the accession numbers KR262833 to KR262839. All sequencing reads are deposited at SRA under study accession number SRP063036.

2.4.5 Fluorescence In Situ Hybridization

Based on 16S rRNA sequences derived from assembled sequence read contigs, as well as on previously published full-length 16S rRNA sequences (Kunapuli *et al.* 2008), a specific FISH probe FliDSB194 (Table 3) was designed for *Desulfobulbaceae* from the Flingern site using the ARB software package (Ludwig *et al.* 2004) (Table 4).

Table 3: Oligonucleotide probes used for FISH

Probe	Sequence	Label	Target organisms
DSB706	5'-ACCGGTATTCCTCCCGAT-3'	6-Fam	Most <i>Desulfobulbaceae</i>
FliDSB194	5'-GGAGAGGTCTCCTTTTCCTTA-3'	Cy3	Groundwater cable bacteria

Fresh sediment samples from lab and field were mixed 1:1 with either 4% paraformaldehyde or 2.5% glutardialdehyde and stored at 4° C until further processing. The sediment was cautiously washed 1:1 in PBS buffer to release filaments to the supernatant. 20 µl supernatant were then diluted in 200 µl MilliQ water, mixed by flipping and pipetted in 40 µl aliquots to 8-well microscope slides.

Cells in samples from culture 1MN were fixed in 1% final concentration of a 4% anoxic paraformaldehyde solution and stored at 4° C for later analysis. For FISH, 20 µl of fixed samples were gently mixed with 40 µl MilliQ water on an adhesion microscope slide (Polysine, Thermo Scientific, USA).

The slides were dried for 90 min at 46° C. Afterwards, they were dehydrated by successively increasing ethanol concentrations of 50%, 80%, and 99% for 3 min each. Hybridization was performed for 2.5 h, followed by a 30 min washing step according to a previously published protocol (Pernthaler *et al.* 2001). Specific oligonucleotide probes DSB706 (Loy *et al.* 2002) and FliDSB194 were used for the detection of filamentous *Desulfobulbaceae* at a hybridization stringency of 35 % formamide (Table 4). Cells were counterstained with DAPI and embedded in

Citiflour AF1 (Citifluor, UK). Labeled cells were detected with fluorescence microscopy (Axioskop 2 plus, Zeiss, Jena, Germany) by using specific filters for 6-Fam (DSB706), Cy3 (FliDSB194) and DAPI (counterstained cells). For imaging, pictures were taken by the digital camera AxioCam HRm (Zeiss) and the software AxioVision (Version 4.8.2; Zeiss).

Table 4: Specificity of probe FliDSB194

Sequence	Accession No.	MM	Alignment
Probe FliDSB194			3'-ATTCCTTTCCTCTGGAGAGG-5'
Target			5'-TAAGGAAAGGAGACCTCTCC-3'
BF enrichment <i>Desulfobulbaceae</i>	EU016449	0
Flingern enrichment culture	HQ625672	0
Lake water	AB754079	0
Trichloroethene-contaminated site	AF529133	0
<i>Desulfobacterales</i> bacterium	JQ723604	0
Aquifer sediment	JX222667	0
Kristineberg tailing dump	KJ650741	0
<i>Desulfobacterales</i> bacterium	JQ723620	1	· G
Lake water	AB754082	2	· G T
Uranium mining mill tailing	AJ296571	2 T T ·
<i>Desulfurivibrio alkaliphilus</i> AHT2	EF422413	2 T T ·
<i>Desulfobulbus</i> sp. DSM 2033	EF442993	4 T · G G A
Marine cable bacteria	JX091072	6	C · · · _ · · · · T · G · · · · A T

Specificity of probe FliDSB194 for selected environmental and cultured sequences in Genbank.

MM: Mismatches. Pairings are indicated as dots.

3. Results

3.1. LDET and Cable Bacteria in Laboratory Sediment Columns

To demonstrate the potential occurrence of LDET in aquifers, sediments from a previously investigated tar oil-contaminated aquifer in Düsseldorf, Germany were amended with $2 \mu\text{mol g}^{-1}$ FeS, saturated with anoxic water and incubated at 20°C in the dark in open-top glass syringes. After 70 days, microsensors measurements in pore water showed that oxygen was penetrating 8 ± 2 mm ($\text{O}_2 < 0.3 \mu\text{M}$) into the sediment (Figure 6A, Table 5). The pH increased to 7.8 within the oxic zone, in accordance with proton consumption by cathodic oxygen reduction. Beneath the oxygen minimum, a suboxic zone of at least 9 mm separated the oxic and sulfidic zones. The coarse resolution of the sulfide profile did not allow for an exact determination of the suboxic-sulfidic transition and might underestimate the width of the suboxic zone. Here, the pH continuously decreased towards a minimum of pH 7.3 within the sulfidic zone at 27.5 mm, in accordance with proton release by anodic sulfide oxidation. The geochemical profiles thus indicated that sulfide oxidation is connected to oxygen reduction over a distance of 15-25 mm (Figure 6A). Calculation of oxygen and alkalinity fluxes from gradient slopes (Nielsen *et al.* 2010; Malkin *et al.* 2014) indicated a cathodic oxygen consumption of $340 \pm 67 \mu\text{mol m}^{-2} \text{d}^{-1}$ and a current density of $1.5 \pm 0.3 \text{ mA m}^{-2}$ (Table 5).

Table 5: Geochemical parameters associated with LDET detected in batch incubations

	OPD [mm]	DOU [$\mu\text{mol m}^{-2} \text{d}^{-1}$]	COC [$\mu\text{mol m}^{-2} \text{d}^{-1}$]	Current density [mA m^{-2}]
Active incubation (n = 4)	8 ± 2	950 ± 360	340 ± 67	1.5 ± 0.3
Abiotic control (n = 2)	18 ± 2	513 ± 95	NA	NA

Abbreviations: COC, cathodic oxygen consumption; DOU, diffusive oxygen uptake; LDET, long-distance electron transfer; NA, not applicable; OPD, oxygen penetration depth. Signal of LDET in four replicate cores in comparison with two abiotic control columns after 70 days of incubation.

This corresponds to a theoretical sulfate recycling of $170 \pm 34 \mu\text{mol m}^{-2} \text{d}^{-1}$ within the sulfidic zone, assuming complete oxidation of sulfide to sulfate and evenly

distributed dissolved inorganic carbon of 5.5 mM as pH buffer over the entire column. In contrast, autoclaved control columns did not show an increase but a 0.7 lower pH in the oxic zone which was most likely caused by chemical FeS oxidation (Figure 6A). Also, abiotic oxygen profiles differed significantly from active incubations by deeper oxygen penetration of 18 ± 2 mm and a corresponding oxygen flux of $513 \pm 85 \mu\text{mol m}^{-2} \text{d}^{-1}$ after 70 days of incubation compared to $950 \pm 360 \mu\text{mol m}^{-2} \text{d}^{-1}$ for active incubations (Figure 6 and Table 5).

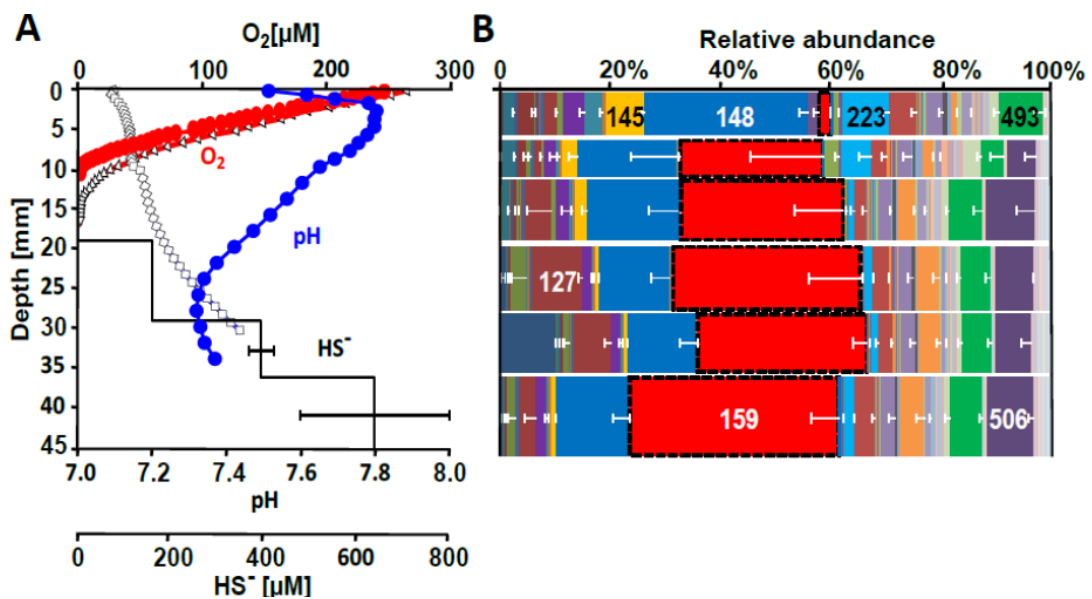


Figure 6. Geochemical gradients and microbial community analysis from a representative incubation of sediments taken from the Flingern aquifer. **A)** Porewater profiles of O₂, pH, and HS⁻ of homogenized sediment amended with 2 μmol g⁻¹ FeS after 70 days of incubation in the dark. One typical replicate out of four is shown. Error bars for sulfide concentrations in different slices of the cut sediment represent standard deviations of 3 technical replicates. Open symbols show porewater profiles of O₂ (triangles) and pH (squares) of one typical abiotic control column out of two. **B)** Corresponding depth-resolved relative abundance of T-RF 159 (dashed frame) representing members of the *Desulfobulbaceae* as mean values of three independent DNA extractions. Error bars show standard deviations of relative abundances determined from triplicate DNA extractions of one typical replicate out of two.

After completing the geochemical measurements, columns were sacrificed and sediment cores cut into 3 to 12 mm slices. Long filamentous bacteria were discovered in the suboxic zone of these sediments by light microscopy. Filament

fragments were up to 5.5 mm long and between 0.4 and 1.5 μm in diameter (Figure 7).

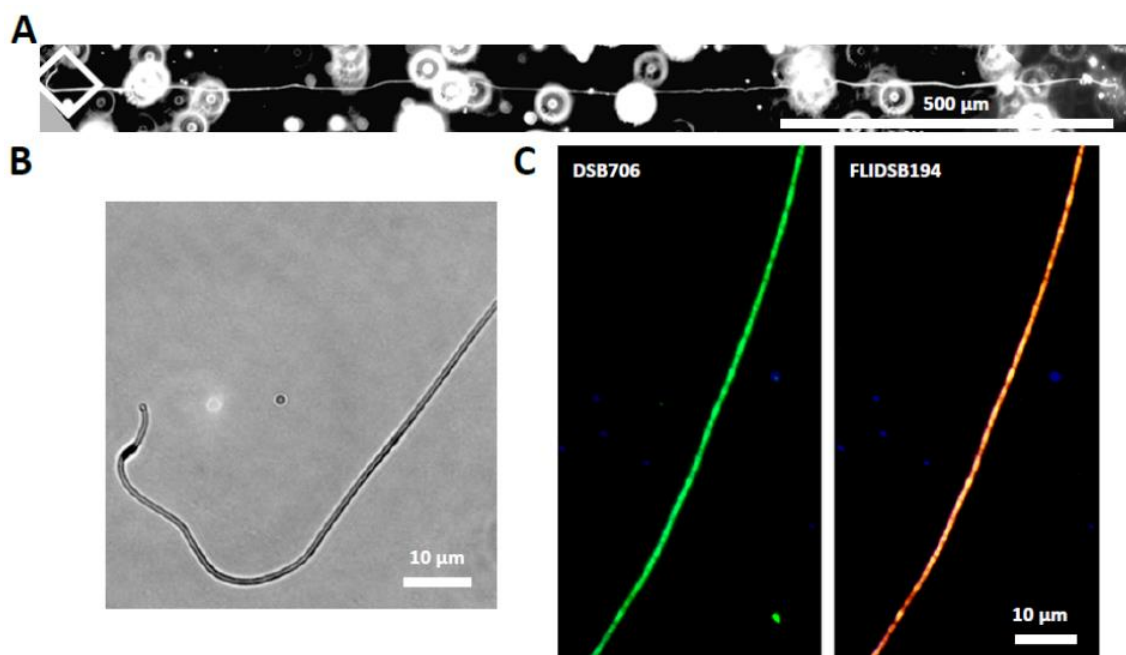


Figure 7. Microscopy of groundwater cable bacteria. **A)** Microscopic image of a filament fragment of approximately 1.7 mm length. Three pictures were merged to cover the full length of the fragment. The white square indicates the part of the filament shown in higher magnification in **B)**. **C)** Micrographs of filaments stained with FISH probes specific for the family *Desulfobulbaceae* (DSB706; 6-FAM labeled) and **D)** for groundwater cable bacteria (FLIDSB194, Cy3 labeled). Each image is presented as overlay of two pictures taken with filters for specific probe fluorescence and DAPI for counterstaining.

In order to elucidate the distribution of these bacteria in the sediment columns and their phylogenetic affiliation, terminal restriction fragment length polymorphism (T-RFLP) and amplicon pyrosequencing were conducted. T-RFLP fingerprinting showed a T-RF of 159 bp length as predominant throughout the columns, with a relative abundance of up to 40% throughout the suboxic and sulfidic zone, where LDET occurred (Figure 6B). Sequencing of 16S rRNA gene fragments from extracted DNA showed *Desulfobulbaceae* to represent up to 34% of all sequencing reads within the anoxic part of the sediment. The comparable abundance of T-RF 159 and *Desulfobulbaceae* sequences – together with a predicted cut size of 162 bp – identified T-RF 159 as member of the family *Desulfobulbaceae* (Figure 8). These molecular techniques included amplification steps of 16S genes and therefore can only provide relative abundances within the bacterial community and

do not reflect absolute cell abundances. Sequence similarity to 16S rRNA genes of marine (Schauer *et al.* 2014) and freshwater (Risgaard-Petersen *et al.* 2015) cable bacteria was only up to 88%. The closest cultivated relative with 91% similarity was *Desulfurivibrio alkaliphilus* AHT2, a facultative chemolithoautotrophic, non-sulfate reducing bacterium (Sorokin *et al.* 2008).

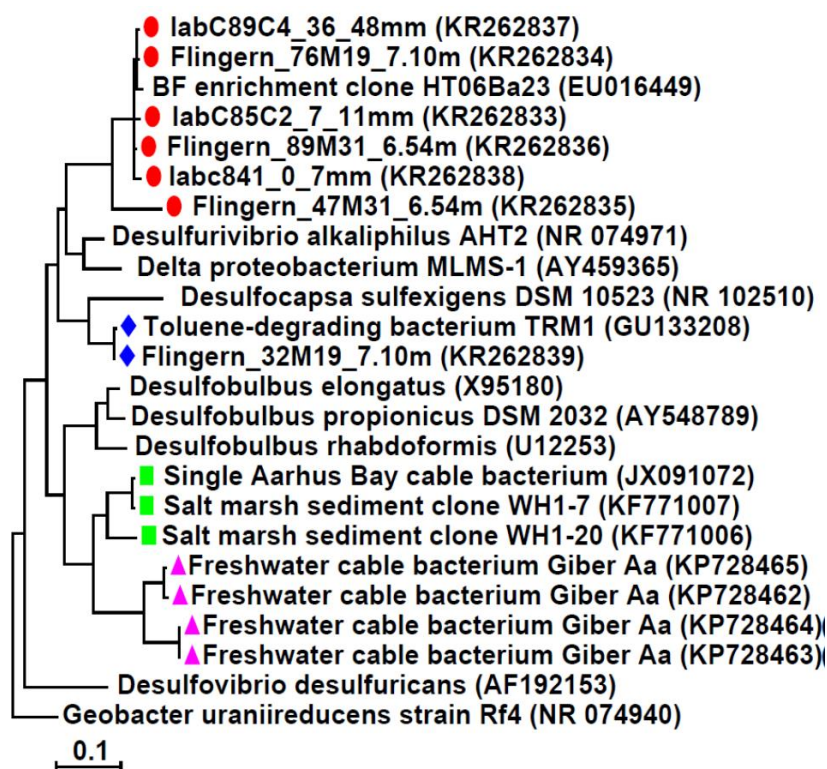


Figure 8. Phylogeny of groundwater cable bacteria. Maximum likelihood phylogenetic tree based on 16S rRNA gene sequences showing the phylogenetic affiliation of groundwater cable bacteria (red circles), marine cable bacteria (green squares), freshwater cable bacteria (violet triangles), and sequences related to the toluene-degrading strain TRM1 (blue diamonds) (Meckenstock 1999). The prefix of sequence names indicates sequences derived from laboratory (lab-) batch incubations or directly from the field (Flingern-). The suffix indicates the sampling depth below sediment surface.

To verify the placement of the filaments within the *Desulfobulbaceae* sequences mentioned above, a specific FISH probe (FlIDSB194) was designed and applied to sediment from laboratory incubations (Figure 7C). The long filamentous bacteria, previously observed by phase contrast microscopy, specifically hybridized with this probe, as well as with the *Desulfobulbaceae* specific probe DSB706 (Loy *et al.* 2002) (Figure 7C).

3.2. Possible LDET at the Capillary Fringe *In Situ*

Sampling of groundwater at 3 cm depth resolution was performed at the same tar oil contaminated aquifer in Düsseldorf, Germany to search for indications of LDET in situ. The toluene plume ranged from the groundwater table at 6.54 m below surface (bls) down to 7.21 m (Figure 9A). Nitrate and sulfate were detectable at the upper plume fringe at 6.54 bls but nitrate decreased below the detection limit at 6.59 m and sulfate at 6.62 m bls. (Figure 9C). The steep geochemical gradients and the depletion of electron acceptors in the plume core suggested strong microbial toluene degradation at the plume fringes (Anneser *et al.* 2008; Winderl *et al.* 2008; Larentis *et al.* 2013). A steep decrease of sulfate from the lower plume fringe towards the plume core indicated sulfate reduction as predominant process between 6.90 m bls and 7.10 m bls. Highest ferrous iron concentrations of 380 μM and the highest number (3×10^6 cells/ml) of active bacteria estimated from intracellular ATP concentrations were also detected at the upper plume fringe at 6.59 m bls (Figure 9D). Such ferrous iron concentrations could be due to microbial biodegradation coupled to iron reduction or an oxygen or nitrate-dependent release of ferrous iron from iron-sulfides by LDET within the suboxic zone.

At 1 m distance from the high resolution monitoring well, intact sediment cores were taken and the microbial communities were studied in 3 cm vertical intervals. Microbial community fingerprinting of DNA extracted from sediment samples showed relatively high abundances of 16% of the same 159 bp T-RF up to the capillary fringe at 6.54 m bls and 22% at the lower plume fringe at 7.10 m and 7.50 m bls (Figure 9B). Sequencing of 16S rRNA gene fragments over depth substantiated this T-RF to represent the filamentous *Desulfobulbaceae* detected in the laboratory incubations (Figure 8). Other abundant sequences found at the capillary fringe and upper plume fringe belonged to *Ignavibacteria* (T-RF 163) and *Thiobacillus denitrificans* (T-RF 477). Dominant taxa within the plume core were *Rhodocyclaceae* (T-RF 502) and *Desulfobulbaceae* related to the toluene-degrading strain TRM1 (Meckenstock 1999) at the lower fringe, previously identified as key toluene degraders in this aquifer (Pilloni *et al.* 2011) (Figure 8).

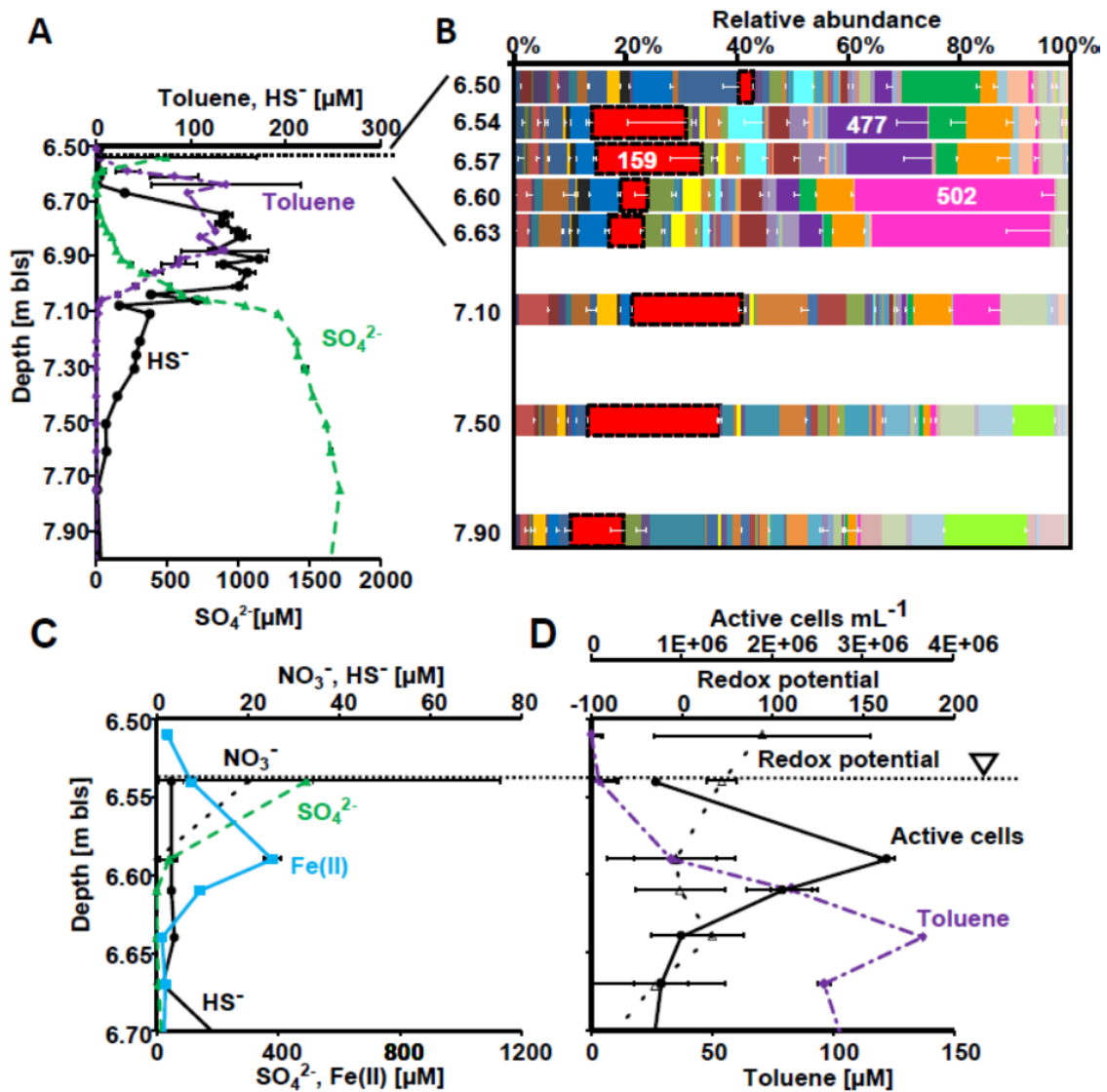


Figure 9. Depth profiles of geochemistry of water samples from a high-resolution monitoring well installed in Flingern and of microbial community compositions from a sediment core drilled at 1 m distance. **A)** Groundwater chemistry of duplicate measurements showing the zone of toluene contamination as well as the sulfide- and sulfate concentrations. **B)** T-RFLP microbial community fingerprints obtained from triplicate DNA extractions of different sediment layers. T-RF 159 (dashed frame) is representing members of the *Desulfobulbaceae*. Data show the mean values and standard deviations of three independent DNA extractions. **C), D)** Geochemistry and active cell densities estimated from intracellular ATP concentrations of groundwater at the upper plume fringe. Bls, below land surface. The dashed horizontal lines indicate the groundwater table.

3.3. Cable Bacteria Couple Nitrate Reduction to Iron and Sulfur Cycles in Anaerobic Enrichment Culture

Desulfobulbaceae closely related to groundwater cable bacteria are found not only in sulfidic freshwater habitats (Handley *et al.* 2012), but also in heavy metal contaminated sites (Wu *et al.* 2010; Fabisch *et al.* 2016), in iron-reducing microcosm experiments (Pilloni *et al.* 2011), and in iron-reducing hydrocarbon-degrading enrichment cultures (Kunapuli *et al.* 2007). In these cultures, *Desulfobulbaceae* are frequently associated with members of the *Firmicutes* that were identified as the key hydrocarbon degraders by DNA stable isotope probing (Kunapuli *et al.* 2007). Motivated by the close relation to groundwater cable bacteria combined with the fact that the growth media are reduced with sulfide, I hypothesized that the *Desulfobulbaceae* catalyze a cryptic sulfur cycle leading to iron reduction. The *Firmicutes* might degrade the pollutants as electron donor and perform either fermentation, or sulfur reduction to sulfide.

Although the *Desulfobulbaceae* are prominent members in these iron-reducing cultures for more than a decade, their function remained enigmatic.

To elucidate the potential function of the *Desulfobulbaceae* in the iron-reducing 1-methylnaphthalene-degrading culture 1MN, the culture was grown in anoxic mineral medium with 1-methylnaphthalene, elemental sulfur, or FeS as electron donor as well as with 2 mM or 0.3 mM HS⁻ as reducing agent (Table 1). As electron acceptors, ferrihydrite was used which contained 0.9 to 3.0 mM nitrate which was not removed by washing after synthesis from Fe(NO₃)₃ (Table 2).

The incubations with 0.35 mM 1-methylnaphthalene as electron donor and 15 mM ferrihydrite and 0.9 mM nitrate as electron acceptors showed a slow decrease in sulfide and HCl-extractible Fe(II) during the first 36 days (Figure 10A) in active incubations as well as in abiotic controls. After this initial phase, active incubations showed increasing Fe(II) concentrations from about 2 mM to 4 mM during the next 24 days. In parallel, sulfide increased for 16 days from 0.4 mM to 0.8 mM and dropped again afterwards. The increase in Fe(II) and sulfide clearly indicated reducing conditions in culture 1MN. At the same time, also 1.6 mM of sulfate was

produced. During the growth phase, the production rates of Fe(II), sulfate and sulfide were 0.08, 0.05 and 0.02 mM d⁻¹, respectively. The 0.9 mM nitrate initially present in the culture was completely reduced to ammonium during the experiment in active incubations. Electron balance calculations allowed for an estimation of nitrate depletion indicating that no nitrate was present after day 60 when sulfate concentrations were still increasing (Figure 10A).

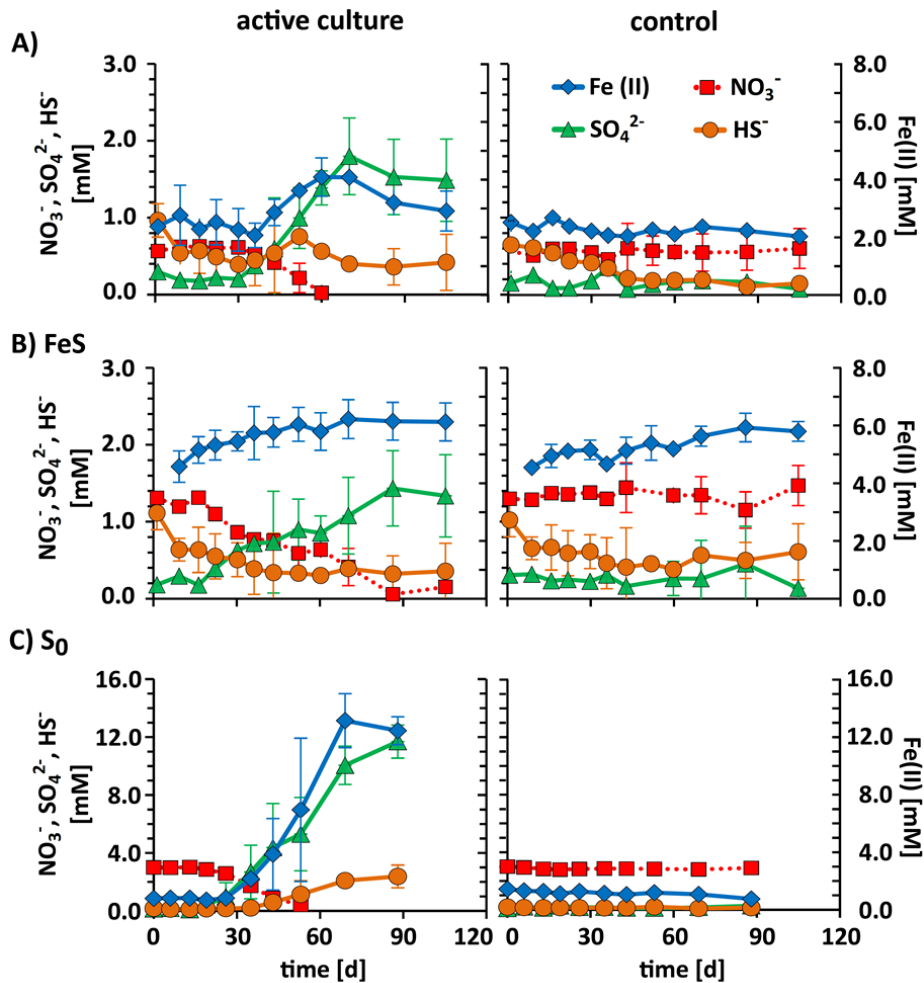


Figure 10. Growth of culture 1MN (left panels) with electron donors 1-methylnaphthalene (A), elemental sulfur (B) and FeS (C) in comparison to not inoculated controls (right panels). Time series of Fe(II) (blue diamonds), SO₄²⁻ (green triangles), and HS⁻ (orange circles). Nitrate concentrations were measured prior to inoculation and after the course of the experiment and in between inferred from electron balance calculations (red squares). Please note the different scale of the y-axis in panel C. Error bars show standard deviations of replicate incubations (1-methylnaphthalene: n = 2; S₀: n = 4, FeS: n = 8, and controls: n = 2).

In abiotic controls, no increase in sulfate was observed but a steady decrease in measurable sulfide and HCl-extractable Fe(II) of ~0.5 mM each (Figure 10A). Dissolution of iron in 10 M HCl after the experiment showed that indeed 0.7 mM Fe(II) were not soluble in 1M HCl which was within the same range like the decrease in Fe(II) over time. Nitrate was not reduced in abiotic controls.

Surprisingly, also incubations with FeS as electron donor showed extensive microbial metabolism. After 16 days, sulfate was produced linearly up to 1.1 mM at 0.02 mM d⁻¹ in contrast to abiotic controls where no sulfate production was observed (Figure 10B). Sulfide concentrations which could be measured by the ADMA assay decreased over time in both active incubations and controls. However, the final sulfide concentrations in active incubations were 0.2 to 0.3 mM lower compared to abiotic controls. In contrast to incubations with 1-methylnaphthalene and elemental sulfur as electron donors, Fe(II) modestly increased also for abiotic controls. Again, the 1.3 mM nitrate initially present were completely reduced to ammonium in active incubations. The electron balance suggests that nitrate was gradually depleted over time, congruent to the increase in sulfate concentration (Figure 10B). In contrast, nitrate was still present in abiotic controls after the experiment.

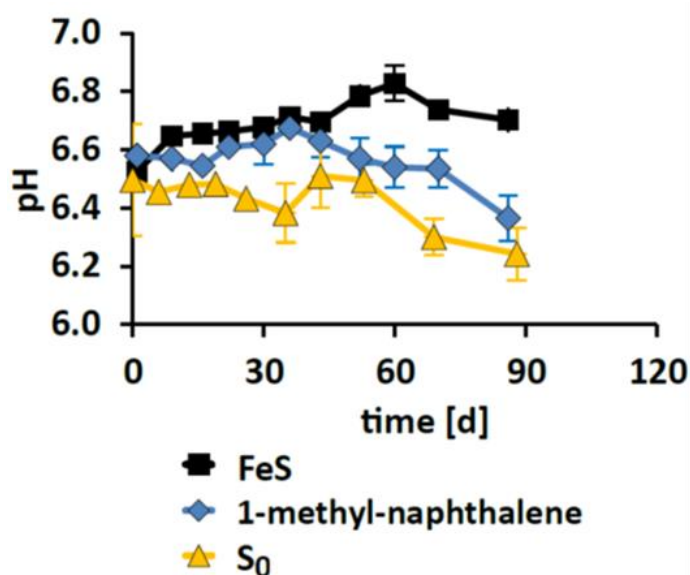


Figure 11. Development of pH values in active incubations of culture 1MN grown on 1-methyl-naphthalene, FeS, and elemental sulfur as electron donors. Error bars indicate standard deviations of replicate incubations (1-methylnaphthalene: n = 2; S₀: n = 4, FeS: n = 4).

Culture 1MN was also capable of growing with 30 mM elemental sulfur as electron donor and 30-40 mM ferric iron and 3 mM nitrate as electron acceptors. Potential carry over of organic carbon was very low in this setting as the inoculation was done with only 2% of a regular 1MN culture. After a lag phase of 30 days, the production of sulfate, sulfide, and Fe(II) indicated growth of culture 1MN (Figure 10C). While Fe(II) and sulfate were produced up to 12 mM, sulfide was only generated up to 2.4 mM. Inferred nitrate concentrations indicate a complete reduction of 3 mM nitrate to ammonium before day 52. The pH dropped during growth from pH 6.5 to 6.2 (Figure 11). The production rates averaged at 0.3 mM d^{-1} Fe(II), 0.2 mM d^{-1} SO_4^{2-} and 0.07 mM d^{-1} HS^- (Figure 10C). Culture 1MN was not able to grow on elemental sulfur alone in the absence of ferrihydrite and nitrate as electron acceptors.

After the course of the experiments, the iron sludge from incubations with FeS or elemental sulfur as electron donor was washed with anoxic deionized water and freeze-dried under anoxic conditions. The mineral composition was analyzed by X-ray diffraction (XRD) and Fourier transform infrared spectrometry (FTIR).

For incubations with FeS as electron donor, XRD spectra revealed goethite (FeOOH), hematite (Fe_2O_3), and vivianite ($\text{Fe}_3(\text{PO}_4)_2 \cdot 8\text{H}_2\text{O}$) as the main iron minerals (Figure 12). However, in one of the two replicates only traces of vivianite were present (Figure 12). Iron sulfide minerals could not be clearly identified in the XRD spectra, even though the medium was amended with 5 mM FeS as electron donor before inoculation. Surprisingly, ferrihydrite was not detected by XRD indicating either a transformation to more crystalline goethite or hematite during the experiment or that goethite, not ferrihydrite, was produced during synthesis. FTIR confirmed the results of XRD, even though Transmission-FTIR additionally detected ferrihydrite which was not supported by ATR-FTIR (Figure 13). The freeze-dried matter showed no magnetic properties.

For incubations with elemental sulfur as electron donor, XRD spectra showed that the freeze-dried matter was mainly composed of goethite, vivianite, and greigite (Fe_3S_4) (Figure 12). The freeze-dried matter exhibited magnetism caused by the greigite in the samples. FTIR spectra confirmed the results from XRD, but additionally exhibited bands for hematite and ferrihydrite (Figure 13). Again, ferrihydrite was only detected by ATR-FTIR and not by Transmission-FTIR. Greigite

does not provide bands in the investigated infrared range and was therefore not detected by FTIR.

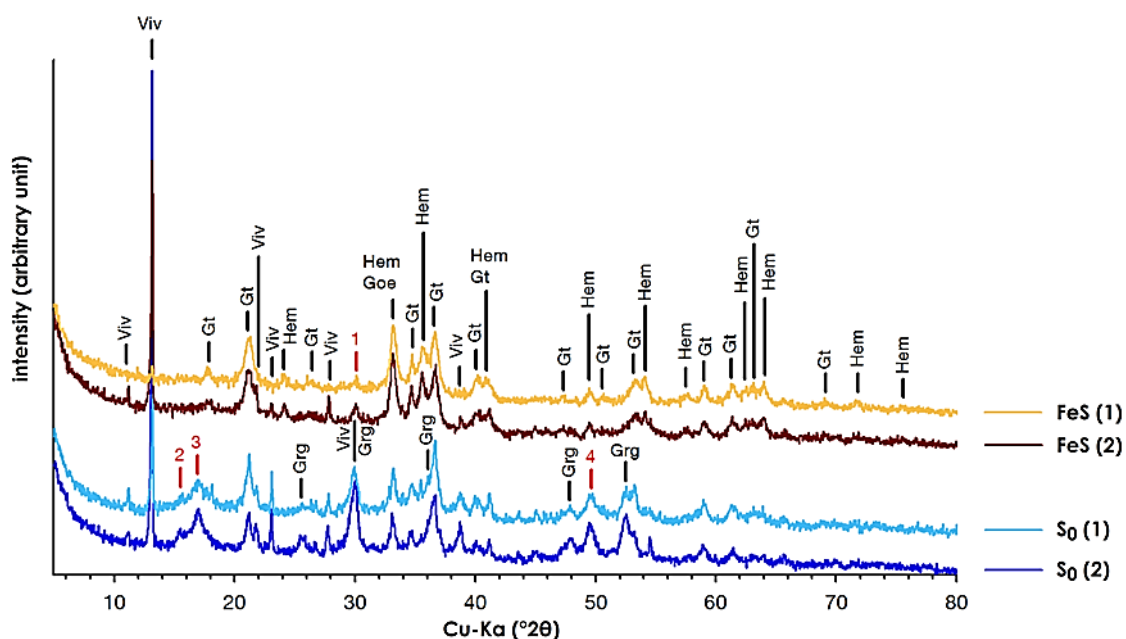


Figure 12. X-ray diffraction patterns of freeze-dried matter from the culture bottles of culture 1MN grown with FeS (yellow and brown) or elemental sulfur (light and dark blue) as electron donors each obtained from two biological replicates. Gt: goethite. Viv: vivianite. Hem: hematite. Grg: greigite. Red numbers: unresolved reflexes.

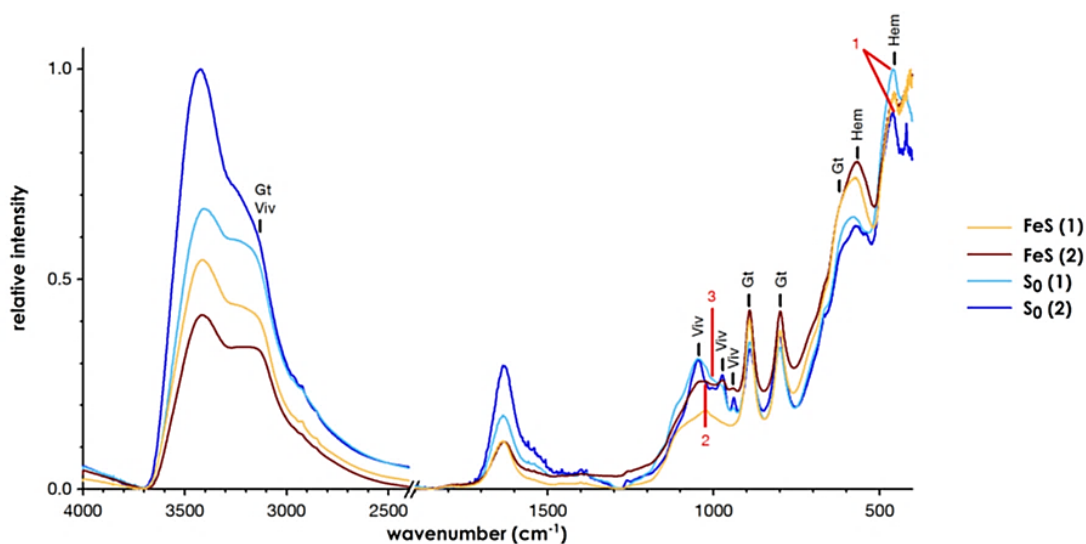


Figure 13. Transmission-Fourier transform infrared spectra of the freeze-dried matter from culture 1MN. Gt: goethite. Viv: vivianite. Hem: hematite. Red numbers: unresolved bands.

The electron recovery during growth of culture 1MN is shown in Table 6. In the original culture 1.5 mM sulfate were produced. This corresponds to the delivery of 9 mM electrons assuming elemental sulfur as electron donor. These electrons reduced 0.9 mM nitrate to ammonium and 1.7 mM ferric iron to Fe(II) which already closes the electron balance. However, sulfide concentrations also decreased by 0.6 mM during the experiment indicating the formation of iron sulfide minerals by precipitation with Fe(II) which was not captured by the sulfide measurements. As the electron balance was already closed by these reactions, 1-Methylnaphthalene likely only played a minor role as electron donor.

Incubations with FeS as electron donor showed a sulfate production of 1.1 mM corresponding to 8.8 mM electrons delivered from FeS oxidation. 11.9 mM electrons were removed by nitrate and iron reduction. The residual 3.1 mM electrons were most likely produced by FeS oxidation to elemental sulfur, as no FeS minerals were identified by XRD (Figure 12, Table 6). However, these reactions only allow for an oxidation of 2.7 mM sulfide from FeS. This “missing” FeS might indicate uncertainties during initial preparation of the media or that some iron sulfide minerals were still present after the experiment, but not clearly identified by XRD.

Table 6: Electron balance of redox reactions in culture 1MN

	1-Methylnaphthalene		FeS		S ₀	
	C [mM]	e ⁻ [mM]	C [mM]	e ⁻ [mM]	C [mM]	e ⁻ [mM]
Fe(III)/Fe(II)	-1.7	-1.7	-1.5	-1.5	-11.5	-11.5
NO₃⁻/NH₄⁺	-0.9	-7.3	-1.3	-10.4	-3.0	-24.0
SO₄²⁻/S₀	+1.5	+9.0	+1.1	+6.6	+11.5	+69.0
S₀/S²⁻	+0.6	+1.2	+0.8	+1.6	-2.2	-4.4
Unknown		-1.2		+3.7		-29.1

Negative values: electron consumption by reduction of electron acceptors. Positive values: electron production by oxidation of electron donors. Unknown: electrons consumed (negative values) or produced (positive values) that cannot be inferred from the measured concentrations (explained in main text).

In incubations with elemental sulfur as electron donor, 11.5 mM sulfate were produced over the course of the experiment. Only about 50% of the produced sulfate can be explained by sulfur oxidation coupled to nitrate and iron reduction. The production of sulfide clearly indicated sulfur disproportionation. However, the

electron balance can only be closed if about 14.6 mM S⁻² escaped the measurement by degassing of H₂S and/or precipitation as greigite. In fact, greigite was identified as main iron sulfide mineral by XRD (Figure 12, Table 6). Thus, a greigite concentration of 3.6 mM can be inferred from the from the electron balance calculations and XRD spectra. The residual 7.9 mM Fe(II) were most likely dissolved in the media and complexed during freeze-drying with phosphate leading to vivianite formation.

After 80 days of incubation, the microbial communities were analyzed with T-RFLP. Restriction fragments of 16S gene amplicons of a native 1MN culture grown with 1-methylnaphthalene were compared to the cultures amended with elemental sulfur or FeS. The original culture was mainly dominated by three T-RFs: 149, 159, and 215 (Figure 14). Pyrosequencing of 16S genes and theoretical calculation of T-RF sizes based on the restriction sites in the amplicons identified T-RFs 149 and 215 belonging to Clostridia. The closest cultivable relatives were *Calderihabitans maritimus* and *Moorella thermoacetica* within the Moorella group with only 88% similarity (Pierce *et al.* 2008; Yoneda *et al.* 2013). With an abundance of >30%, T-RF 159 was affiliated to two different sequences within the *Desulfobulbaceae* closely related (>97%) to groundwater cable bacteria and the *Desulfobulbaceae* in the benzene-degrading iron-reducing culture BF (Kunapuli *et al.* 2007) (Figure 14A). When growing the culture on FeS or elemental sulfur, Clostridia T-RFs almost completely disappeared indicating that only the *Desulfobulbaceae* were responsible sulfur oxidation coupled to nitrate and iron reduction. T-RF 159 got highly enriched in these cultures with an abundance of up to 95%. The only other prominent T-RF under these conditions had a size of 506 which could not be assigned from pyrosequencing results of the native culture (Figure 14B).

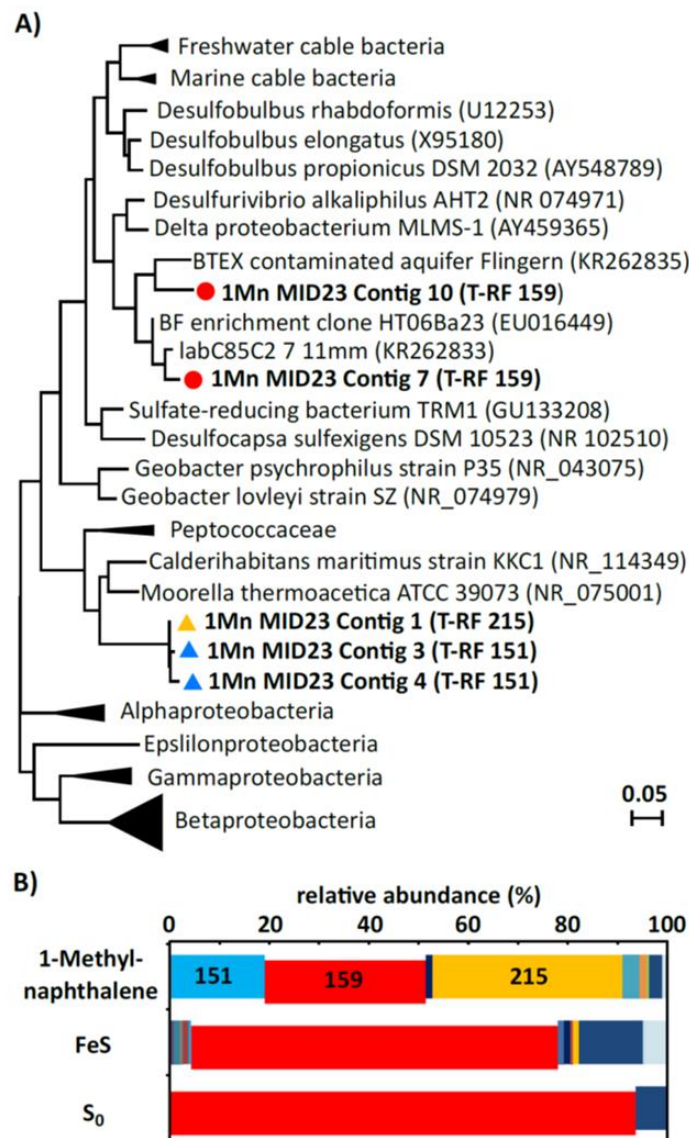


Figure 14. Bacterial community composition and phylogenetic affiliations of bacteria in culture 1MN **A)** Maximum likelihood phylogenetic tree of 16S rRNA gene sequences in culture 1MN within the Clostridia (triangles) and *Desulfobulbaceae* (red circles). Both contigs affiliated with *Desulfobulbaceae* are closely related to sequences of groundwater cable bacteria (KR262835 and KR262833) and to sequences in iron-reducing benzene-degrading culture BF. In parentheses: Predicted T-RF length of contigs with restriction enzyme MSPI. The color of each symbol reflects the respective T-RFs in B. **B)** Microbial community fingerprints by T-RFLP of 16S rRNA gene PCR amplicons of culture 1MN grown under different conditions. 1-Mn: Regular culture 1MN grown with 0.35 mM 1-methylnaphtalene and 20 mM ferrihydrite. FeS: Culture 1MN grown in the presence of 5 mM FeS and 30 mM ferrihydrite. S₀: Culture 1MN grown on elemental sulfur and 30 mM ferrihydrite.

Fluorescence in situ hybridization with the specific probes FliDSB194 and DSB706 for groundwater cable bacteria and *Desulfobulbaceae* revealed hybridization for filaments of 1-1.5 μm width and several hundred micrometers length. However, the high background fluorescence created by the iron oxides in the incubations often hampered filament detection. Besides these long filaments, also shorter filaments and single cells were identified as *Desulfobulbaceae* by FISH. The filamentous *Desulfobulbaceae* were frequently attached with one end to iron minerals (Figure 15).

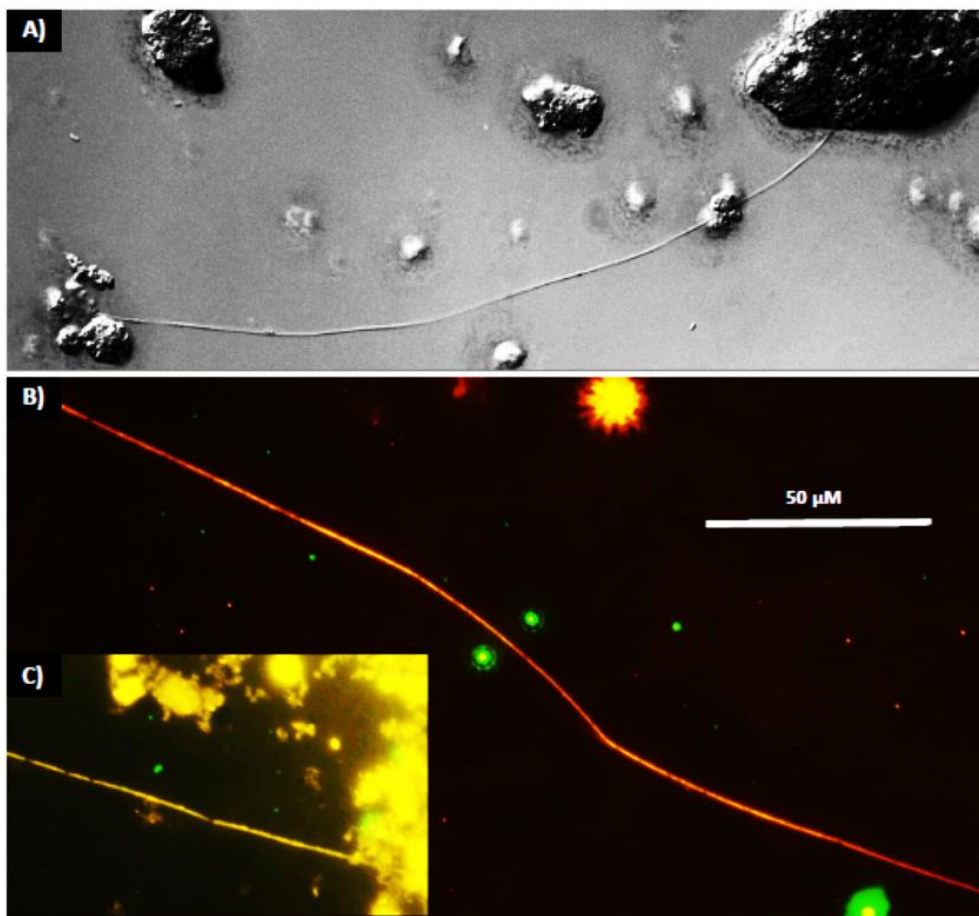


Figure 15. Filaments in culture 1MN. **A)** Filament attached to iron particles observed by light microscopy. The picture was created by focus-z-stacking of six individual pictures with picolay (www.picolay.de). **B, C)** Fluorescence in situ hybridization of filaments in 1MN. Picture are shown as overlays of two pictures taken with filters for FAM-labeled probe FLIDSB194 (red) for groundwater cable bacteria and Cy3-labeled probe DSB706 (green) for *Desulfobulbaceae*. Yellow labeling indicates that both probes were positively hybridizing. The scale bar in B) applies to all pictures in Figure 3.

3.4. Geochemistry of Dissolved Organic Matter in a Spatially Highly Resolved Groundwater Petroleum Hydrocarbon Plume Cross-Section

The aim of this study was to combine on-site high resolution spatial sampling across a well-defined petroleum hydrocarbon plume with high resolution molecular characterization of DOM to study the interaction of the contaminants in addition to redox processes and their reaction products with natural DOM. Samples collected from the petroleum hydrocarbon contaminated aquifer in Düsseldorf Flingern showed steep small-scale gradients for monocyclic aromatic hydrocarbons of the BTEX-group (Benzene, Toluene, Ethylbenzene, Xylenes) and naphthalene as the major contaminants (Figure 16 A, B). The contaminant plume, at the time of sampling, was located at the groundwater table extending to 0.8 m beneath (6.51–7.31 m below surface (bls)).

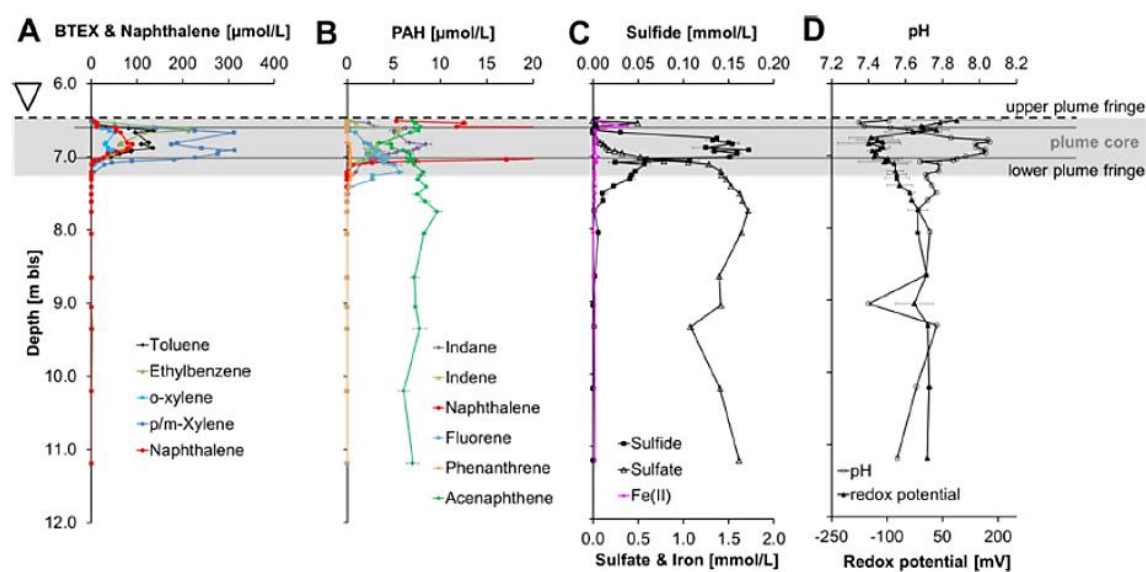


Figure 16. High-resolution vertical concentration profiles at the Düsseldorf-Flingern site of BTEX (A), PAHs (B), sulfide, sulfate, iron (C) and hydro-chemical parameters pH and redox potential (D) in groundwater sampled from the tar-oil contaminated aquifer in Düsseldorf-Flingern (Dvorski *et al.* 2016).

According to the scheme of Anneser *et al.*, the contaminant plume was subdivided into three compartments (Figure 16) (Anneser *et al.* 2008). The first, the plume core, was defined as the zone exhibiting BTEX concentrations $>50\%$ of the observed maximum of $616 \mu\text{mol/L}$ (6.61–7.01 m bls). The second compartment, the upper

plume fringe (6.51–6.61 m bls), was bound at the upper side by the groundwater table including the capillary fringe, which was located right above the groundwater table and only partially filled with water. The lower plume fringe, which was the third compartment and located below the plume core, extended from 7.01–7.31 m bls.

Polycyclic aromatic hydrocarbons (PAHs), in particular naphthalene, exhibited a high abundance (maximum of 89.5 $\mu\text{mol/L}$ at 6.78 m bls) in the plume core (Figure 16A, B). The three-ring PAHs showed highest abundances ~ 0.3 m deeper (Figure 16A, B). Acenaphthene was present at approximate concentrations of 7 $\mu\text{mol/L}$ all along the sampled vertical profile (Figure 16B).

Redox potentials between +89 mV at the groundwater table and –149 mV in the plume core indicated strictly anoxic conditions except for the capillary fringe (Figure 16D). The pH profile showed elevated values of up to pH 8.05 in the plume core and a minimum of pH 7.35 at the upper plume fringe (Figure 16D).

Sulfate as the predominant electron acceptor was almost absent in the plume core and showed a steep counter gradient to the major contaminants at the lower plume fringe. Outside of the contaminant plume, sulfate exhibited a rather constant high concentration of approximately 1.5 mmol/L (Figure 16C). Sulfide peaked at concentrations of up to 0.17 mmol/L in the plume core and lower plume fringe. Extraordinary high Fe(II) concentrations of up to 0.38 mmol/L were found close to the groundwater table.

(–)ESI FT-ICR-MS spectra from solid phase extracted DOM (SPE-DOM) showed distinct compositional variation along the aquifer (Figure 18A). In general, sample similarity followed spatial proximity, and hierarchical cluster analysis revealed three distinct subclusters, 6.51–6.64 m bls, 6.67–7.06 m bls, and 7.08–10.20 m bls (Figure 17A). The extensive chemical dissimilarity between the subclusters is depicted in Figure 17B. The van Krevelen diagrams and ring charts display the most representative molecular formulas (correlation coefficient $r > 0.9$) for each subcluster. The differences between (–)ESI FT-ICR mass spectra of the SPE-DOM isolates corresponded to the respective prevailing and clearly distinct zone-dependent redox chemistry (Figure 16 and Figure 18A). The specific DOM chemistry in the upper part of the aquifer, including the upper fringe, plume core,

and 5 cm of the lower plume fringe (cf. blue and red subcluster, Figure 17), was dominated by sulfur organic molecules.

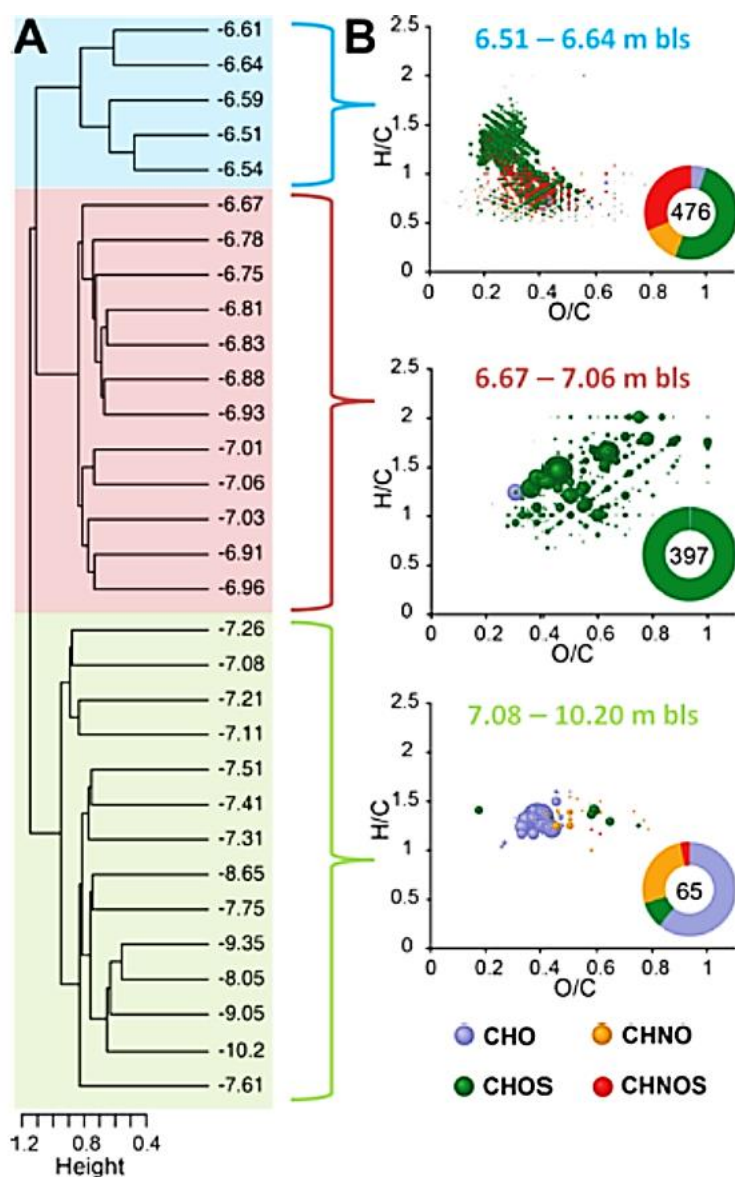


Figure 17. (A) Hierarchical cluster analysis of the assigned (-)ESI FT-ICR-MS derived molecular formulas observed in SPE-DOM along the aquifer with samples named according to their sampling depth (bls = below surface). (B) Van Krevelen diagrams depict the most representative characteristic molecular formulas (correlation coefficient >0.9; cf. SI) for the three main subclusters, representing the specific DOM chemistry. Elemental composition of the molecular formulas are represented as CHO (blue), CHNO (orange), CHOS (green), and CHNOS (red), and the bubble area depicts the mean mass peak intensity within the respective subcluster.

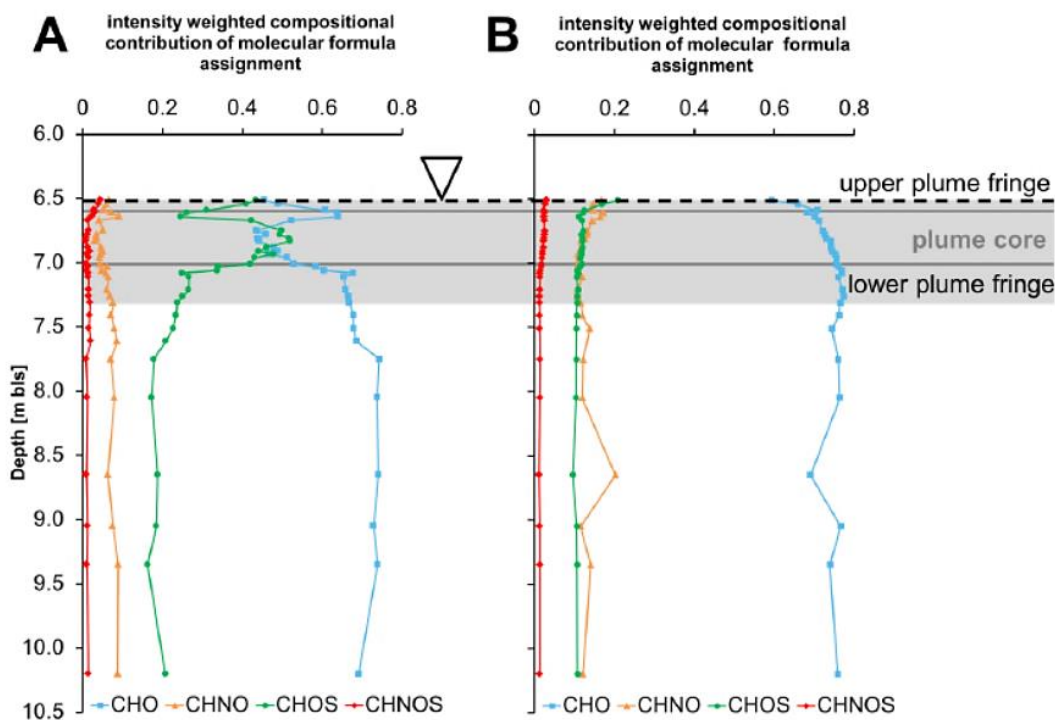


Figure 18. (A) (-)ESI and **(B)** (+)APPI FT-ICR mass spectra derived intensity weighted compositions of assigned molecular formulas showed increased contribution of CHOS and decreased CHO compounds in the highly sulfidic region from 6.67–7.06 m bls in (-)ESI FT-ICR mass spectra. (+) APPI FT-ICR mass spectra did not show this trend, thereby suggesting that CHOS compounds were formed from highly functionalized CHO molecules as a result of bacterial sulfate reduction.

The samples from 6.67–7.06 m bls (red subcluster, Figure 19) were dominated by CHOS compounds with a contribution to the total intensity of assigned molecular formulas of up to 52% (Figure 18A). The relative proportion of CHO compounds from 6.67–7.06 m bls decreased (Figure 18A). With respect to contaminants, the influence of ionizable aromatic molecules ($H/C < 1$) was higher in the top centimeters close to the groundwater table, thereby indicating fewer degraded contaminants present inside the upper plume fringe. A substantial portion of characteristic CHNO and especially CHNOS compounds suggested significant nitrogen DOM chemistry in the upper plume fringe where dissolved sulfide was almost absent. The characteristic mass peaks of SPE-DOM from the deep zone below 7.08 m bls showed mainly CHO and CHNO compounds in the polyphenolic region of the van Krevelen diagram ($1.5 > H/C > 0.7$ and $0.7 > O/C > 0.1$) (Figure 17).

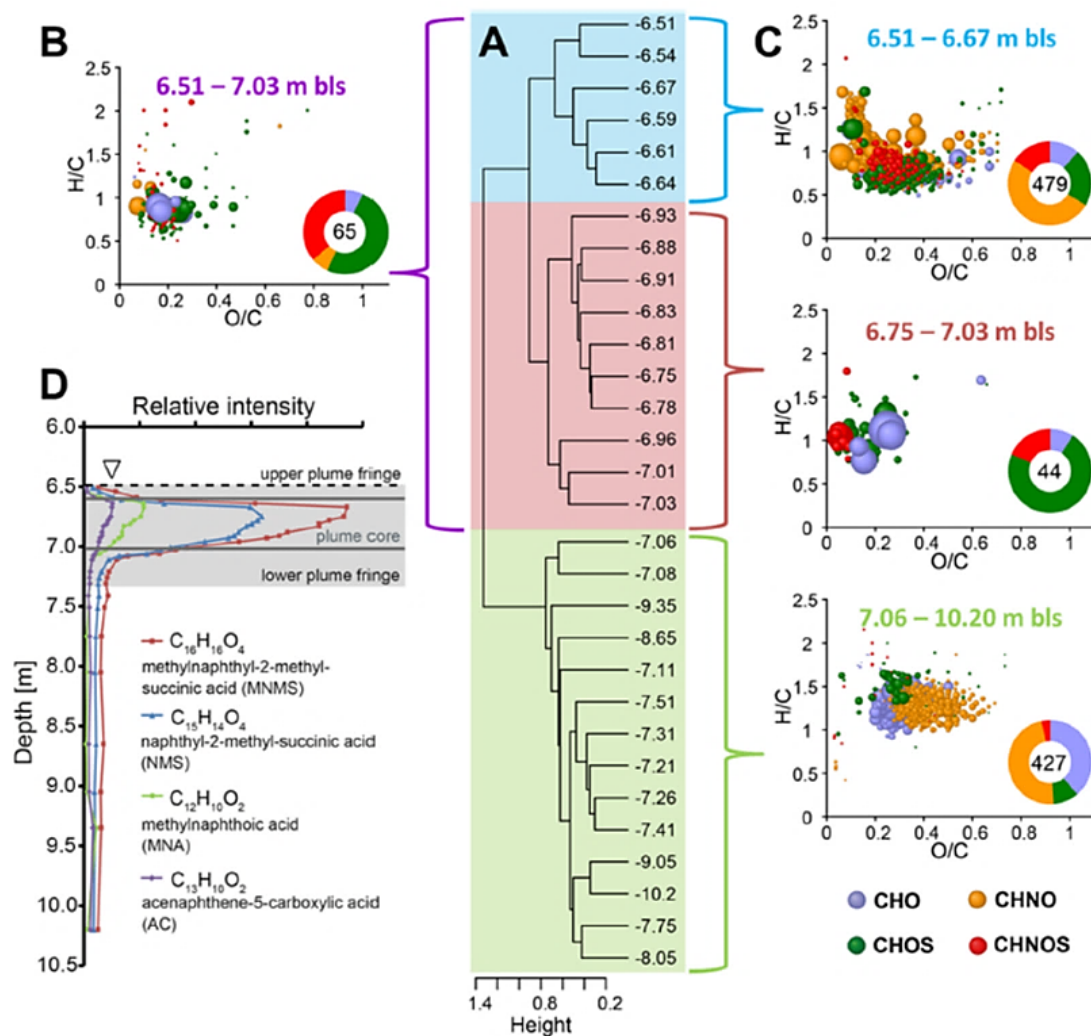


Figure 19. (A) Hierarchical cluster analysis of the assigned (+)APPI FT-ICR-MS derived molecular formulas observed in SPE-DOM along the aquifer with samples named according to their sampling depth. **(B)** Van Krevelen diagram of shared characteristic molecular formulas of the two upper subclusters, which were highly affected by the contamination plume and **(C)** van Krevelen diagrams of the characteristic molecular formulas for the three main subclusters representing the specific SPE-DOM chemistry. Elemental composition of the molecular formulas are represented as CHO (blue), CHNO (orange), CHOS (green), and CHNOS (red), and the bubble area depicts the mean mass peak intensity within the respective subcluster. Note that the size of the three and four most abundant CHO (blue) bubbles of the purple **(B)** and red subcluster **(C)** had to be downsized because of their very high mass peak intensity. **(D)** (+)APPI FT-ICR-MS derived abundance profile of main petroleum contamination degradation products.

Hierarchical cluster analysis of (+)APPI FT-ICR mass peaks and the associated van Krevelen diagrams of characteristic molecular formulas of the subclusters showed that all samples above 7.06 m bls were dominated by aromatic and even condensed

aromatic molecules (low H/C and O/C ratios) (Figure 19B, C). These molecules are typically derived from petroleum; thus, the segmentation of the cluster was clearly driven by the elevated contamination input in the top ~50 cm beneath the groundwater table (6.54 m bls). Analogous to the (-)ESI FT-ICR-MS results, the proportion of characteristic CHNO and CHNOS compounds in the contamination plume and fringes was greater in the samples taken close to the groundwater table. Furthermore, (+)APPI FT-ICR-MS showed that a large proportion of characteristic formulas were sulfur organic compounds, which was in accordance with the (-)ESI FT-ICR-MS results (Figure 19B, C). However, the intensity-weighted contribution of assigned molecular formulas did not show any clear trend in the highly sulfidic region (Figure 18B). On the contrary, SPE-DOM isolates from the deeper zone of the aquifer were characterized by a large combined abundance (greater 80% of the observed characteristic mass peaks describing the overall diversity) of CHO and CHNO compounds with $1.5 > \text{H/C} > 1$ and $0.6 > \text{O/C} > 0.2$ (Figure 19, note that due to limitations in the visualization, CHO compounds are partially hidden by the CHNO compounds).

Field and culture degradation studies of BTEX, PAHs, and heteroatom PAHs at the same or similar conditions identified typical degradation products (Coble 1996; Annweiler *et al.* 2001; Martus and Püttmann 2003; Safinowski *et al.* 2006; Jobelius *et al.* 2010; Jarling *et al.* 2015). Due to the high accuracy in molecular formula annotation combined with the profound literature knowledge, the respective mass peaks most probably derive from these known degradation products. Figure 19D shows the relative mass peak intensities for the four highest abundant putative degradation products originating from BTEX, PAHs, and heteroatom PAHs as well as their methylated relatives methyl-naphthyl-2-methylsuccinic acid (MNMS, $\text{C}_{16}\text{H}_{16}\text{O}_4$), naphthyl-2-methyl-succinic acid (NMS, $\text{C}_{15}\text{H}_{14}\text{O}_4$), methyl-naphthoic acid (MNA, $\text{C}_{12}\text{H}_{10}\text{O}_2$), and acenaphthene-5-carboxylic acid (AC, $\text{C}_{13}\text{H}_{10}\text{O}_2$) (Annweiler *et al.* 2001; Martus and Püttmann 2003; Griebler *et al.* 2004; Safinowski *et al.* 2006; Jobelius *et al.* 2010; Jarling *et al.* 2015). The depth profile was in accordance with the distribution of plume marker compounds, hydrochemical parameters, and redox chemistry markers (Figure 16 and Figure 19D). Moreover, MNMS, NMS, AC, and an unknown compound ($\text{C}_{15}\text{H}_{12}\text{O}_2$) represented the highly abundant characteristic masses of the 6.75 to 7.03 m bls subcluster (Figure 19).

4. Discussion

4.1. Long-distance Electron Transfer by Cable Bacteria in Aquifer Sediments

Recently, filamentous cable bacteria were discovered in organic-rich marine sediments to spatially bridge the redox half reactions of sulfide oxidation and oxygen reduction via long-distance electron transfer (LDET) over 1-2 cm (Nielsen *et al.* 2010; Pfeffer *et al.* 2012; Malkin *et al.* 2014). Here, I investigated if microbially mediated LDET may also occur in freshwater sediments, specifically in hydrocarbon-contaminated groundwater, where it could recycle sulfate as electron acceptor and thus increase biodegradation rates.

In FeS-amended laboratory incubations of sediments from the investigated site, a suboxic zone developed with no detectable oxygen or sulfide but with distinct cathodic pH maxima and anodic pH minima indicative of LDET (Nielsen *et al.* 2010). Oxygen only penetrated 8 mm into the sediment and yet served as a direct sink for electrons from oxidation of sulfide up to 19 mm below, congruent with the LDET hypothesis. The calculated current density between the oxic and the anoxic layers was higher than $1.5 \text{ mA} / \text{m}^2$ corresponding to a cathodic oxygen consumption of $340 \text{ } \mu\text{mol m}^{-2} \text{ d}^{-1}$ and representing 40% of the total oxygen consumption. This calculation does not include calcite precipitation and ferrous iron oxidation and might therefore underestimate cathodic oxygen consumption (Risgaard-Petersen *et al.* 2014). Moreover, the coarse sediment did not allow for microsensor measurements of pH profiles, but only for a macroelectrode with a tip size of 3 mm at a resolution of 1 mm. This smoothed the pH profile, resulting in lower calculated alkalinity fluxes and cathodic oxygen consumption. So, the electron transfer rate inferred for groundwater cable bacteria was 1-2 orders of magnitude lower than the 4.6 to 92 mA m^{-2} reported for marine sediments (Nielsen *et al.* 2010; Nielsen and Risgaard-Petersen 2015). This discrepancy could be also caused – besides the underestimation of fluxes – by up to 100-fold lower sulfide concentrations in the investigated sediment compared to marine sediments (Rao *et al.* 2016).

16S rRNA gene sequencing and FISH identified groundwater cable bacteria as members of the *Desulfobulbaceae*. The marine cable bacteria are only distantly related with 88% similarity on 16S rRNA level. The closest cultivated relative with 91% 16S rRNA gene similarity was *Desulfurivibrio alkaliphilus* AHT 2, which can grow chemo-litho-auto-trophically with H₂ as electron donor. The strain cannot perform sulfate reduction but utilizes elemental sulfur, thiosulfate, and nitrate as electron acceptor (Sorokin *et al.* 2008). The genome exhibits a complete aerobic respiratory chain with a terminal cytochrome c oxidase *cbb3* type. Sox genes for sulfide oxidation are not present, but a reverse sulfate reduction pathway seems possible. The second-most closely related chemo-litho-auto-trophic organism, the arsenate-reducing strain MLMS-1, is able to grow with sulfide as electron donor and shows 90% 16S rRNA gene similarity to the groundwater cable bacteria (Hoeft *et al.* 2004).

The high abundance of cable bacteria at the oxic-anoxic interface of aquifers indicates an ecological competitiveness to other sulfide-oxidizing, chemo-litho-auto-trophs such as e.g. *Thiobacillus*. A possible explanation is fluctuations of the groundwater table leading to shifting redox gradients at the capillary fringe (Meckenstock *et al.* 2015). Under such dynamic conditions, uni-cellular microorganisms will often not be located in the zone of overlapping counter-gradients and lack either electron donor or acceptor. Such unfavorable conditions can be overcome by spatially decoupling of the oxidation and reduction half reactions by cable bacteria. Only some cells at both ends of the filaments need to have access to electron donors or acceptors, respectively. Thus, cable bacteria could still be active as long as the spatial shifts of redox gradients do not exceed the lengths of the filaments. Even though, groundwater table fluctuations of around 20 cm within one year have been reported from this site (Einsiedl *et al.* 2015), cable bacteria could still have a competitive advantage by buffering short-term fluctuations in a smaller scale. Cable bacteria can also adapt rapidly to changing conditions, as it was shown for laboratory incubations (Nielsen *et al.* 2010) and seasonal hypoxic basins (Seitaj *et al.* 2015). The longest filament which could be found microscopically was approximately 5 mm. However, natural filaments and cable networks which are not disrupted by sampling could be much longer. For marine

sediments, fragments lengths of filaments up to 1.5 cm have been reported (Pfeffer *et al.* 2012).

The detection of LDET in situ remains a difficult task. The monitoring well provided water samples at 3 cm vertical resolution. Although this is probably the highest resolution for water sampling in aquifers of that depths reported to date, it is obviously not sufficient to record pH profiles at the mm range, which might be necessary to map LDET in situ. Moreover, pH profiles could also not be determined from fresh sediment cores, since cores commonly de-water upon retrieval during drilling, prohibiting the reconstruction of pore water geochemistry. Thus, analyzing sediment cores with molecular and microscopic tools is the only reliable way for detecting cable bacteria in aquifers so far. However, LDET might potentially be traced in situ by remotely assessing associated electric fields (Revil *et al.* 2010; Risgaard-Petersen *et al.* 2014; Revil *et al.* 2015). In fact, my results provide the first field evidence for bio-geobatteries in aquifers comprising cable bacteria as electron conductors (Revil *et al.*, 2010). By oxidizing sulfide, groundwater cable bacteria resemble the anode of a microbial fuel cell. Revil *et al.* 2015 showed direct oxidation of propylene glycol by electric currents through a conductive iron body in laboratory experiments (Revil *et al.* 2015). Such electric currents create electric potential anomalies which might be a good monitoring tool for localizing hotspots of LDET in situ (Naudet *et al.* 2004; Atekwana and Slater 2009; Revil *et al.* 2010; Revil *et al.* 2015). However, the direct link between LDET and the observation of electric potentials at contaminated sites still remains to be proven.

Our field geochemical data indicated that oxygen and nitrate were at least 6 cm apart from detectable dissolved sulfide. Since only distances below 3 cm for LDET have been reported so far, LDET might be fueled by other reduced sulfur compounds as electron donor such as precipitated FeS. This would be supported by the laboratory incubations where FeS turned out to be an excellent electron donor for LDET. It is also likely that sulfide produced by sulfate reducing toluene degradation is immediately re-oxidized by LDET (Figure 21B) or precipitated as FeS. In fact, a previous study conducted at the same site demonstrated strong sulfur cycling at the upper plume fringe, the place of LDET reported here (Einsiedl *et al.* 2015).

4.2. Cable Bacteria Couple Nitrate Reduction to Iron and Sulfur Cycles in Anaerobic Enrichment Culture

The iron-reducing enrichment culture 1MN was capable of growing in medium amended with 1-methylnaphthalene, elemental sulfur, and FeS as electron donor in the presence of ferrihydrite and nitrate as electron acceptors. Astonishingly, the culture produced sulfate, ferrous iron, and sulfide simultaneously during growth on 1-methylnaphthalene and elemental sulfur. Thus, sulfur disproportionation, abiotic reduction of ferrihydrite by sulfide, and FeS oxidation with nitrate as electron acceptor were taking place at the same time leading to a direct coupling of iron and sulfur cycle in 1MN. Based on time series of reduced and oxidized species involved in iron and sulfur cycling as well as estimations for nitrate concentrations during growth of 1MN, a conceptual model for redox cycling processes can be developed (Figure 20).

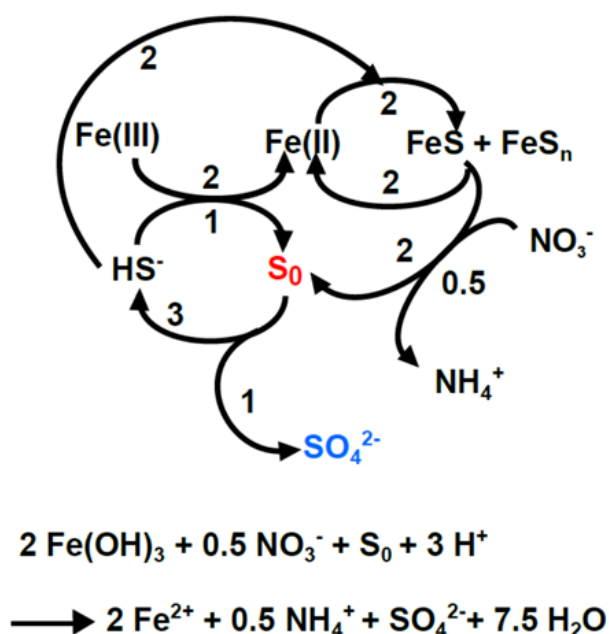
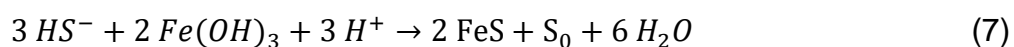


Figure 20. Conceptual model of reactions involved in nitrogen, iron, and sulfur metabolism in culture 1MN during growth with 1-methylnaphthalene, FeS, and elemental sulfur as electron donors with ferrihydrite and nitrate as electron acceptors. Numbers on arrows indicate stoichiometric factors of each reaction. Below: net reaction of the cycling processes if all reactants are sufficiently available in the culture in the absence of limiting reaction steps.

Prior to inoculation, the reducing agent Na₂S already reacted with ferrihydrite abiotically according to (Melton *et al.* 2014):



Polysulfide as precursor of pyrite formation might also have been formed by this reaction (Wan *et al.* 2014). Pyrite formation might also explain the decrease in sulfide and iron extractable with 1 M HCl in both active and abiotic settings. When growing the culture with 1-methylnaphthalene as electron donor, the production of sulfate, Fe(II), and sulfide in parallel after 36 days of incubation indicated growth of culture 1MN by sulfur disproportionation. However, the 2 mM sulfide initially used for reduction of the medium would have only provided about 0.7 mM elemental sulfur according to the stoichiometry of equation 7. Based on a sulfate to sulfide ratio of 1:3 for sulfur disproportionation, only 0.2 mM sulfate and 0.5 mM sulfide could have been produced from sulfur disproportionation alone unless the elemental sulfur pool was replenished by sulfide oxidation to elemental sulfur by the residual nitrate in the medium. A complete oxidation of the sulfide from FeS to sulfate by nitrate reduction can explain the high sulfate concentrations, but not the parallel increase in Fe(II) and sulfide. Consequently, FeS was incompletely oxidized by nitrate to elemental sulfur which was then disproportionated to sulfate and sulfide. Again, the sulfide could have abiotically reacted with ferrihydrite to elemental sulfur and FeS and thereby closing the cycle.

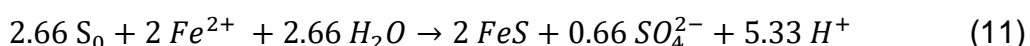
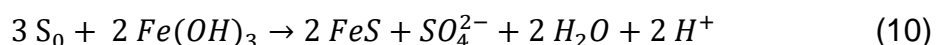
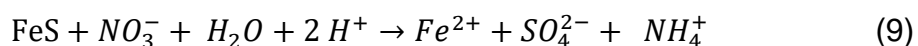
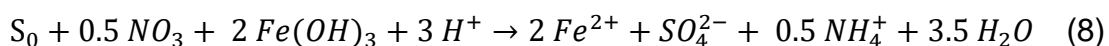
Incubations with FeS as sole electron donor showed FeS oxidation by nitrate to sulfate and Fe(II). Nitrate was converted completely to ammonium with about the same amount of sulfate produced over the course of the experiment. Nevertheless, this does not exclude a partial oxidation of FeS to elemental sulfur for sulfur disproportionation. Electron balance calculations as well as the absence of ferrous sulfide minerals in the XRD spectra support this assumption. In this case, free sulfide can directly precipitate with free Fe(II) which might explain the low amount of Fe(II) produced.

The most extensive metabolism was observed in inoculations with elemental sulfur as sole electron donor with ferrihydrite and nitrate as electron acceptor. The parallel increase in sulfate and Fe(II) indicated strong sulfur disproportionation. Most likely,

the product sulfide reduced ferrihydrite abiotically to FeS which was then re-oxidized to elemental sulfur with nitrate as electron acceptor. Even though nitrate was completely converted to ammonium, the electron balance can only be closed if S²⁻ was mainly present as iron sulfide minerals and therefore escaped the measurements. This is consistent with the detection of greigite by XRD after the course of the experiment. Electron balances indicate concentrations of 3.6 mM greigite and 7.9 mM dissolved Fe(II). Together with the 2.2 mM dissolved sulfide in the medium the total concentration of S²⁻ can be estimated to be 16.8 mM leading to a sulfide to Fe(II) ratio of around 3:2 which is consistent with values from literature. For instance, a production of FeS and FeS₂ in a 1:1 ratio is documented for sulfur disproportionating *Desulfocapsa sulfexigens* (Finster et al. 1998). There, iron sulfides were quantified as acid volatile sulfides and chromium reducible sulfides. A determination of the iron mineral composition by XRD might have also revealed predominant greigite formation.

Surprisingly, goethite and hematite were detected as dominant ferric iron minerals after the experiments by XRD and FTIR. This might indicate a transformation from ferrihydrite to more stable iron minerals catalyzed by aqueous Fe(II) as previously described (Pedersen *et al.* 2005). However, also a production of goethite during synthesis of ferrihydrite is possible, as the mineral composition of ferric iron was not measured before the experiments.

Taken together, I propose that sulfide produced by sulfur disproportionation reduced ferrihydrite. This led to recycling of elemental sulfur and formation of reduced, ferrous iron in culture 1MN. The ferrous iron can further react with additional sulfide to FeS. The sulfide from FeS is then oxidized by nitrate to elemental sulfur and liberation of Fe(II) depending on the presence or absence of nitrate and ferrihydrite. This led to the following net reactions:



As long as nitrate was sufficiently present, the pH increased for both FeS and S₀ as electron donor (Equations 8 and 9). When nitrate is depleted microbial growth proceeds via sulfur disproportionation leading to acidification of the medium (Equations 10 and 11) which is in consistence with the pH measurements during growth of 1MN (Figure 11).

T-RFLP and pyrosequencing showed a high enrichment of *Desulfobulbaceae* during growth on elemental sulfur and FeS. This indicates that *Desulfobulbaceae* with more than 90% abundance are the main catalysts of sulfur cycling coupled to iron and nitrate reduction. *Clostridia* represented by the most prominent T-RFs 149 and 215 played no role at all when growing with elemental sulfur or FeS. In fact, the *Clostridia* in culture 1MN were identified as the main 1-methylnaphthalene degraders by stable isotope probing in a different study which is not part of this thesis (unpublished results).

Fluorescence in situ hybridization detected long filamentous bacteria with similar morphology to groundwater cable bacteria as members of the *Desulfobulbaceae*. Besides the filamentous morphology, also single cells were positively labeled for *Desulfobulbaceae*. Therefore, cable bacteria in the 1MN culture might not be obligate filaments, but can also grow as single cells.

Cable bacteria might have lived from FeS oxidation with nitrate as electron acceptor, as previously shown for incubations of marine sediments (Marzocchi *et al.* 2014). As ferrihydrite and elemental sulfur deposited to the bottom of the bottles in contrast to nitrate which was freely dissolved in the medium, FeS oxidation and nitrate reduction might have been spatially separated. Such conditions could promote cable bacterial growth by long-distance electron transfer.

From a thermodynamic point of view, cable bacteria might facilitate sulfur disproportionation by keeping concentrations of free sulfide by oxidizing sulfide to elemental sulfur coupled to reduction of nitrate. In fact, first indications for high rates of sulfur disproportionation have been found in marine sediments in the presence of cable bacteria (Rao *et al.* 2016; Vasquez-Cardenas *et al.* 2015; van de Velde *et al.* 2016). In culture 1MN, a strong enrichment of *Desulfobulbaceae* was observed concomitant with sulfur disproportionation. At the beginning of the growth

experiments, nitrate was present which was not completely removed by washing after the synthesis of ferrihydrite from $\text{Fe}(\text{NO}_3)_3$. Nevertheless, cable bacteria formed a stable community in culture 1MN for more than a decade when ferrihydrite was synthesized from $\text{Fe}(\text{Cl})_3$ in the absence of nitrate as electron acceptor. Intriguingly, sulfur disproportionation leads to acidity production and might contribute to the anodic pH minimum during long-distance electron transfer.

4.3. Geochemistry of Dissolved Organic Matter in a Spatially Highly Resolved Groundwater Petroleum Hydrocarbon Plume Cross-Section

Dissolved organic matter (DOM) in pristine groundwater is generally composed of organic molecules from natural carbon sources, such as plants, microbes, and fungi, whereas DOM at contaminated sites considerably derives from the anthropogenic carbon input (Shen *et al.* 2015). Biogeochemical gradients and distribution patterns of major contaminants and signature metabolites provide critical information on the redox processes involved in transformation of contaminants and active biodegradation pathways (Meckenstock *et al.* 2015). Typically, biodegradation in organic contaminant plumes in porous aquifers is most pronounced at the plume fringes as repeatedly confirmed by (1) steep and opposing gradients of contaminants and electron acceptors such as sulfate, (2) peaking of the metabolic end products sulfide and Fe(II) from sulfate and iron reduction, respectively, and (3) bacterial cell counts and contaminant specific stable carbon isotope values at the plume fringes (Anneser *et al.* 2008; Bauer *et al.* 2008; Meckenstock *et al.* 2015).

Analysis of groundwater sampled in high-resolution at the Düsseldorf-Flingern site showed a comparable distribution of the major contaminants like in previous studies, however, with slightly different concentrations of the individual compounds (Anneser *et al.* 2008). As already shown in previous studies (Anneser *et al.* 2008; Winderl *et al.* 2008; Anneser *et al.* 2010), sulfate reduction was the key redox process involved in biodegradation of organic contaminants in the Düsseldorf-Flingern aquifer. However, in contrast to earlier surveys, sulfate, sulfide, and BTEX profiles indicated biodegradation by sulfate reduction taking place not only at the lower plume fringe but also in parts of the plume core. These changing patterns may be related to temporal dynamics of contaminant concentrations and biodegradation activities.

The high Fe(II) concentrations at the upper plume fringe indicated, in accordance with previous studies (Anneser *et al.* 2008), iron reduction to be a relevant redox process in the aquifer.

Non-targeted high resolution analytics in combination with spatially highly resolved sampling revealed DOM signatures from petroleum contaminants and specific degradation products (Figure 17). Additionally, this approach enabled a comprehensive molecular level understanding of natural DOM and its role in petroleum hydrocarbon bioremediation. Previous studies at the investigated site identified bacterial sulfate reduction as the major redox process involved in the contaminant biodegradation by isotope ratio analysis (Anneser *et al.* 2008; Anneser *et al.* 2010). The current study demonstrates that the DOM characteristics were highly affected by bacterial sulfate reduction. Both (+)APPI FT-ICR-MS, which favors the detection of petroleum derived compounds, and (-)ESI FTICR- MS, which is preferably applied for the characterization of natural DOM, revealed characteristic CHOS compounds at the depths where sulfate reduction is active. Organosulfur compounds were found by far more abundant in the (-)ESI FT-ICR mass spectra (Figure 18). Thus, reduced sulfur mainly reacts with natural DOM. CHOS compounds represented >50% of the total mass peak intensity of the corresponding assigned molecular formulas derived from (-)ESI FT-ICR mass spectra in the zone with maximum sulfide concentrations (Figure 16, Figure 17, Figure 18).

Especially in zones where Fe(II) and other complexation partners were limited, sulfide remained in solution. Contaminant biodegradation is limited by the availability of sulfate as electron acceptor at the investigated site. Elevated sulfide concentrations may even further decelerate petroleum biodegradation at low sulfate concentrations; indeed, high concentrations of sulfide are toxic to many microbes (Muyzer and Stams 2008). In this context, natural DOM may act as a beneficial key player in the mediation of sulfide resulting from bacterial sulfate reduction. In consequence, natural DOM may be applied in bioremediation.

5. Conclusions and Outlook

The discovery of LDET catalyzed by cable bacteria in laboratory incubations with sediments from hydrocarbon-contaminated aquifers might provide a new perspective of microbial activities at the capillary or plume fringes. Even though the presence of cable bacteria at the plume fringes provides a first evidence for LDET in situ, the quantitative impact on the biogeochemistry and contaminant degradation remains to be investigated. The electric short-cut by the filaments could strongly increase electron fluxes (Risgaard-Petersen *et al.* 2014) across redox interphases (Figure 21).

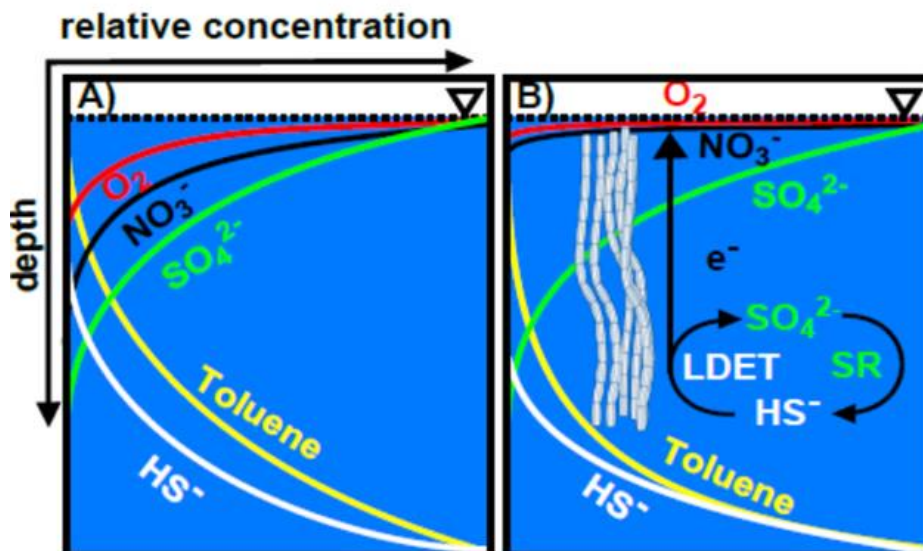


Figure 21. Conceptual model of the impact of LDET by cable bacteria on sulfur cycling and contaminant degradation at the plume fringe. **A)** Redox zonation at a toluene plume fringe only controlled by dispersive/diffusive mixing in the absence of cable bacteria. **B)** A plume fringe scenario including sulfide re-oxidation by cable bacteria leads to higher availability of sulfate for toluene degradation by sulfate reduction (SR) and a broader zone of biodegradation at the plume fringes. Steeper gradients indicate higher fluxes of solutes.

Thus, it could extend the recently established plume fringe concept (Cirpka *et al.* 1999; Mayer *et al.* 2001; Thornton *et al.* 2001; Maier and Grathwohl 2006; Anneser *et al.* 2008; Bauer *et al.* 2008; Winderl *et al.* 2008; Meckenstock *et al.* 2015), which states that electron acceptors are depleted in the core of contaminant plumes. Biodegradation is accordingly restricted to the plume fringes where electron acceptors are supplied from the outside by dispersion or diffusion (Figure 21A).

Recycling of sulfate by LDET at the plume fringes might overcome the spatial separation of electron donors and acceptors to a certain extent and consequently lead to an enhancement of biodegradation as compared to a system otherwise fully controlled by dispersion (Figure 21B) (Anneser *et al.* 2008; Bauer *et al.* 2008; Anneser *et al.* 2010; Pilloni *et al.* 2011).

High resolution mass spectrometry showed that dissolved organic matter composition is strongly influenced by the sulfur chemistry in the tar oil contaminated aquifer in Düsseldorf-Flingern. By removing toxic sulfide as product of sulfate reduction, natural dissolved organic matter might support microbial contaminant degradation.

The presence of groundwater cable bacteria together with hydrocarbon degraders in the 1-methylnaphthalene degrading culture 1MN over years is the first evidence that cable bacteria might support contaminant degradation. Indeed, recent findings show that *Desulfobulbaceae* were enriched at the anode of microbial fuel cells powered with toluene as substrate (Daghio *et al.* 2016). The production of sulfate supports the proposal of the recycling of electron acceptors for hydrocarbon degradation by cable bacteria.

6. References

- American Public Health Association, American Water Works Association, Water Environment Federation. (1998). *Standard methods for the examination of water and wastewater*, 20th (edn). Washington, DC.
- Anneser B, Einsiedl F, Meckenstock RU, Richters L, Wisotzky F, Griebl C (2008). High-resolution monitoring of biogeochemical gradients in a tar oil-contaminated aquifer. *Applied Geochemistry* **23**: 1715-1730.
- Anneser B, Pilloni G, Bayer A, Lueders T, Griebl C, Einsiedl F *et al.* (2010). High Resolution Analysis of Contaminated Aquifer Sediments and Groundwater—What Can be Learned in Terms of Natural Attenuation? *Geomicrobiology Journal* **27**: 130-142.
- Annweiler E, Michaelis W, Meckenstock RU (2001). Anaerobic cometabolic conversion of benzothiophene by a sulfate-reducing enrichment culture and in a tar-oil-contaminated aquifer. *Applied and environmental microbiology* **67**: 5077-5083.
- Atekwana EA, Slater LD (2009). Biogeophysics: A new frontier in Earth science research. *Reviews of Geophysics* **47**: RG4004.
- Bauer RD, Maloszewski P, Zhang Y, Meckenstock RU, Griebl C (2008). Mixing-controlled biodegradation in a toluene plume -results from two-dimensional laboratory experiments. *Journal of Contaminant Hydrology* **96**: 150-168.
- Bethke CM, Sanford RA, Kirk MF, Jin Q, Flynn TM (2011). The thermodynamic ladder in geomicrobiology. *American Journal of Science* **311**: 183-210.
- Bigalke J, Grabner EW (1997). The Geobattery model: A contribution to large scale electrochemistry. *Electrochimica Acta* **42**: 3443-3452.
- Bird LJ, Bonnefoy V, Newman DK (2011). Bioenergetic challenges of microbial iron metabolisms. *Trends in microbiology* **19**: 330-340.
- Bjerg JT, Damgaard LR, Holm SA, Schramm A, Nielsen LP (2016). Motility of electric cable bacteria. *Applied and environmental microbiology* **82**: 3816-3821.

- Borch T, Kretzschmar R, Kappler A, Cappellen PV, Ginder-Vogel M, Voegelin A *et al.* (2009). Biogeochemical redox processes and their impact on contaminant dynamics. *Environmental science & technology* **44**: 15-23.
- Burdorf L, Hidalgo-Martinez S, Cook P, Meysman F (2016). Long-distance electron transport by cable bacteria in mangrove sediments. *Mar Ecol Prog Ser* **545**: 1-8.
- Carta D, Casula MF, Corrias A, Falqui A, Navarra G, Pinna G (2009). Structural and magnetic characterization of synthetic ferrihydrite nanoparticles. *Materials Chemistry and Physics* **113**: 349-355.
- Chapelle FH (2000). The significance of microbial processes in hydrogeology and geochemistry. *Hydrogeology Journal* **8**: 41-46.
- Choi B-Y, Yun S-T, Kim K-H (2016). Role of oxbow lakes in controlling redox geochemistry of shallow groundwater under a heterogeneous fluvial sedimentary environment in an agricultural field: Coexistence of iron and sulfate reduction. *Journal of Contaminant Hydrology*. **185-186**: 28-41.
- Christensen TH, Kjeldsen P, Albrechtsen HJr, Heron G, Nielsen PH, Bjerg PL *et al.* (1994). Attenuation of landfill leachate pollutants in aquifers. *Critical Reviews in Environmental Science and Technology* **24**: 119-202.
- Christensen TH, Bjerg PL, Banwart SA, Jakobsen R, Heron G, Albrechtsen HJ (2000). Characterization of redox conditions in groundwater contaminant plumes. *Journal of Contaminant Hydrology* **45**: 165-241.
- Cirpka OA, Frind EO, Helmig R (1999). Numerical simulation of biodegradation controlled by transverse mixing. *Journal of Contaminant Hydrology* **40**: 159-182.
- Cirpka OA, Rolle M, Chiogna G, de Barros FP, Nowak W (2012). Stochastic evaluation of mixing-controlled steady-state plume lengths in two-dimensional heterogeneous domains. *Journal of contaminant hydrology* **138**: 22-39.
- Cline JD (1969). Spectrophotometric determination of hydrogen sulfide in natural waters. *Limnology and Oceanography*: **14**: 454-458.
- Coble PG (1996). Characterization of marine and terrestrial DOM in seawater using excitation-emission matrix spectroscopy. *Marine chemistry* **51**: 325-346.

- Culman SW, Bukowski R, Gauch HG, Cadillo-Quiroz H, Buckley DH (2009). T-REX: software for the processing and analysis of T-RFLP data. *Bmc Bioinformatics* **10**: 171.
- Cussler E (2009). *Diffusion: Mass Transfer in Fluid Systems, 3rd edn*. Cambridge University Press, Cambridge, UK.
- D'Andrilli J, Dittmar T, Koch BP, Purcell JM, Marshall AG, Cooper WT (2010). Comprehensive characterization of marine dissolved organic matter by Fourier transform ion cyclotron resonance mass spectrometry with electrospray and atmospheric pressure photoionization. *Rapid communications in mass spectrometry* **24**: 643-650.
- Daghio M, Vaiopoulou E, Patil SA, Suárez-Suárez A, Head IM, Franzetti A *et al.* (2016). Anodes Stimulate Anaerobic Toluene Degradation via Sulfur Cycling in Marine Sediments. *Applied and environmental microbiology* **82**: 297-307.
- Damgaard LR, Risgaard-Petersen N, Nielsen LP (2014). Electric potential microelectrode for studies of electrobiogeophysics. *Journal of Geophysical Research: Biogeosciences* **119**: 1906-1917.
- Dittmar T, Koch B, Hertkorn N, Kattner G (2008). A simple and efficient method for the solid-phase extraction of dissolved organic matter (SPE-DOM) from seawater. *Limnol Oceanogr Methods* **6**: 230-235.
- Dvorski SE-M, Gonsior M, Hertkorn N, Uhl J, Müller H, Griebler C *et al.* (2016). Geochemistry of Dissolved Organic Matter in a Spatially Highly Resolved Groundwater Petroleum Hydrocarbon Plume Cross-Section. *Environmental science & technology* **50**: 5536-5546.
- Edgar RC (2004). MUSCLE: multiple sequence alignment with high accuracy and high throughput. *Nucleic acids research* **32**: 1792-1797.
- Einsiedl F, Pilloni G, Ruth-Anneser B, Lueders T, Griebler C (2015). Spatial distributions of sulphur species and sulphate-reducing bacteria provide insights into sulphur redox cycling and biodegradation hot-spots in a hydrocarbon-contaminated aquifer. *Geochimica Et Cosmochimica Acta* **156**: 207-221.

- Fabisch M, Freyer G, Johnson C, Büchel G, Akob D, Neu T *et al.* (2016). Dominance of 'Gallionella capsiferriformans' and heavy metal association with Gallionella-like stalks in metal-rich pH 6 mine water discharge. *Geobiology* **14**: 68-90.
- Fahrenfeld N, Cozzarelli IM, Bailey Z, Pruden A (2014). Insights into Biodegradation Through Depth-Resolved Microbial Community Functional and Structural Profiling of a Crude-Oil Contaminant Plume. *Microbial ecology* **68**: 453-462.
- Finster K, Liesack W, Thamdrup B (1998). Elemental sulfur and thiosulfate disproportionation by *Desulfocapsa sulfoexigens* sp. nov., a new anaerobic bacterium isolated from marine surface sediment. *Applied and environmental microbiology* **64**: 119-125.
- Flynn TM, O'Loughlin EJ, Mishra B, DiChristina TJ, Kemner KM (2014). Sulfur-mediated electron shuttling during bacterial iron reduction. *Science* **344**: 1039-1042.
- Forté SA, Bentley LR (2013). Mapping Degrading Hydrocarbon Plumes with Self Potentials: Investigation on Causative Mechanisms using Field and Modeling Data. *Journal of Environmental & Engineering Geophysics* **18**: 27-42.
- Frindte K, Allgaier M, Grossart HP, Eckert W (2016). Redox stability regulates community structure of active microbes at the sediment–water interface. *Environmental Microbiology Reports* **8**: 798–804.
- Fuchs G, Boll M, Heider J (2011). Microbial degradation of aromatic compounds—from one strategy to four. *Nature Reviews Microbiology* **9**: 803-816.
- Gorby YA, Yanina S, McLean JS, Rosso KM, Moyles D, Dohnalkova A *et al.* (2006). Electrically conductive bacterial nanowires produced by *Shewanella oneidensis* strain MR-1 and other microorganisms. *Proceedings of the National Academy of Sciences of the United States of America* **103**: 11358-11363.
- Gorski CA, Edwards R, Sander M, Hofstetter TB, Stewart SM (2016). Thermodynamic characterization of iron oxide-aqueous Fe²⁺ redox couples. *Environmental science & technology* **50**: 8538–8547.
- Griebler C, Safinowski M, Vieth A, Richnow HH, Meckenstock RU (2004). Combined application of stable carbon isotope analysis and specific metabolites determination

for assessing in situ degradation of aromatic hydrocarbons in a tar oil-contaminated aquifer. *Environmental science & technology* **38**: 617-631.

Griebler C, Lueders T (2009). Microbial biodiversity in groundwater ecosystems. *Freshwater Biology* **54**: 649-677.

Hammes F, Goldschmidt F, Vital M, Wang Y, Egli T (2010). Measurement and interpretation of microbial adenosine tri-phosphate (ATP) in aquatic environments. *Water research* **44**: 3915-3923.

Handley KM, Wrighton KC, Piceno YM, Andersen GL, DeSantis TZ, Williams KH *et al.* (2012). High-density PhyloChip profiling of stimulated aquifer microbial communities reveals a complex response to acetate amendment. *FEMS microbiology ecology* **81**: 188-204.

Hansel CM, Lentini CJ, Tang Y, Johnston DT, Wankel SD, Jardine PM (2015). Dominance of sulfur-fueled iron oxide reduction in low-sulfate freshwater sediments. *The ISME journal* **9**: 2400-2412.

Hertkorn N, Frommberger M, Witt M, Koch B, Schmitt-Kopplin P, Perdue E (2008). Natural organic matter and the event horizon of mass spectrometry. *Analytical chemistry* **80**: 8908-8919.

Hoefl SE, Kulp TR, Stolz JF, Hollibaugh JT, Oremland RS (2004). Dissimilatory arsenate reduction with sulfide as electron donor: experiments with mono lake water and isolation of strain MLMS-1, a chemoautotrophic arsenate respirer. *Applied and environmental microbiology* **70**: 2741-2747.

Hoehler TM, Jørgensen BB (2013). Microbial life under extreme energy limitation. *Nature Reviews Microbiology* **11**: 83-94.

Holmes D, Bond D, O'neil R, Reimers C, Tender L, Lovley D (2004a). Microbial communities associated with electrodes harvesting electricity from a variety of aquatic sediments. *Microbial Ecology* **48**: 178-190.

Holmes DE, Bond DR, Lovley DR (2004b). Electron transfer by *Desulfobulbus propionicus* to Fe (III) and graphite electrodes. *Applied and environmental microbiology* **70**: 1234-1237.

- Holmkvist L, Ferdelman TG, Jørgensen BB (2011). A cryptic sulfur cycle driven by iron in the methane zone of marine sediment (Aarhus Bay, Denmark). *Geochimica et Cosmochimica Acta* **75**: 3581-3599.
- Höss S, Fritzsche A, Meyer C, Bosch J, Meckenstock RU, Totsche KU (2014). Size- and composition-dependent toxicity of synthetic and soil-derived Fe oxide colloids for the nematode *Caenorhabditis elegans*. *Environmental science & technology* **49**: 544-552.
- Jarling R, Kühner S, Janke EB, Gruner A, Drozdowska M, Golding BT *et al.* (2015). Versatile transformations of hydrocarbons in anaerobic bacteria: substrate ranges and regio- and stereo-chemistry of activation reactions. *Frontiers in microbiology* **6**.
- Jelen BI, Giovannelli D, Falkowski PG (2016). The Role of Microbial Electron Transfer in the Coevolution of the Biosphere and Geosphere. *Annual Review of Microbiology* **70**: 45-62.
- Jobelius C, Ruth B, Griebler C, Meckenstock RU, Hollender J, Reineke A *et al.* (2010). Metabolites indicate hot spots of biodegradation and biogeochemical gradients in a high-resolution monitoring well. *Environmental science & technology* **45**: 474-481.
- Jost D, Haberer CM, Grathwohl P, Winter J, Gallert C (2015). Oxygen transfer in a fluctuating capillary fringe: Impact of microbial respiratory activity. *Vadose Zone Journal* **14**.
- Jost G, Pollehne F (2012). The energetic balance of microbial exploitation of pelagic redox gradients. *The Handbook of Environmental Chemistry* **22**: 47-65.
- Kappler A, Benz M, Schink B, Brune A (2004). Electron shuttling via humic acids in microbial iron (III) reduction in a freshwater sediment. *FEMS microbiology ecology* **47**: 85-92.
- Kato S, Hashimoto K, Watanabe K (2012). Microbial interspecies electron transfer via electric currents through conductive minerals. *Proceedings of the National Academy of Sciences of the United States of America* **109**: 10042-10046.
- Kato S, Yamagishi A (2016). A novel large filamentous deltaproteobacterium on hydrothermally inactive sulfide chimneys of the Southern Mariana Trough. *Deep Sea Research Part I: Oceanographic Research Papers* **110**: 99-105.

- Klüpfel L, Piepenbrock A, Kappler A, Sander M (2014). Humic substances as fully regenerable electron acceptors in recurrently anoxic environments. *Nature Geoscience* **7**: 195-200.
- Kunapuli U, Lueders T, Meckenstock RU (2007). The use of stable isotope probing to identify key iron-reducing microorganisms involved in anaerobic benzene degradation. *The ISME journal* **1**: 643-653.
- Kunapuli U, Griebler C, Beller HR, Meckenstock RU (2008). Identification of intermediates formed during anaerobic benzene degradation by an iron-reducing enrichment culture. *Environmental microbiology* **10**: 1703-1712.
- Larentis M, Hoermann K, Lueders T (2013). Fine-scale degrader community profiling over an aerobic/anaerobic redox gradient in a toluene-contaminated aquifer. *Environmental Microbiology Reports* **5**: 225-234.
- LaRowe DE, Amend JP (2015). Power limits for microbial life. *Frontiers in microbiology* **6**: 718.
- Larsen S, Nielsen LP, Schramm A (2014). Cable Bacteria Associated with Long Distance Electron Transport in New England Salt Marsh Sediment. *Environmental Microbiology Reports* **7**: 175-179.
- Lovley DR, Phillips EJ (1988). Novel mode of microbial energy metabolism: organic carbon oxidation coupled to dissimilatory reduction of iron or manganese. *Applied and environmental microbiology* **54**: 1472-1480.
- Lower SK (2014). Redox equilibria in natural waters. *Chem1 Environmental Chemistry, Reference text, Simon Fraser University*.
- Loy A, Lehner A, Lee N, Adamczyk J, Meier H, Ernst J *et al.* (2002). Oligonucleotide microarray for 16S rRNA gene-based detection of all recognized lineages of sulfate-reducing prokaryotes in the environment. *Applied and environmental microbiology* **68**: 5064-5081.
- Ludwig W, Strunk O, Westram R, Richter L, Meier H, Buchner A *et al.* (2004). ARB: a software environment for sequence data. *Nucleic Acids Research* **32**: 1363-1371.

- Lueders T, Manefield M, Friedrich MW (2004). Enhanced sensitivity of DNA-and rRNA-based stable isotope probing by fractionation and quantitative analysis of isopycnic centrifugation gradients. *Environmental microbiology* **6**: 73-78.
- Maier U, Grathwohl P (2006). Numerical experiments and field results on the size of steady state plumes. *Journal of contaminant hydrology* **85**: 33-52.
- Malkin S, Meysman F (2014). Rapid redox signal transmission by cable bacteria beneath a photosynthetic biofilm. *Applied and environmental microbiology* **81**: 948-956.
- Malkin SY, Rao AM, Seitaj D, Vasquez-Cardenas D, Zetsche EM, Hidalgo-Martinez S *et al.* (2014). Natural occurrence of microbial sulphur oxidation by long-range electron transport in the seafloor. *The ISME journal* **8**: 1843-1854.
- Marsili E, Baron DB, Shikhare ID, Coursolle D, Gralnick JA, Bond DR (2008). Shewanella secretes flavins that mediate extracellular electron transfer. *Proceedings of the National Academy of Sciences* **105**: 3968-3973.
- Martus P, Püttmann W (2003). Formation of alkylated aromatic acids in groundwater by anaerobic degradation of alkylbenzenes. *Science of the total environment* **307**: 19-33.
- Marzocchi U, Trojan D, Larsen S, Meyer RL, Revsbech NP, Schramm A *et al.* (2014). Electric coupling between distant nitrate reduction and sulfide oxidation in marine sediment. *The ISME journal* **8**: 1682–1690.
- Mayer K, Benner S, Frind E, Thornton S, Lerner D (2001). Reactive transport modeling of processes controlling the distribution and natural attenuation of phenolic compounds in a deep sandstone aquifer. *Journal of Contaminant Hydrology* **53**: 341-368.
- McCarty PL, Criddle CS (2012). Chemical and Biological Processes: The Need for Mixing. *Delivery and Mixing in the Subsurface: Processes and Design Principles for In Situ Remediation*: 7-52.
- Meckenstock RU (1999). Fermentative toluene degradation in anaerobic defined syntrophic cocultures. *FEMS Microbiology Letters* **177**: 67-73.
- Meckenstock RU, Elsner M, Griebler C, Lueders T, Stumpp C, Dejonghe W *et al.* (2015). Biodegradation: Updating the concepts of control for microbial clean-up in contaminated aquifers. *Environmental science & technology* **49**: 7073–7081.

- Melton ED, Swanner ED, Behrens S, Schmidt C, Kappler A (2014). The interplay of microbially mediated and abiotic reactions in the biogeochemical Fe cycle. *Nature Reviews Microbiology* **12**: 797-808.
- Meysman FJ, Risgaard-Petersen N, Malkin SY, Nielsen LP (2015). The geochemical fingerprint of microbial long-distance electron transport in the seafloor. *Geochimica et Cosmochimica Acta* **152**: 122-142.
- Müller H, Bosch J, Griebler C, Damgaard LR, Nielsen LP, Lueders T *et al.* (2016). Long-distance electron transfer by cable bacteria in aquifer sediments. *The ISME journal* **10**: 2010-2019.
- Muyzer G, Stams AJ (2008). The ecology and biotechnology of sulphate-reducing bacteria. *Nature Reviews Microbiology* **6**: 441-454.
- Naudet V, Revil A, Bottero JY, Bégassat P (2003). Relationship between self-potential (SP) signals and redox conditions in contaminated groundwater. *Geophysical Research Letters* **30**: 2091.
- Naudet V, Revil A, Rizzo E, Bottero JY, Bégassat P (2004). Groundwater redox conditions and conductivity in a contaminant plume from geoelectrical investigations. *Hydrology and Earth System Sciences* **8**: 8-22.
- Nielsen LP, Risgaard-Petersen N, Fossing H, Christensen PB, Sayama M (2010). Electric currents couple spatially separated biogeochemical processes in marine sediment. *Nature* **463**: 1071-1074.
- Nielsen LP, Risgaard-Petersen N (2015). Rethinking Sediment Biogeochemistry After the Discovery of Electric Currents. *Annual review of marine science* **7**: 425-442.
- Nielsen LP (2016). Ecology: Electrical Cable Bacteria Save Marine Life. *Current Biology* **26**: R32-R33.
- Osburn MR, LaRowe DE, Momper LM, Amend JP (2014). Chemolithotrophy in the continental deep subsurface: Sanford Underground Research Facility (SURF), USA. *Frontiers in microbiology* **5**: 610.
- Pedersen HD, Postma D, Jakobsen R, Larsen O (2005). Fast transformation of iron oxyhydroxides by the catalytic action of aqueous Fe (II). *Geochimica et Cosmochimica Acta* **69**: 3967-3977.

- Pernthaler J, Glöckner F-O, Schönhuber W, Amann R (2001). Fluorescence in situ hybridization (FISH) with rRNA-targeted oligonucleotide probes. *Methods in Microbiology* **30**: 207-226.
- Pfeffer C, Larsen S, Song J, Dong M, Besenbacher F, Meyer RL *et al.* (2012). Filamentous bacteria transport electrons over centimetre distances. *Nature* **491**: 218-221.
- Pierce E, Xie G, Barabote RD, Saunders E, Han CS, Detter JC *et al.* (2008). The complete genome sequence of *Moorella thermoacetica* (f. *Clostridium thermoaceticum*). *Environmental microbiology* **10**: 2550-2573.
- Pilloni G, von Netzer F, Engel M, Lueders T (2011). Electron acceptor-dependent identification of key anaerobic toluene degraders at a tar-oil-contaminated aquifer by Pyro-SIP. *FEMS microbiology ecology* **78**: 165-175.
- Podgorski DC, McKenna AM, Rodgers RP, Marshall AG, Cooper WT (2012). Selective ionization of dissolved organic nitrogen by positive ion atmospheric pressure photoionization coupled with Fourier transform ion cyclotron resonance mass spectrometry. *Analytical chemistry* **84**: 5085-5090.
- Rao A, Risgaard-Petersen N, Neumeier U (2016). Electrogenic sulfur oxidation in a northern saltmarsh (St. Lawrence Estuary, Canada). *Canadian journal of microbiology* **62**: 530-537.
- Rao AM, Malkin SY, Hidalgo-Martinez S, Meysman FJ (2016). The impact of electrogenic sulfide oxidation on elemental cycling and solute fluxes in coastal sediment. *Geochimica et Cosmochimica Acta* **172**: 265–286
- Reguera G, McCarthy KD, Mehta T, Nicoll JS, Tuominen MT, Lovley DR (2005). Extracellular electron transfer via microbial nanowires. *Nature* **435**: 1098-1101.
- Reguera G (2016). Microbes, cables, and an electrical touch. *International Microbiology* **18**: 151-157.
- Reimers CE, Tender LM, Fertig S, Wang W (2001). Harvesting energy from the marine sediment-water interface. *Environmental science & technology* **35**: 192-195.
- Revil A, Mendonca CA, Atekwana EA, Kulesa B, Hubbard SS, Bohlen KJ (2010). Understanding biogeobatteries: Where geophysics meets microbiology. *J Geophys Res-Biogeophys* **115**.

- Revil A, Fernandez P, Mao D, French H, Bloem E, Binley A (2015). Self-potential monitoring of the enhanced biodegradation of an organic contaminant using a bioelectrochemical cell. *The Leading Edge* **34**: 198-202.
- Revsbech NP (1989). An oxygen microsensor with a guard cathode. *Limnology and Oceanography* **34**: 474-478.
- Risgaard-Petersen N, Revil A, Meister P, Nielsen LP (2012). Sulfur, iron-, and calcium cycling associated with natural electric currents running through marine sediment. *Geochimica et Cosmochimica Acta* **92**: 1-13.
- Risgaard-Petersen N, Kristiansen M, Frederiksen RB, Dittmer AL, Bjerg JT, Trojan D *et al.* (2015). Cable Bacteria in Freshwater Sediments. *Applied and environmental microbiology* **81**: 6003-6011.
- Risgaard-Petersen N, Damgaard LR, Revil A, Nielsen LP (2014). Mapping electron sources and sinks in a marine biogeobattery. *Journal of Geophysical Research: Biogeosciences* **119**: 1475-1486.
- Rolle M, Maier U, Grathwohl P (2011). Contaminant fate and reactive transport in groundwater. *Dealing with Contaminated Sites*: 851-885.
- Ryckelynck N, Stecher HA, Reimers CE (2005). Understanding the anodic mechanism of a seafloor fuel cell: interactions between geochemistry and microbial activity. *Biogeochemistry* **76**: 113-139.
- Safinowski M, Griebl C, Meckenstock RU (2006). Anaerobic cometabolic transformation of polycyclic and heterocyclic aromatic hydrocarbons: evidence from laboratory and field studies. *Environmental science & technology* **40**: 4165-4173.
- Sato M, Mooney HM (1960). The electrochemical mechanism of sulfide self-potentials. *Geophysics* **25**: 226-249.
- Schauer R, Risgaard-Petersen N, Kjeldsen KU, Tataru Bjerg JJ, B BJ, Schramm A *et al.* (2014). Succession of cable bacteria and electric currents in marine sediment. *The ISME journal* **8**: 1314-1322.
- Schmitt R, Langguth H-R, Püttmann W, Rohns H, Eckert P, Schubert J (1996). Biodegradation of aromatic hydrocarbons under anoxic conditions in a shallow sand

and gravel aquifer of the Lower Rhine Valley, Germany. *Organic Geochemistry* **25**: 41-50.

Schoepp-Cothenet B, van Lis R, Atteia A, Baymann F, Capowiez L, Ducluzeau A-L *et al.* (2013). On the universal core of bioenergetics. *Biochimica et Biophysica Acta (BBA)-Bioenergetics* **1827**: 79-93.

Schüring J, Schulz HD, Fischer WR, Böttcher J, Duijnisveld WH (2013). *Redox: fundamentals, processes and applications*. Springer Science & Business Media.

Seitaj D, Schauer R, Sulu-Gambari F, Hidalgo-Martinez S, Malkin SY, Burdorf LD *et al.* (2015). Cable bacteria generate a firewall against euxinia in seasonally hypoxic basins. *Proceedings of the National Academy of Sciences of the United States of America* **112**: 13278-13283.

Shen Y, Chapelle FH, Strom EW, Benner R (2015). Origins and bioavailability of dissolved organic matter in groundwater. *Biogeochemistry* **122**: 61-78.

Shrestha PM, Rotaru A-E (2014). Plugging in or going wireless: strategies for interspecies electron transfer. *Frontiers in microbiology* **5**.

Sleighter RL, Hatcher PG (2011). Fourier transform mass spectrometry for the molecular level characterization of natural organic matter: Instrument capabilities, applications, and limitations. *Fourier Transforms—Approach to Scientific Principles, edited by G. Nikolic*: 295–320. InTech, Vienna.

Sorokin DY, Tourova T, Mußmann M, Muyzer G (2008). *Dethiobacter alkaliphilus* gen. nov. sp. nov., and *Desulfurivibrio alkaliphilus* gen. nov. sp. nov.: two novel representatives of reductive sulfur cycle from soda lakes. *Extremophiles* **12**: 431-439.

Sousa FL, Thiergart T, Landan G, Nelson-Sathi S, Pereira IA, Allen JF *et al.* (2013). Early bioenergetic evolution. *Philosophical Transactions of the Royal Society of London B: Biological Sciences* **368**: 20130088.

Stookey LL (1970). Ferrozine -a new spectrophotometric reagent for iron. *Analytical Chemistry* **42**: 779-781.

Sulu-Gambari F, Seitaj D, Meysman FJ, Schauer R, Polerecky L, Slomp CP (2016). Cable Bacteria Control Iron-Phosphorus Dynamics in Sediments of a Coastal Hypoxic Basin. *Environmental science & technology* **50**: 1227–1233.

- Sulu-Gambari F, Seitaj D, Behrends T, Banerjee D, Meysman FJ, Slomp CP (2016). Impact of Cable Bacteria on Sedimentary Iron and Manganese Dynamics in a Seasonally-Hypoxic Marine Basin. *Geochimica et Cosmochimica Acta* **192**: 49–69.
- Tabatabai M (1974). A rapid method for determination of sulfate in water samples. *Environmental Letters* **7**: 237-243.
- Tamura K, Stecher G, Peterson D, Filipski A, Kumar S (2013). MEGA6: molecular evolutionary genetics analysis version 6.0. *Molecular biology and evolution* **30**: 2725-2729.
- Tender LM, Reimers CE, Stecher HA, Holmes DE, Bond DR, Lowy DA *et al.* (2002). Harnessing microbially generated power on the seafloor. *nature biotechnology* **20**: 821-825.
- Thornton SF, Quigley S, Spence MJ, Banwart SA, Bottrell S, Lerner DN (2001). Processes controlling the distribution and natural attenuation of dissolved phenolic compounds in a deep sandstone aquifer. *Journal of Contaminant Hydrology* **53**: 233-267.
- Trojan D, Schreiber L, Bjerg JT, Bøggild A, Yang T, Kjeldsen KU *et al.* (2016). A taxonomic framework for cable bacteria and proposal of the candidate genera *Electrothrix* and *Electronema*. *Systematic and Applied Microbiology* **39**: 297-306.
- Tziotis D, Hertkorn N, Schmitt-Kopplin P (2011). Letter: Kendrick-analogous network visualisation of ion cyclotron resonance Fourier transform mass spectra: improved options for the assignment of elemental compositions and the classification of organic molecular complexity. *European Journal of Mass Spectrometry* **17**: 415-421.
- Van de Velde S, Lesven L, Burdorf LD, Hidalgo-Martinez S, Geelhoed JS, Van Rijswijk P *et al.* (2016). The impact of electrogenic sulfur oxidation on the biogeochemistry of coastal sediments: a field study. *Geochimica et Cosmochimica Acta* **194**: 211–232.
- Van Krevelen D (1950). Graphical-statistical method for the study of structure and reaction processes of coal. *Fuel* **29**: 269-284.
- Vasquez-Cardenas D, van de Vossenberg J, Polerecky L, Malkin SY, Schauer R, Hidalgo-Martinez S *et al.* (2015). Microbial carbon metabolism associated with electrogenic sulphur oxidation in coastal sediments. *The ISME journal* **9**: 1966-1978.

- Wan M, Shchukarev A, Lohmayer R, Planer-Friedrich B, Peiffer S (2014). The occurrence of surface polysulphides during the interaction between ferric (hydr) oxides and aqueous sulphide. *Environmental science & technology* **48**: 5076–5084.
- Weber KA, Achenbach LA, Coates JD (2006). Microorganisms pumping iron: anaerobic microbial iron oxidation and reduction. *Nature reviews Microbiology* **4**: 752-764.
- Widdel F, Bak F (1992). Gram-negative mesophilic sulfate-reducing bacteria. *The prokaryotes*. Springer. pp 3352-3378.
- Wiedemeier TH (1999). *Natural attenuation of fuels and chlorinated solvents in the subsurface*. John Wiley & Sons.
- Winderl C, Anneser B, Griebl C, Meckenstock RU, Lueders T (2008). Depth-resolved quantification of anaerobic toluene degraders and aquifer microbial community patterns in distinct redox zones of a tar oil contaminant plume. *Applied and environmental microbiology* **74**: 792-801.
- Wu W-M, Carley J, Green SJ, Luo J, Kelly SD, Nostrand JV *et al.* (2010). Effects of nitrate on the stability of uranium in a bio-reduced region of the subsurface. *Environmental science & technology* **44**: 5104-5111.
- Yoneda Y, Yoshida T, Yasuda H, Imada C, Sako Y (2013). A thermophilic, hydrogenogenic and carboxydophilic bacterium, *Calderihabitans maritimus* gen. nov., sp. nov., from a marine sediment core of an undersea caldera. *International journal of systematic and evolutionary microbiology* **63**: 3602-3608.
- Zehnder AJ (1988). *Biology of anaerobic microorganisms*. John Wiley and Sons.
- Zhu T, Dittrich M (2016). Carbonate Precipitation through Microbial Activities in Natural Environment, and Their Potential in Biotechnology: A Review. *Frontiers in bioengineering and biotechnology* **4**.

Appendix

Table 7: Concentrations of O₂ and HS⁻; and pH values for Figure 6A

Active					Abiotic control				
Depth [mm]	O ₂ [μM]	Depth [mm]	pH	Depth [mm]	HS ⁻ [μM]	Depth [mm]	O ₂ [μM]	Depth [mm]	pH
0.00	245.94	0.00	7.51	(-2)-0	0.00	0.00	262.39	0.00	7.08
0.25	237.10	0.50	7.61	0-7	0.00	0.50	249.66	0.50	7.08
0.50	227.82	1.00	7.69	7-11	0.00	1.00	228.77	1.00	7.09
0.75	220.37	1.50	7.78	11-19	0.00	1.50	213.43	1.50	7.10
1.00	213.24	2.50	7.80	19-29	160.19	2.00	199.75	2.00	7.11
1.25	204.12	3.50	7.79	29-36	396.56	2.50	182.22	2.50	7.11
1.50	192.40	4.50	7.79	36-48	640.68	3.00	169.59	3.00	7.11
1.75	183.36	5.50	7.77			3.50	160.83	3.50	7.12
2.00	175.87	6.50	7.75			4.00	145.75	4.00	7.12
2.25	170.44	7.50	7.73			4.50	134.42	4.50	7.12
2.50	161.10	8.50	7.69			5.00	124.33	5.00	7.13
2.75	151.59	9.50	7.65			5.50	105.63	5.50	7.13
3.00	142.25	11.50	7.60			6.00	93.20	6.00	7.13
3.25	134.67	13.50	7.56			6.50	81.34	6.50	7.13
3.50	128.50	15.50	7.51			7.00	68.95	7.00	7.13
3.75	121.36	17.50	7.47			7.50	58.29	7.50	7.13
4.00	113.64	19.50	7.41			8.00	50.23	8.00	7.13
4.25	104.77	21.50	7.37			8.50	42.77	8.50	7.13
4.50	98.47	23.50	7.33			9.00	38.22	9.00	7.13
4.75	91.17	25.50	7.32			9.50	28.95	9.50	7.14
5.00	91.92	27.50	7.31			10.00	22.63	10.00	7.16
5.25	77.18	29.50	7.32			10.50	17.54	11.00	7.16
5.50	70.46	31.50	7.33			11.00	14.03	12.00	7.17
5.75	63.34	33.50	7.36			11.50	10.70	13.00	7.17
6.00	58.84					12.00	8.34	14.00	7.18
6.25	54.77					12.50	5.94	15.00	7.18
6.50	49.28					13.00	2.94	16.00	7.19
6.75	42.53					13.50	1.97	17.00	7.20
7.00	36.10					14.00	0.83	18.00	7.21
7.25	30.39					14.50	0.65	19.00	7.22
7.50	24.80					15.00	0.47	20.00	7.23
7.75	21.29					15.50	0.19	21.00	7.25
8.00	18.32					16.00	0.13	22.00	7.26
8.25	13.38					16.50	0.00	23.00	7.28
8.50	9.48							24.00	7.30
8.75	5.94							25.00	7.32
9.00	3.59							26.00	7.34
9.25	1.46							27.00	7.36
9.50	0.98								
9.75	0.43								
10.00	0.11								
10.25	0.00								
10.50	0.00								

Table 8: Relative abundances of TRFs for Figure 6B

Depth	0 - 07 mm		07 - 11 mm		11 - 19 mm		19 - 29 mm		29 - 36 mm		36 -48 mm	
	TRF	Mean (%)	SD	Mean (%)	SD	Mean (%)	SD	Mean (%)	SD	Mean (%)	SD	Mean (%)
7B	0.16	0.00	0.00	0.00	0.12	0.00	0.20	0.00	0.22	0.06	0.00	0.00
12B	0.00	0.00	0.00	0.00	0.15	0.02	0.21	0.00	0.23	0.15	0.00	0.00
14B	1.72	0.94	0.84	0.49	2.68	2.22	2.43	2.95	2.07	2.35	3.36	4.10
20B	0.00	0.00	0.35	0.00	0.13	0.00	1.55	1.24	0.40	0.32	2.17	0.00
35B	0.00	0.00	0.00	0.00	0.00	0.00	0.88	0.76	10.88	0.00	0.19	0.00
56B	0.14	0.00	0.20	0.00	0.11	0.00	0.00	0.00	0.00	0.00	0.00	0.00
61B	0.36	0.07	0.23	0.04	0.35	0.02	0.17	0.05	0.20	0.08	0.23	0.00
66B	0.34	0.08	0.20	0.03	0.11	0.00	0.12	0.00	0.15	0.00	0.15	0.00
70B	1.87	0.30	2.45	0.34	1.31	0.27	0.50	0.13	0.38	0.05	0.46	0.02
73B	0.00	0.00	0.00	0.00	0.16	0.01	0.00	0.00	0.14	0.00	0.13	0.00
76B	0.64	0.28	0.34	0.09	0.45	0.14	0.00	0.00	0.13	0.00	0.00	0.00
79B	2.95	0.41	1.71	0.58	0.60	0.17	0.43	0.04	0.47	0.20	0.45	0.05
89B	0.25	0.09	0.69	0.49	0.49	0.18	3.06	2.96	1.10	0.91	1.47	1.73
111B	0.75	0.18	0.00	0.00	0.10	0.00	0.00	0.00	0.00	0.00	0.00	0.00
114B	0.00	0.00	0.00	0.00	0.10	0.00	0.24	0.00	0.21	0.00	0.00	0.00
120B	0.21	0.00	0.20	0.02	0.21	0.06	0.44	0.00	0.20	0.07	0.17	0.00
123B	0.67	0.08	0.60	0.16	0.73	0.17	0.39	0.04	0.52	0.21	0.57	0.00
127B	2.18	0.32	1.24	0.28	4.77	4.37	9.77	0.70	7.27	1.34	3.23	2.09
130B	1.10	0.28	0.50	0.31	0.82	0.28	0.00	0.00	0.00	0.00	0.00	0.00
136B	3.89	1.04	2.15	1.19	2.48	1.38	1.76	0.06	1.85	0.48	2.12	0.23
139B	3.14	0.38	0.72	0.59	0.73	0.34	0.43	0.08	0.42	0.09	0.43	0.01
143B	0.65	0.21	0.57	0.06	0.41	0.03	0.28	0.05	0.31	0.10	0.47	0.00
145B	7.03	0.52	2.89	1.76	2.15	1.07	0.77	0.11	0.68	0.17	0.91	0.08
148B	29.45	1.60	18.32	8.46	16.87	5.58	13.74	3.57	13.05	3.03	14.46	3.31
152B	0.00	0.00	0.22	0.00	0.00	0.00	0.23	0.00	0.19	0.00	0.00	0.00
155B	1.89	0.96	0.60	0.34	0.21	0.08	0.35	0.00	0.21	0.03	0.00	0.00
159B	2.11	0.13	26.54	13.67	29.51	8.75	36.12	9.80	32.57	2.67	40.62	5.31
164B	0.37	0.05	0.31	0.19	0.13	0.04	0.13	0.00	0.17	0.00	0.61	0.00
168B	0.20	0.05	0.00	0.00	0.18	0.04	0.14	0.00	0.19	0.04	0.18	0.00
171B	0.18	0.02	0.00	0.00	0.13	0.00	0.13	0.00	0.13	0.01	0.00	0.00
179B	0.83	0.10	2.81	0.73	0.41	0.19	0.18	0.04	0.16	0.04	0.15	0.00
196B	0.50	0.08	0.27	0.10	0.23	0.06	0.18	0.03	0.21	0.03	0.23	0.00
205B	0.00	0.00	0.00	0.00	0.00	0.00	0.28	0.14	0.15	0.01	0.16	0.00
210B	0.15	0.01	0.00	0.00	0.00	0.00	0.00	0.00	0.00	0.00	0.00	0.00
223B	8.23	1.05	5.67	2.32	1.10	0.65	1.48	0.05	1.24	0.46	1.84	0.18
225B	5.07	1.10	2.96	1.10	2.16	0.60	3.08	0.11	2.78	0.33	3.97	0.49
262B	0.22	0.07	0.00	0.00	0.08	0.00	0.00	0.00	0.00	0.00	0.00	0.00
276B	0.19	0.04	0.00	0.00	0.08	0.00	0.00	0.00	0.00	0.00	0.00	0.00
279B	0.00	0.00	0.00	0.00	0.10	0.00	0.17	0.04	0.15	0.01	0.16	0.00
288B	0.37	0.09	0.66	0.09	0.49	0.06	0.47	0.15	0.66	0.15	0.39	0.00
290B	0.20	0.00	0.00	0.00	0.15	0.02	0.14	0.00	0.19	0.05	0.22	0.00
297B	0.00	0.00	0.16	0.00	0.10	0.01	0.19	0.00	0.00	0.00	0.00	0.00
299B	0.00	0.00	0.29	0.00	0.20	0.01	0.17	0.06	0.16	0.00	0.00	0.00
302B	0.00	0.00	0.36	0.00	0.24	0.04	0.17	0.08	0.14	0.00	0.00	0.00
305B	0.23	0.05	0.00	0.00	0.08	0.00	0.23	0.00	0.00	0.00	0.00	0.00
310B	0.00	0.00	0.00	0.00	0.13	0.01	0.00	0.00	0.00	0.00	0.00	0.00
356B	0.15	0.01	0.00	0.00	0.08	0.00	0.00	0.00	0.00	0.00	0.00	0.00
373B	0.00	0.00	0.14	0.00	0.13	0.00	0.25	0.03	0.24	0.04	0.25	0.00
398B	0.28	0.04	0.30	0.06	0.39	0.03	0.11	0.00	0.14	0.00	0.17	0.00
402B	3.07	0.77	2.69	1.73	2.49	0.48	2.71	0.93	2.79	1.14	2.65	1.07
411B	0.00	0.00	0.15	0.00	0.13	0.04	0.00	0.00	0.00	0.00	0.00	0.00
422B	0.85	0.16	0.55	0.07	0.73	0.03	0.53	0.18	0.51	0.09	0.64	0.11
428B	0.71	0.24	1.44	0.54	0.21	0.01	0.30	0.00	0.29	0.06	0.37	0.00

Depth	0 - 07 mm		07 - 11 mm		11 - 19 mm		19 - 29 mm		29 - 36 mm		36 - 48 mm		
	TRF	Mean (%)	SD	Mean (%)	SD	Mean (%)	SD	Mean (%)	SD	Mean (%)	SD	Mean (%)	SD
431B		1.09	0.21	1.93	0.02	3.15	0.37	4.47	1.40	3.95	0.60	4.79	1.71
434B		0.67	0.07	0.35	0.12	0.53	0.20	0.28	0.00	0.25	0.10	0.14	0.00
438B		1.87	0.09	1.08	0.23	1.48	0.25	0.87	0.05	0.83	0.02	1.08	0.25
442B		0.14	0.01	0.20	0.01	0.29	0.06	0.43	0.05	0.44	0.12	0.45	0.00
446B		0.40	0.11	1.06	0.14	0.22	0.09	0.11	0.00	0.13	0.00	0.16	0.00
452B		0.30	0.07	0.21	0.05	0.19	0.01	0.25	0.01	0.26	0.07	0.30	0.00
459B		0.33	0.09	0.56	0.25	0.15	0.00	0.00	0.00	0.11	0.00	0.00	0.00
463B		0.28	0.04	0.17	0.00	0.16	0.00	0.14	0.04	0.14	0.00	0.00	0.00
469B		0.57	0.27	0.19	0.04	0.15	0.08	0.00	0.00	0.00	0.00	0.00	0.00
475B		0.15	0.00	0.18	0.05	0.00	0.00	0.00	0.00	0.00	0.00	0.00	0.00
477B		0.16	0.00	0.20	0.00	0.28	0.07	0.25	0.03	0.28	0.03	0.32	0.00
484B		0.62	0.19	0.46	0.15	0.88	0.25	0.60	0.18	0.51	0.16	0.82	0.23
488B		0.31	0.04	0.82	0.00	0.60	0.47	0.32	0.18	0.29	0.07	0.55	0.35
490B		1.58	0.98	3.35	0.72	1.15	0.51	0.87	0.87	1.11	1.01	1.11	1.01
493B		7.89	1.50	4.27	2.50	6.16	1.62	5.77	1.03	5.60	0.72	6.35	0.57
497B		0.17	0.00	0.20	0.05	0.34	0.03	0.34	0.12	0.42	0.07	0.48	0.07
502B		0.32	0.04	0.58	0.28	0.44	0.10	0.47	0.02	0.44	0.10	0.53	0.04
506B		0.00	0.00	5.27	2.01	8.74	3.21	7.50	0.11	6.75	1.88	9.01	1.18
510B		0.00	0.00	0.24	0.00	0.22	0.01	0.44	0.08	0.48	0.06	0.43	0.01
513B		0.00	0.00	0.00	0.00	0.10	0.00	0.12	0.00	0.16	0.04	0.00	0.00
526B		0.30	0.10	0.63	0.19	0.45	0.08	0.49	0.06	0.57	0.16	0.57	0.03
531B		0.00	0.00	0.00	0.00	0.00	0.00	0.11	0.00	0.14	0.03	0.00	0.00
538B		0.00	0.00	0.31	0.05	0.22	0.01	0.51	0.15	0.43	0.06	0.42	0.03
579B		0.20	0.01	0.42	0.13	0.46	0.10	0.47	0.04	0.54	0.19	0.54	0.04
590B		0.00	0.00	0.00	0.00	0.00	0.00	0.11	0.00	0.16	0.03	0.00	0.00
604B		0.18	0.04	0.13	0.00	0.17	0.06	0.10	0.00	0.26	0.00	0.16	0.00
644B		0.15	0.01	0.38	0.16	0.38	0.09	0.44	0.08	0.52	0.18	0.47	0.03
685B		0.00	0.00	0.49	0.00	0.87	0.54	0.37	0.02	0.42	0.04	0.60	0.34

* Mean: Mean values of relative TRF abundance derived from replicate DNA extractions (n = 3);
SD: standard deviation

Table 9: Chemical composition of groundwater sampled at the Düsseldorf-Flingern site, in 2013, for Figures 9 and 16

depth [m bls]	Redox [mV]		pH	Sulfide [μM]		Sulfate [μM]		Fe(II) [μM]		Active cells mL^{-1}		Nitrate [μM]		Toluene [μM]	
	Mean	SD		Mean	SD	Mean	SD	Mean	SD	Mean	SD	Mean	SD	Mean	SD
6.51	89	119	7.51	3.2	0.9			34.3	4.4					0.0	0.0
6.54	44	16	7.35	3.2	0.9	492.4	637.8	112.1	7.6	7.2E+05	1.3E+01	20.0	14.2	3.2	0.0
6.59	-7	46	7.38	3.2	0.9	40.4	28.6	380.0	26.8	3.3E+06	1.2E+01	0.0	0.0	33.0	1.3
6.61	-2	49	7.52	3.9	0.0	0.0	0.0	143.3	8.8	2.1E+06	1.6E+01	0.0	0.0	82.8	12.7
6.64	34	34	7.62	1.3	0.0	0.0	0.0	17.4	1.0	1.0E+06	3.0E+01	0.0	0.0	137.2	25.3
6.67	-30	77	7.67	30.2	0.9	6.1	0.0	27.9	2.7	7.8E+05	9.6E+01	0.0	0.0	96.3	79.5
6.75	-144	59	7.85	136.8	0.9	28.6	0.3	20.0	2.2	6.0E+05	4.4E+00	0.0	0.0	125.9	0.2
6.78	-125	57	8.04	132.3	7.3	49.4	1.9	47.2	12.1	6.1E+05	3.2E+00	0.0	0.0	109.7	0.8
6.81	-112	45	8.05	149.6	11.8	77.5	0.3	22.4	4.3	4.4E+05	1.0E+01	0.0	0.0	135.5	2.3
6.83	-149	85	7.98	154.1	7.3	111.9	0.5	26.5	6.5	5.0E+05	2.1E+01	0.0	0.0	89.0	45.4
6.88	-111	19	7.98	124.6	14.5	143.9	0.9	7.6	2.8	7.5E+05	6.2E+00	0.0	0.0	87.5	5.5
6.91	-121	24	8.03	172.1	1.8	177.4	0.6	11.8	2.6	9.7E+05	8.2E+00	0.0	0.0	62.1	18.7
6.93	-140	12	8.01	134.2	4.5	241.1	13.2	8.4	4.9	9.6E+05	2.0E+00	0.0	0.0	41.8	8.3
6.96	-131	7	8.03	159.3	5.4	321.2	1.6	18.5	10.3	6.8E+05	3.6E+00	0.0	0.0	22.9	3.2
7.01	-135	2	7.92	150.9	4.5	520.4	8.5	59.2	17.6	8.1E+05	1.6E+01	0.0	0.0	5.9	2.5
7.04	-97	38	7.88	57.8	12.7	603.0	4.7	31.1	8.8	7.1E+05	4.0E+00	0.0	0.0	2.6	0.1
7.06	-105	35	7.86	106.6	10.9	782.8	0.3	17.9	1.9	7.5E+05	5.0E+00	0.0	0.0	2.5	0.2
7.08	-106	71	7.68	24.4	7.3	1.050.7	0.6	43.6	11.7	6.6E+05	1.3E+01	0.0	0.0	0.0	0.2
7.11	-80	35	7.78	56.5	7.3	1.280.2	2.5	16.9	4.1	5.3E+05	9.2E+00	0.0	0.0	0.0	0.0
7.21	-78	23	7.78	46.2	3.6	1.412.2	0.8	13.7	0.8	4.5E+05	2.3E+00	0.0	0.0	0.0	0.0
7.26	-74	27	7.71	42.4	3.6	1.419.4	2.7	15.5	0.9	7.8E+05	1.1E+01	0.0	0.0	0.0	0.0
7.31	-73	33	7.71	40.5	6.4	1.473.3	20.6	15.0	0.5	5.7E+05	3.3E-01	0.0	0.0	0.0	0.0
7.41	-66	34	7.74	22.5	0.9	1.526.3	3.1	27.9	2.5	4.4E+05	1.7E+00	0.0	0.0	0.0	0.0
7.51	-38	12	7.77	10.3	5.4	1.619.4	1.2	16.5	1.5	3.1E+05	5.8E+00	0.0	0.0	0.0	0.0
7.61	-33	7	7.72	10.9	0.9	1.651.4	9.2	16.3	0.9	3.2E+05	2.2E+00	0.0	0.0	0.0	0.0
7.75	-16	27	7.67	1.3	0.0	1.715.5	1.4	12.3	2.6	2.0E+05	9.3E-01	0.0	0.0	0.0	0.0
8.05	-17	9	7.73	5.8	0.9	1.641.6	10.1	3.1	0.4	2.4E+05	4.5E+00	0.0	0.0	0.0	0.0
8.65	6	4	7.71	1.9	0.9	1.394.6	0.3	8.4	0.7	1.8E+05	3.5E+00	0.0	0.0	0.0	0.0
9.05	-26	52	7.40	0.0	0.0	1.414.6	0.0	18.3	0.3	1.2E+05	6.9E+00	0.0	0.0	0.0	0.0
9.35	11	5	7.77	1.3	0.0	1.077.7	2.3	12.4	1.8	1.1E+05	1.2E+01	0.0	0.0	0.0	0.0
10.20	14	7	7.66	0.0	0.0	1.403.8	7.4	17.4	1.4	2.2E+05	1.2E+01	0.0	0.0	0.0	0.0

* Mean: Mean values of replicate groundwater samples (n = 2); SD: standard deviation

Table 10: Relative abundances of TRFs for Figure 9B

Depth [m bls]	6.50 m		6.54 m		6.57 m		6.63 m		7.10 m		7.50 m		7.90 m		
	TRF	Mean* (%)	SD*	Mean (%)	SD	Mean (%)*	SD*	Mean (%)	SD	Mean (%)	SD	Mean (%)	SD	Mean (%)	SD
7B		0.00	0.00	0.06	0.10	0.07	0.13	0.00	0.00	0.00	0.00	0.00	0.00	0.10	0.13
12B		0.00	0.00	0.34	0.46	0.18	0.32	0.00	0.00	0.00	0.00	0.00	0.00	0.13	0.18
14B		0.76	0.45	1.15	1.54	0.50	0.65	0.98	0.20	4.70	0.19	0.61	0.26	1.70	0.58
20B		0.00	0.00	0.08	0.14	0.15	0.25	0.00	0.00	0.00	0.00	0.19	0.26	0.14	0.19
34B		0.30	0.42	0.00	0.00	0.00	0.00	0.00	0.00	14.02	8.90	0.00	0.00	0.00	0.00
61B		0.55	0.09	0.00	0.00	0.00	0.00	0.00	0.00	0.00	0.00	0.00	0.00	2.52	1.22
66B		1.15	0.07	1.89	0.68	1.56	1.01	0.14	0.20	0.00	0.00	0.00	0.00	0.00	0.00
70B		1.82	0.31	0.00	0.00	0.00	0.00	0.00	0.00	0.00	0.00	0.47	0.01	0.09	0.13
74B		0.43	0.04	0.78	0.13	0.55	0.03	0.13	0.18	0.00	0.00	0.00	0.00	0.10	0.13
77B		2.33	0.10	0.27	0.30	0.19	0.33	0.13	0.18	0.72	0.06	0.00	0.00	0.71	0.45
79B		0.66	0.07	0.22	0.38	0.00	0.00	0.00	0.00	0.00	0.00	0.00	0.00	0.00	0.00
84B		0.34	0.07	0.15	0.25	0.47	0.11	0.00	0.00	0.00	0.00	0.00	0.00	0.00	0.00
87B		1.12	0.13	1.23	0.55	1.49	0.32	1.96	0.16	4.22	0.21	3.29	0.19	1.34	0.45
91B		0.00	0.00	0.00	0.00	0.00	0.00	0.00	0.00	1.52	0.04	0.72	0.05	0.11	0.16
110B		0.00	0.00	0.00	0.00	0.00	0.00	0.00	0.00	0.00	0.00	0.41	0.05	0.26	0.36
117B		1.82	0.08	0.57	0.17	0.73	0.18	0.68	0.03	1.15	0.01	0.66	0.04	0.15	0.21
122B		1.43	0.01	0.08	0.14	0.43	0.12	1.16	0.16	0.68	0.08	0.00	0.00	0.00	0.00
127B		1.89	0.19	0.35	0.31	0.65	0.16	4.20	0.15	2.87	0.76	2.19	0.02	0.30	0.42
130B		3.36	0.04	3.17	1.18	3.35	0.39	1.54	0.04	1.02	0.07	0.00	0.00	0.17	0.24
136B		2.46	0.50	0.32	0.32	0.53	0.09	0.21	0.29	2.82	0.25	1.47	0.08	2.10	0.64
139B		1.64	0.09	0.81	0.09	1.14	0.24	1.24	0.15	0.46	0.04	0.40	0.01	0.15	0.21
144B		0.65	0.06	0.07	0.13	0.00	0.00	0.10	0.14	0.32	0.01	0.94	0.06	0.50	0.71
148B		6.87	0.35	3.17	0.47	3.37	0.45	5.18	0.69	1.38	0.09	0.49	0.00	1.50	0.36
151B		1.10	0.22	0.13	0.22	0.00	0.00	0.00	0.00	0.00	0.00	0.00	0.00	0.00	0.00
154B		10.51	2.62	0.49	0.44	0.00	0.00	0.12	0.17	0.00	0.00	2.07	0.08	2.11	0.92
159B		2.71	0.09	16.53	10.38	18.88	5.58	6.03	0.54	15.98	0.35	23.57	0.37	9.05	2.29
164B		0.00	0.00	1.34	0.41	2.19	0.55	3.51	0.21	0.61	0.04	0.14	0.20	3.08	0.92
168B		1.60	0.11	1.07	0.34	0.74	0.26	0.18	0.25	0.74	0.06	0.40	0.06	1.48	0.51
172B		0.16	0.23	0.00	0.00	0.13	0.22	0.80	0.08	0.00	0.00	2.16	0.02	9.62	2.44
179B		0.00	0.00	0.00	0.00	0.00	0.00	0.00	0.00	0.00	0.00	0.42	0.05	0.21	0.29
183B		1.25	0.18	0.25	0.43	0.00	0.00	0.53	0.13	0.00	0.00	0.00	0.00	2.04	0.86
187B		0.00	0.00	0.82	0.19	1.13	0.15	2.56	0.30	0.58	0.06	0.78	0.12	0.55	0.77
197B		2.24	0.10	0.08	0.13	0.00	0.00	0.00	0.00	0.48	0.03	0.00	0.00	0.00	0.00
203B		0.00	0.00	0.21	0.37	0.16	0.27	0.00	0.00	0.00	0.00	0.86	0.01	0.91	0.30
206B		0.00	0.00	0.00	0.00	0.00	0.00	0.11	0.16	0.00	0.00	6.04	0.41	1.04	0.45
211B		0.56	0.03	2.48	0.43	2.39	0.32	1.75	0.01	7.42	1.00	4.75	0.21	1.50	0.21
224B		0.00	0.00	0.00	0.00	0.00	0.00	0.00	0.00	1.44	0.19	0.96	0.05	1.44	0.81
228B		0.00	0.00	0.00	0.00	0.00	0.00	0.00	0.00	4.22	0.57	1.23	0.03	0.99	0.08
243B		0.16	0.22	1.30	0.03	1.04	0.21	1.05	0.09	2.76	0.51	1.72	0.13	0.33	0.46
260B		0.39	0.05	0.00	0.00	0.00	0.00	0.11	0.15	1.02	0.06	0.34	0.02	0.23	0.33
263B		0.83	0.04	0.09	0.15	0.10	0.17	0.00	0.00	0.00	0.00	0.00	0.00	0.17	0.24
268B		0.00	0.00	0.00	0.00	0.00	0.00	0.00	0.00	0.00	0.00	1.45	0.02	1.44	0.10
272B		0.00	0.00	0.00	0.00	0.00	0.00	0.00	0.00	0.15	0.21	0.00	0.00	0.00	0.00
276B		3.62	0.34	6.11	3.42	3.78	0.81	1.29	0.13	0.23	0.00	0.00	0.00	0.26	0.36
279B		0.20	0.28	0.00	0.00	0.00	0.00	0.00	0.00	0.25	0.01	1.19	0.08	0.09	0.13
282B		0.00	0.00	0.24	0.29	0.23	0.23	0.76	0.26	0.52	0.06	0.00	0.00	0.00	0.00
287B		1.55	0.15	0.12	0.21	0.09	0.15	0.13	0.18	0.34	0.05	4.39	0.25	2.28	0.29
292B		0.58	0.07	0.18	0.32	0.19	0.18	0.22	0.31	0.24	0.02	0.48	0.00	0.13	0.18
295B		0.00	0.00	0.00	0.00	0.00	0.00	0.27	0.37	0.00	0.00	0.15	0.21	0.26	0.36
297B		0.00	0.00	0.00	0.00	0.00	0.00	0.60	0.18	0.00	0.00	0.00	0.00	0.16	0.23
301B		0.13	0.18	0.10	0.17	0.00	0.00	0.00	0.00	0.00	0.00	0.00	0.00	0.10	0.13

Depth [m bls]	6.50 m		6.54 m		6.57 m		6.63 m		7.10 m		7.50 m		7.90 m		
	TRF	Mean (%)	SD	Mean (%)	SD	Mean (%)	SD	Mean (%)	SD	Mean (%)	SD	Mean (%)	SD	Mean (%)	SD
303B		0.00	0.00	0.05	0.08	0.00	0.00	0.11	0.16	0.00	0.00	0.62	0.02	0.20	0.28
325B		0.00	0.00	0.05	0.09	0.00	0.00	0.12	0.16	0.31	0.00	0.00	0.00	0.00	0.00
372B		0.00	0.00	0.08	0.14	0.00	0.00	0.00	0.00	0.00	0.00	1.02	0.10	3.25	1.04
398B		0.00	0.00	0.07	0.12	0.09	0.16	1.75	0.22	0.27	0.04	0.00	0.00	0.00	0.00
402B		0.43	0.01	0.07	0.12	0.35	0.06	0.17	0.23	0.00	0.00	0.00	0.00	0.00	0.00
419B		0.00	0.00	0.07	0.12	0.08	0.13	0.22	0.31	0.00	0.00	0.00	0.00	0.00	0.00
422B		0.69	0.01	0.05	0.09	0.00	0.00	0.00	0.00	0.00	0.00	0.00	0.00	0.00	0.00
430B		0.82	0.00	0.08	0.14	0.00	0.00	0.11	0.16	0.25	0.01	0.00	0.00	2.46	0.21
433B		0.40	0.00	0.07	0.12	0.30	0.27	1.08	0.06	0.00	0.00	0.00	0.00	0.00	0.00
438B		1.35	0.04	3.39	0.53	4.61	1.11	4.87	0.15	0.72	0.06	0.00	0.00	0.00	0.00
441B		0.00	0.00	0.00	0.00	0.00	0.00	0.00	0.00	0.00	0.00	0.00	0.00	0.00	0.00
445B		0.00	0.00	0.09	0.15	0.26	0.23	0.00	0.00	0.34	0.01	0.00	0.00	0.00	0.00
449B		0.67	0.01	3.33	0.82	4.17	0.88	1.63	0.10	0.14	0.20	0.61	0.16	1.09	1.54
453B		0.00	0.00	0.00	0.00	0.00	0.00	0.00	0.00	0.00	0.00	3.92	0.05	0.18	0.25
455B		0.00	0.00	0.84	0.10	0.73	0.15	0.00	0.00	0.00	0.00	0.00	0.00	0.00	0.00
459B		0.40	0.06	1.27	0.38	1.03	0.48	0.48	0.02	0.00	0.00	0.51	0.01	0.86	1.21
461B		0.81	0.06	0.18	0.32	0.13	0.23	0.13	0.18	0.00	0.00	0.00	0.00	0.00	0.00
466B		1.97	0.22	0.10	0.18	0.24	0.21	0.54	0.05	0.00	0.00	0.80	0.04	1.44	0.13
469B		0.76	0.07	0.78	0.35	1.25	0.51	3.03	0.08	0.71	0.06	0.00	0.00	0.00	0.00
472B		0.00	0.00	0.20	0.34	0.47	0.23	0.00	0.00	0.00	0.00	0.00	0.00	0.00	0.00
477B		3.04	0.86	17.86	5.64	15.32	5.17	4.12	0.70	0.51	0.06	0.00	0.00	0.11	0.15
480B		1.13	0.18	0.00	0.00	0.00	0.00	0.13	0.18	0.00	0.00	0.74	0.07	0.00	0.00
485B		0.83	0.29	0.16	0.28	0.83	0.17	0.00	0.00	0.33	0.08	0.00	0.00	0.47	0.66
489B		13.86	0.76	6.60	2.93	3.69	0.32	1.61	0.10	0.82	0.08	0.72	0.01	0.37	0.52
492B		2.85	0.62	8.20	1.27	9.37	2.18	5.84	0.34	5.68	0.38	1.51	0.08	1.50	2.11
496B		1.97	0.73	1.06	0.41	1.70	0.47	0.61	0.03	0.12	0.17	0.00	0.00	0.12	0.17
499B		3.66	0.39	3.15	0.46	2.50	0.12	0.66	0.03	0.00	0.00	0.00	0.00	0.19	0.27
502B		0.68	0.06	0.45	0.57	0.87	0.60	31.76	7.94	6.85	1.68	0.81	0.13	0.32	0.45
506B		1.09	0.01	0.39	0.37	0.80	0.72	0.80	0.10	0.00	0.00	0.95	0.00	3.80	1.08
509B		1.50	0.02	3.43	0.61	3.56	0.48	2.29	0.21	6.88	1.20	6.09	0.03	4.12	0.04
513B		0.44	0.00	0.32	0.34	0.47	0.20	0.00	0.00	0.00	0.00	0.75	0.04	1.01	0.53
518B		0.53	0.03	0.15	0.26	0.44	0.06	0.00	0.00	0.68	0.08	6.01	0.06	5.63	0.16
520B		0.60	0.06	0.48	0.43	0.00	0.00	0.00	0.00	0.00	0.00	0.00	0.00	0.09	0.12
526B		0.13	0.18	0.14	0.25	0.00	0.00	0.00	0.00	0.00	0.00	7.42	0.09	14.01	0.44
533B		0.14	0.19	0.00	0.00	0.00	0.00	0.00	0.00	0.00	0.00	0.00	0.00	1.54	0.29
538B		0.00	0.00	0.00	0.00	0.00	0.00	0.00	0.00	0.00	0.00	0.00	0.00	0.00	0.00
542B		0.48	0.01	0.00	0.00	0.00	0.00	0.00	0.00	1.15	0.14	0.38	0.04	0.19	0.27
546B		0.00	0.00	0.00	0.00	0.00	0.00	0.00	0.00	0.00	0.00	0.31	0.02	0.30	0.42
549B		0.00	0.00	0.00	0.00	0.09	0.15	0.00	0.00	0.87	0.15	0.39	0.03	0.00	0.00
579B		0.00	0.00	0.08	0.14	0.00	0.00	0.00	0.00	0.00	0.00	0.58	0.04	0.22	0.30
603B		0.00	0.00	0.35	0.35	0.26	0.24	0.00	0.00	0.00	0.00	0.00	0.00	4.32	2.42
611B		1.09	0.04	0.08	0.13	0.00	0.00	0.00	0.00	0.00	0.00	0.13	0.18	0.12	0.16
613B		0.00	0.00	0.00	0.00	0.00	0.00	0.41	0.06	0.00	0.00	0.00	0.00	0.00	0.00
629B		0.00	0.00	0.00	0.00	0.00	0.00	0.00	0.00	0.65	0.35	0.47	0.14	0.18	0.25
644B		0.53	0.01	0.07	0.12	0.00	0.00	0.00	0.00	0.00	0.00	0.46	0.04	0.44	0.62
668B		0.17	0.23	0.00	0.00	0.00	0.00	0.00	0.00	0.00	0.00	0.00	0.00	0.00	0.00
685B		0.00	0.00	0.00	0.00	0.00	0.00	0.00	0.00	0.00	0.00	0.00	0.00	0.10	0.14

* Mean: Mean values of relative TRF abundance derived from replicate DNA extractions (n = 3);
SD: standard deviation

Table 11: Concentrations of Fe(II), sulfate, sulfide, and nitrate during growth of culture 1MN and in abiotic controls for Figure 10

	Time [d]	Fe(II) [mM]				Sulfate [mM]				Sulfide [mM]				Nitrate [mM]			
		Active		Control		Active		Control		Active		Control		Active		Control	
		Mean*	SD*	Mean	SD	Mean	SD	Mean	SD	Mean	SD	Mean	SD	Mean	SD	Mean	SD
A)	1	2.4	0.2	2.5	0.0	0.3	0.0	0.2	0.1	1.0	0.2	0.7	0.1	0.6	0.0	0.6	0.0
	9	2.7	1.0	2.2	0.1	0.2	0.1	0.3	0.1	0.5	0.1	0.6	0.1	0.6	0.0	0.5	0.0
	16	2.3	0.4	2.7	0.1	0.2	0.0	0.1	0.1	0.6	0.3	0.5	0.2	0.6	0.0	0.6	0.0
	22	2.5	0.8	2.4	0.1	0.2	0.0	0.1	0.1	0.5	0.3	0.4	0.0	0.6	0.0	0.6	0.0
	30	2.2	0.7	2.2	0.0	0.2	0.0	0.2	0.0	0.4	0.2	0.4	0.1	0.6	0.0	0.6	0.0
	36	2.1	0.4	2.1	0.1	0.4	0.1	0.4	0.0	0.4	0.3	0.3	0.0	0.5	0.0	0.5	0.0
	43	2.8	0.5	2.0	0.3	0.6	0.7	0.1	0.0	0.5	0.5	0.2	0.1	0.4	0.3	0.6	0.0
	52	3.6	0.2	2.3	0.1	1.0	0.4	0.1	0.0	0.8	0.1	0.2	0.1	0.2	0.2	0.6	0.0
	60	4.1	0.7	2.1	0.1	1.4	0.2	0.2	0.0	0.6	0.1	0.2	0.0	0.0	0.1	0.6	0.0
	70	4.1	0.3	2.4	0.0	1.8	0.5	0.2	0.0	0.4	0.1	0.2	0.0	0.0	0.0	0.6	0.0
	86	3.2	0.4	2.2	0.1	1.5	0.5	0.2	0.0	0.4	0.2	0.1	0.0	0.0	0.0	0.6	0.0
105	2.9	0.7	2.0	0.1	1.5	0.5	0.1	0.0	0.4	0.4	0.1	0.1	0.0	0.0	0.6	0.1	
B) FeS	1	ND*	ND*	ND*	ND*	0.2	0.1	0.3	0.1	1.1	0.1	1.0	0.2	1.3	0.0	1.3	0.0
	9	4.6	0.5	4.6	0.1	0.3	0.1	0.3	0.1	0.6	0.1	0.7	0.1	1.2	0.1	1.3	0.1
	16	5.1	0.5	5.0	0.4	0.2	0.1	0.2	0.1	0.6	0.1	0.7	0.1	1.3	0.1	1.4	0.1
	22	5.3	0.5	5.1	0.1	0.4	0.2	0.3	0.1	0.5	0.2	0.6	0.0	1.1	0.2	1.4	0.2
	30	5.4	0.3	5.2	0.3	0.6	0.1	0.2	0.0	0.5	0.1	0.6	0.1	0.9	0.1	1.4	0.1
	36	5.7	0.9	4.7	0.2	0.7	0.1	0.3	0.1	0.4	0.1	0.5	0.1	0.8	0.1	1.3	0.2
	43	5.7	0.5	5.1	0.5	0.7	0.2	0.2	0.0	0.3	0.1	0.4	0.1	0.7	0.2	1.4	0.1
	52	6.0	0.6	5.4	0.6	0.9	0.1	0.3	0.1	0.3	0.1	0.5	0.1	0.6	0.1	1.3	0.1
	60	5.8	0.7	5.2	0.3	0.8	0.2	0.3	0.1	0.3	0.1	0.4	0.1	0.6	0.1	1.3	0.2
	70	6.2	0.7	5.6	0.3	1.1	0.2	0.3	0.1	0.4	0.1	0.6	0.1	0.4	0.2	1.3	0.1
	86	6.1	0.7	5.9	0.5	1.4	0.2	0.5	0.1	0.3	0.1	0.5	0.1	0.0	0.2	1.2	0.1
105	6.1	0.7	5.8	0.3	1.3	0.3	0.1	0.0	0.3	0.1	0.6	0.1	0.1	0.3	1.5	0.1	
C) S ₀	0	0.9	0.4	1.4	0.1	0.1	0.0	0.1	0.0	0.2	0.1	0.2	0.0	3.0	0.0	3.0	0.0
	6	0.9	0.1	1.3	0.1	0.2	0.1	0.2	0.1	0.1	0.0	0.2	0.0	3.0	0.1	2.9	0.0
	13	0.9	0.1	1.3	0.1	0.1	0.0	0.1	0.1	0.1	0.0	0.1	0.0	3.0	0.0	2.8	0.0
	19	0.7	0.1	1.1	0.0	0.4	0.2	0.3	0.1	0.1	0.0	0.1	0.0	2.9	0.1	2.8	0.0
	26	0.9	0.1	1.3	0.1	1.0	1.0	0.2	0.0	0.2	0.1	0.1	0.0	2.6	0.5	2.8	0.0
	35	2.2	0.7	1.1	0.2	2.7	1.8	0.2	0.1	0.2	0.1	0.1	0.0	1.7	0.9	2.9	0.0
	43	3.9	2.5	1.1	0.0	4.4	3.0	0.1	0.0	0.6	0.5	0.1	0.0	0.9	1.5	2.9	0.0
	53	7.0	4.9	1.2	0.1	5.3	2.5	0.1	0.0	1.1	1.0	0.2	0.0	0.4	1.3	2.8	0.0
	69	13.1	1.9	1.1	0.1	10.1	1.3	0.2	0.0	2.1	0.5	0.1	0.0	0.0	0.0	2.8	0.0
	88	12.4	1.0	0.8	0.1	11.7	1.1	0.3	0.0	2.4	0.8	0.1	0.0	0.0	0.0	2.9	0.0

* Mean: Mean values of replicate incubations (1-methylnaphthalene: n = 2; S₀: n = 4; FeS: n = 8; and controls: n = 2);
SD: standard deviation; ND: not determined

Table 12: Values of pH during growth of culture 1MN for Figure 11

	Time [d]	Mean	SD
A)	1	6.58	0.03
	9	6.57	0.04
	16	6.55	0.02
	22	6.61	0.03
	30	6.62	0.07
	36	6.68	0.04
	43	6.63	0.06
	52	6.57	0.07
	60	6.54	0.07
	70	6.54	0.06
	86	6.37	0.08
B) FeS	1	6.53	0.03
	9	6.65	0.03
	16	6.66	0.03
	22	6.66	0.03
	30	6.68	0.04
	36	6.71	0.02
	43	6.70	0.03
	52	6.79	0.04
	60	6.83	0.06
	70	6.74	0.02
	86	6.70	0.04
C) S₀	0	6.50	0.19
	6	6.46	0.04
	13	6.48	0.03
	19	6.48	0.04
	26	6.43	0.03
	35	6.38	0.10
	43	6.51	0.11
	53	6.50	0.05
	69	6.30	0.06
	88	6.24	0.09

* Mean: Mean values of replicate incubations (1-methylnaphthalene: n = 2; S₀: n = 4; FeS: n = 4);
SD: standard deviation)

Publications

Müller H, Bosch J, Griebler C, Damgaard LR, Nielsen LP, Lueders T, Meckenstock, RU (2016). "Long-distance electron transfer by cable bacteria in aquifer sediments." *ISME J* 10(8): 2010-2019. (*published*)

Müller H, Marozava S, Fritzsche A, Lueders T, Meckenstock, RU. "Cable bacteria couple iron and sulfur cycles in anaerobic enrichment culture." (*in preparation*)

Dvorski SEM, Gonsior M, Hertkorn N, Uhl J, **Müller H**, Griebler C, Schmitt-Kopplin P. (2016). "Geochemistry of Dissolved Organic Matter in a Spatially Highly Resolved Groundwater Petroleum Hydrocarbon Plume Cross-Section." *Environ Sci Technol* **50**(11): 5536-5546. (*published*)

Authorship Clarification

I) Long-distance electron transfer by cable bacteria in aquifer sediments

This study addressed the hypothesis of this thesis that long-distance electron transfer by cable bacteria is present in sediments from a contaminated aquifer. This was done via laboratory incubations and high-resolution field sampling. Prof. Meckenstock together with the author developed the concept of this study and planned laboratory experiments. Prof. Meckenstock, Dr. Lüders, Dr. Griebler, Dr. Kellermann, and the author planned the sampling campaign in Düsseldorf-Flingern, 2013. Dr. Griebler, Dr. Kellermann, Dr. Uhl, Sabine Dvorski, Katrin Hörmann, and the author conducted the field sampling and sample analyses. The setup of laboratory sediment incubations was done by the author. Dr. Damgaard (Aarhus University) and the author measured the pore water chemistry by microsensors. Molecular analyses and data processing were done by the author. Dr. Lüders together with the author designed the specific probes for fluorescence in situ hybridization. Katrin Hörmann conducted pyrosequencing with purified amplicons provided by the author. Data processing was done by the author. Prof. Meckenstock, Dr. Lüders, Dr. Griebler and Dr. Nielsen (Aarhus University) supported the author by data assessment and revision of the manuscript. The work was published in the ISME Journal (Müller *et al.* 2016).

II) Cable bacteria couple nitrate reduction to iron and sulfur cycles in anaerobic enrichment culture

This study elucidated the role of cable bacteria in nitrogen, iron and sulfur cycling. Cable bacteria from an iron-reducing 1-methyl-naphthalene-degrading enrichment culture were grown in the laboratory in the presence of different electron donor. The author developed the conceptual framework of this study. Prof. Meckenstock and the author planned the experimental design. The experimental setup, chemical analyses and data processing were done by the author. Niklas Gassen and Gabriele Barthel measured nitrate concentrations by ion chromatography. Dr. Fritzsche (University Jena) did anoxic freeze-drying and analyses of solid phase mineral

composition by XRD and FTIR of washed samples provided by the author. Prof. Meckenstock assessed the data together with the author and revised the manuscript.

III) Geochemistry of Dissolved Organic Matter in a Spatially Highly Resolved Groundwater Petroleum Hydrocarbon Plume Cross-Section

This study combined high resolution ground water sampling to high-resolution analysis of DOM composition. This work is based on parts of the published manuscript of Sabine Dvorski which the author co-authored. The main contributions of the author were support during field sampling and groundwater analyses. The author also assisted Sabine Dvorski in data interpretation and evaluation and in writing of the manuscript which was published to ES&T (Dvorski *et al.* 2016).

Selected Contributions to Scientific Meetings

Oral presentations:

Müller H, Bosch J, Griebler C, Damgaard LR, Nielsen LP, Lueders T, Meckenstock, RU (2013) "Long distance electron transfer in groundwater." VAAM 2013 in Bremen, March 10-13, 2013.

Müller H, Bosch J, Griebler C, Damgaard LR, Nielsen LP, Lueders T, Meckenstock, RU (2014). "Microbial long distance electron transfer in contaminated aquifers." ISSM 2014 in Pacific grove (CA, USA), October 05-10, 2014

Müller H, Bosch J, Griebler C, Damgaard LR, Nielsen LP, Lueders T, Meckenstock, RU (2015). "Long distance electron transfer by cable bacteria in contaminated aquifers." VAAM 2015 in Marburg, March 1-4, 2015

Poster:

Müller H, Marozava S, Lueders T, Nielsen LP, Meckenstock RU (2016). "Cable bacteria in 1-methyl-naphthalene degrading enrichment culture." VAAM 2016 in Jena, March 13-16, 2016

Lebenslauf

Name: Hubert Müller
Adresse: Tölzer Straße 109
83607 Holzkirchen
Telefon: 017621202593
E-Mail: hubert.mueller83@gmail.com
Familienstand: ledig
Geburtsdatum: 13.07.1983
Geburtsort: Bad Tölz



Bildungsweg

Seit April 2013	Doktorarbeit am Institut für Grundwasserökologie des Helmholtz Zentrum München bei Prof. Meckenstock und P.D. Dr. Lueders
Juli 2012 – März 2013	Diplomarbeit am Lehrstuhl für Grundwasserökologie bei Prof. Dr. Meckenstock
2003 - 2013	Studium der Biologie an der TU München; Hauptfach: Mikrobiologie Nebenfächer: Biochemie und Umweltmikrobiologie
1994 – 2003	Gymnasium Tegernsee Abschluss: Abitur

Acknowledgments

First, I like to thank my supervisor Rainer Meckenstock for his support throughout this thesis. He was always highly interested in my work, supported me in all possible ways, and pushed the project by valuable suggestions and discussions.

As well, I like to thank Tillmann Lüders, not only for taking over the supervision of this thesis after Rainer Meckenstock received his call from the University Duisburg-Essen, but also for warmly welcoming me to his group, his scientific input, and extensive support in many ways.

I also like to acknowledge Christian Griebler as commissary head of the institute for guiding the IGOE through stormy weather and for his help during the sampling campaign in Düsseldorf, in 2013. I like to thank all members of the anaerobic degradation and the molecular ecology group for scientific help and for the fun we had over the years. I like to thank Katrin Hörmann and Gabriele Barthel for technical support and for providing excellent conditions for doing science. I also like to thank my colleagues Anne, Anna, Claudia, Clemens, Niklas, Philip, Sviatlana, Lauren, and many more, for their help and the discussion we had during the daily laboratory work; and all colleagues at the IGÖ for the great working atmosphere.

Many thanks to Prof. Nielsen from the Aarhus University whose pioneering work on cable bacteria provided the basics of this thesis. Furthermore, many thanks for being part of my thesis committee and for the interesting discussions we had during our meetings and the yearly workshops on cable bacteria.

I like to thank the Helmholtz Wasserzentrum München and the European Research Council for funding. I am also very grateful to Prof. Liebl for taking over the chair of my examination committee.

Finally, many thanks to my family and friends for their unconditional support during this period of my life.